Australian Government
Department of Defence
Defence Science and
Technology Organisation

DSTO

Fatigue Crack Growth in Several 7050T7451 Aluminium Alloy Thick Section Plates with Aircraft Manufacturer's and Laboratory Surface Finishes Representing Some Regions of the F / A-18 Structure

S. A. Barter

DSTO-TR-1539

Australian Government
Department of Defence
Defence Science and
Technology Organisation

Fatigue Crack Growth in Several 7050T7451 Aluminium Alloy Thick Section Plates with Aircraft Manufacturer's and Laboratory Surface Finishes Representing Some Regions of the F/A-18 Structure

S A Barter

Air Vehicles Division
Platforms Sciences Laboratory

DSTO-TR-1539

ABSTRACT

This is the third in a series of papers that examine material factors likely to influence the fatigue life of F/A-18 structure. Work leading up to these papers has highlighted a number of concerns about the fatigue variability of the 7050 aluminium alloy thick section plate and the effect that the surface condition of finished components has on service fatigue crack initiation and life. This report examines a series of fatigue test specimens that were cut from three different 7050 plates, including two aircraft manufacturer's plates. Following the tests, quantitative fractography was used to produce crack growth curves for each fatigue specimen allowing a detailed interpretation of the crack growth to be made, including a measure of the severity of the flaws from which the main fatigue cracks initiated. Comparisons between previously tested 7050 plate, and the three plates tested here were made, with the finding that the crack growth rates and the flaws from which the cracking initiated were very similar to those previously examined.

Published by

DSTO Platforms Sciences Laboratory
506 Lorimer St
Fishermans Bend, Victoria 3207 Australia

Telephone: (03) 9626 7000
Fax: (03) 9626 7999

AR-012-856
December 2003

APPROVED FOR PUBLIC RELEASE

Fatigue Crack Growth in Several 7050T7451 Aluminium Alloy Thick Section Plates with Aircraft Manufacturer's and Laboratory Surface Finishes Representing Some Regions of the F/A-18 Structure

Executive Summary

DSTO research into material factors likely to affect F/A-18 fatigue life has highlighted a number of concerns about the fatigue variability of the 7050 thick section plate and the effect that the surface condition has on service fatigue crack initiation. This report presents the results of a fatigue coupon test program, which tested samples cut from three different 7050 plates.

The test coupons were drawn from two previously tested Y488 bulkheads that had the original aircraft manufacturer's surface finish intact, and from one plate that had been purchased for coupon testing by DSTO. The surfaces of the coupons made from the DSTO plate were etched to simulate the surface on the two Y488 bulkheads, which was preserved on the coupons cut from these bulkheads. All specimens were loaded with a representative wing root-bending spectrum derived from the F/A-18 FT488/2 bulkhead fatigue test. Several peak stress levels were used to test the low Kt coupons cut from the Y488 bulkheads, and a single stress level was tested with specimens from another DSTO plate. The spectrum used had additional marker loads added to aid quantitative fractography. These marker loads are briefly discussed.

Following the tests, quantitative fractography was used to produce crack growth curves for each of the fatigued specimens. This allowed a detailed interpretation of the crack growth to be made, including a measure of the severity of the flaws from which the fatigue cracks initiated. Comparisons between a previously tested 7050 plate, the plate purchased for the coupon testing for this report, and the coupons cut from the two Y488 bulkheads were made. It was found that the crack growth rates and the discontinuities from which the cracking initiated were very similar and they could be characterised by the way that cracking grew from them.

Author

Simon Barter
Air Vehicles Division

Simon Barter completed a Diploma of Applied Science in Secondary Metallurgy and a Graduate Diploma in Surface Finishing and Corrosion Control at RMIT and is currently completing a PhD in Engineering Science at Monash University. During his time at DSTO he has been involved with the metallurgical investigation of failures in aircraft structures and components and the investigation of aircraft oxygen system fires. These studies have included quantitative fractographic studies on Macchi, F111 and F/A-18 aircraft and research into fatigue crack growth in aircraft metals. He now works in the Structural Integrity area as the manager of the Australian F/A-18 aft empennage test, FT46 and undertakes investigations into the fatigue and fracture of high strength aluminium alloys found in this aircraft. His involvement in the investigation of numerous aircraft accidents has been a highlight of his employment, having completed the Aircraft Accident Investigation course held at Cranfield Aviation Safety Centre, and is a member of the DSTO Accident Investigation Committee.

Contents

This page intentionally left blank

Nomenclature

Al	Aluminium alloy.
ASME	American Society of Mechanical Engineers.
AVD	Air Vehicles Division, a division of DSTO.
CF	Canadian Forces.
DSTO	Defence Science and Technology Organisation.
EPS	Equivalent Pre-crack Size.
FT 488/1	First stand alone Y488 bulkhead fatigue test, performed in Australia.
FT 488/2	Second stand alone Y488 bulkhead fatigue test, performed in Australia.
FT55	IFOSTP F/A-18 centre fuselage fatigue test.
IARP03a	Canadian Forces flying sequence.
IARP03a+markers	IARP03a spectrum modified for testing of a stand alone Y488 bulkhead with the addition of five compressive loads before the highest peak load in the spectrum.
IFOSTP	International Follow on Structural Fatigue Project.
IVD	Ion Vapour Deposited aluminium coating used as a corrosion preventative on 7050 fatigue critical components, as well as many other components in the F/A-18.
MDA	McDonnell Douglas Aircraft Corporation. (now Boeing Aircraft).
QF	Quantitative Fractography.
RAAF	Royal Australian Air Force.
SFH	Simulated Flying Hours.
USN	United States Navy.
μ_{log}	mean (based on log normal distribution).
σ_{log}	Standard deviation (based on log normal distributions.
Y488	Rear most of the three centre barrel wing carry-through bulkheads in the F/A-18 aircraft.

1. Introduction

This is the third paper in a series that examines material factors likely to influence the fatigue life of F/A-18 structure. Work leading up to these papers has highlighted a number of concerns about the fatigue variability of the thick section plate 7050 aluminium alloy and the effect that the surface condition of finished components has on service fatigue crack initiation and therefore life. This material is used extensively in the critical structure of the F/A-18 aircraft. The surface condition aspect has been partially addressed elsewhere, Barter, 2003, although the validity of the laboratory simulated pre-IVD[1] etch used on these previously fatigue tested coupons has not been fully investigated. This report tests coupons cut from two OEM F/A-18 Y488 bulkheads with the OEM IVD coating intact on their surfaces, and compares these results to previously tested coupons and coupons from another 7050 Al plate held at DSTO.

During the production run of the RAAF F/A-18 aircraft the 7050-T7451 thick section plate used in most of the main bulkheads was improved in quality by the plate manufacturers, particularly Alcoa, Owen et al. 1988. This report partially addresses this unknown improvement by carrying out fatigue tests on specimens cut from several sources of material. In addition to this test objective, two of the sources of material had surfaces which had been IVD coated by the aircraft manufacturer (OEM IVD) which allowed the comparison of the effect of production pre-IVD coating preparation-induced etching over an OEM machined surface to be compared to the laboratory etched (pre-IVD simulation) specimens tested previously.

The low Kt 'dog bone' type specimens, cut for testing as part of this study, were loaded with a spectrum typical of aircraft in-service loading, using several peak stress levels to produce life data that may be applicable in the estimation of the life of the most critical structure in the F/A-18 aircraft. The spectrum used was the International Follow on Structural Fatigue Project (IFOSTP) IARPO3a spectrum with the addition of marker loads. These marker loads have been discussed in some detail by Barter, 2003.

2. Test Procedure & Results

2.1 Specimen geometry

The specimens were of the simple 'dog bone' type with a continuous 100mm radius on either side resulting in a 25mm wide test section. The thickness of the specimens varied depending on the source. Specimens were cut from the remains of two Y488 bulkheads that had been fatigue tested to failure in previous programs, Barter et al., 1991 and Athiniotis et al, 2003. These tests are known as FT488/1 and FT488/2

[1] IVD is an Ion Vapour Deposited coating of aluminium, with or without a small percentage of zinc which is applied to the surfaces of high strength aluminium alloy parts (and many other parts) of the F/A-18 aircraft. To achieve adequate adhesion for the coating, the 7050 Al parts were acid etched prior to the application of the IVD; this is termed the 'pre-IVD etch'.

respectively. These specimens were typically about 4.5mm thick depending on the thickness of the web from which they were cut and were orientated so that cracking would occur in the T-S direction. All specimens cut from OEM prepared Y488 bulkheads were from the web that lay along the central plane of the bulkhead and therefore the central plane of the original plate. It is this region of the thick section plates that were improved to reduce the occurrence of large porosity during the quality improvement program carried out by Alcoa in the mid 80's, Owen et al, 1988. The specimens cut from stock plate were similar in dimensions to the Y488 specimens except they had a thickness of 6.35mm as per the previous coupons tested in Barter, 2003. These specimens were taken from a larger group of specimens in a random manner so that they represented random positions through the plate thickness. A schematic showing the general form of the specimens is presented in Figure 1, although the thickness of the Y488 bulkhead specimens varied as indicated above. The size of the specimens was dictated by the availability of the material from the two Y488 bulkheads, and were therefore shorter than the specimens tested previously and reported on in Barter, 2003. With the 100mm radius used in these specimens the K_t was calculated to be 1.08 which is somewhat higher than the 1.037 of the previous specimens tested and reported on in Barter, 2003. This specimen was a modification of the previous design, which mimicked a critical low K_t detail of an F/A-18 Y488 centre-section bulkhead and for which much data have already been generated. Although the Y488 bulkhead detail in question has a 6" (152.4mm) radius, the K_t was not significantly different (Molent, Ogden and Pell, 2000) and the 100mm radius allowed a shorter specimen; a necessity as they were to be cut from the Y488 bulkheads, while leaving the IVD on the web surface intact and providing sufficient specimens for this test program. Since part of the purpose of these tests was to examine the effect of the OEM IVD procedure on fatigue life, the Y488 specimens were peened on the cut edges and in the grips to prevent failure at these locations, negating the Kt region of the specimens - none of these specimens failed from the radii during the testing. The stock plate KW specimens were not peened on the edges.

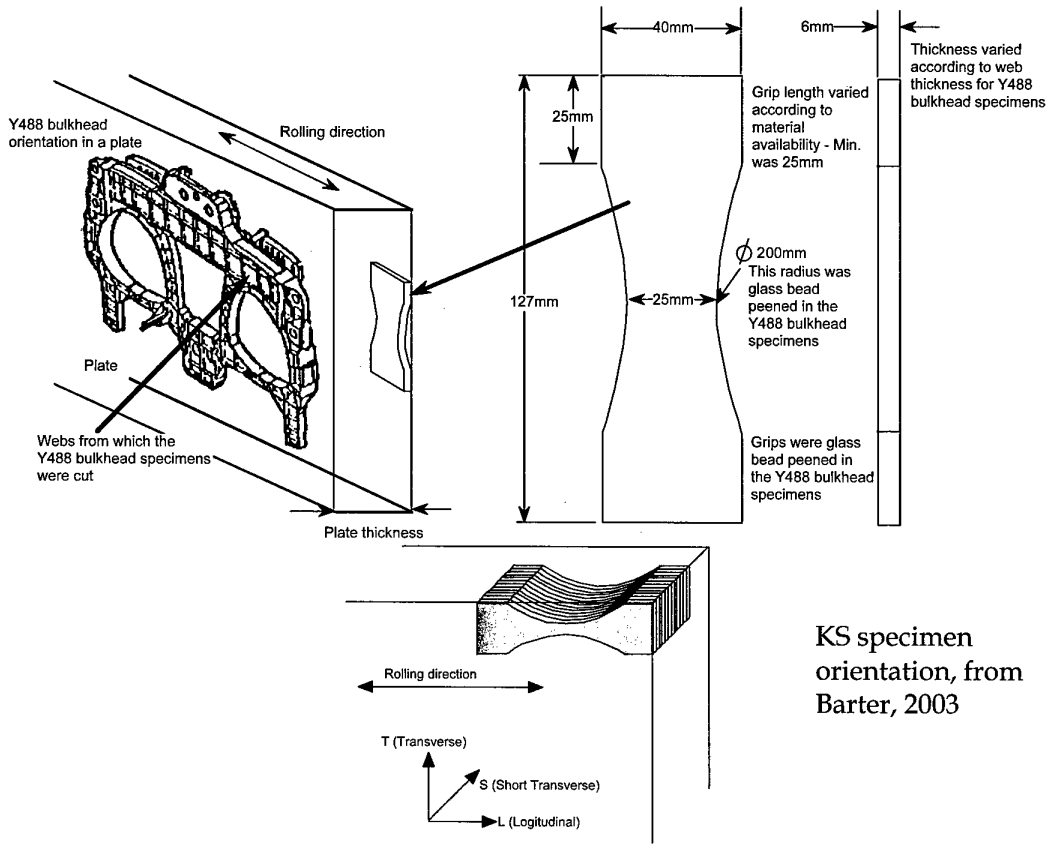

KS specimen orientation, from Barter, 2003

Figure 1 A schematic drawing of the specimens used in this test program and their orientation in the plate along with the orientation of a typical F/A-18 aircraft bulkhead in the plate is shown in the upper view. The webs from which the Y488 bulkhead specimens were cut are marked. The lower view shows the orientation of the KS specimens which will be used for comparison to the results reported here, showing their orientation.

The stock plate specimens were machined from a 6inch thick (150mm) 7050-T7451 aluminium alloy plate (DSTO designation KW) produced by British Aluminum USA, Ellisville, Missouri. The long axis of the specimens was aligned across the rolling direction as shown in Figure 1 to duplicate the orientation of the FT488/1 and 2 specimens. This gave the coupons a grain orientation that was consistent with cracking occurring in many areas of the bulkhead (away from where the coupons were cut) during the two Y488 bulkhead tests carried out at DSTO. It was found for the peened edge Y488 specimens the cracks were all in the TS orientation while the non-peened edge KW specimens had cracking in the TS and TL directions. Cracking in these directions was expected to be faster than the cracking in the KS specimens tested previously, to which these results are compared. Those specimens had cracks in the LS and LT orientation, Barter, 2003. Figure 2 shows a prepared Y488 and KW specimen, and a KS specimen from Barter, 2003, for comparison.

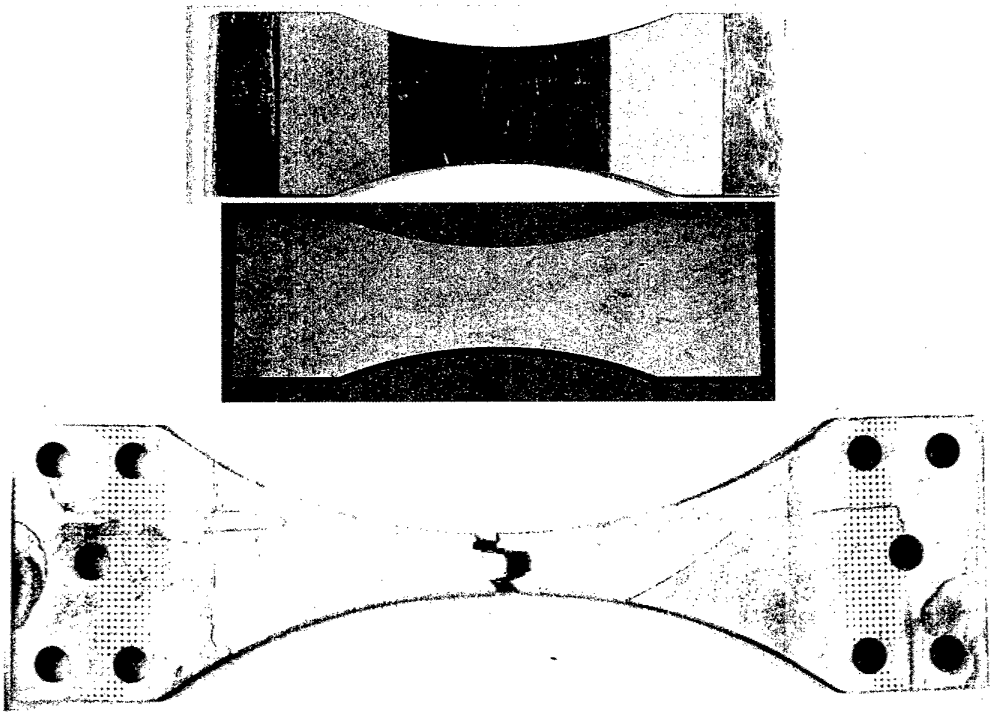

Figure 2 Pictures of the three types of specimens – the first shows a specimen cut from the FT488/1 bulkhead, peened in the grip areas and on the cut edges, and the second picture is of an etched specimen cut from the KW plate. The third picture is of one of the KS specimens (after failure), which were used for comparison purposes in this report.

Since the specimens cut from the two Y488 bulkheads had been subjected to fatigue loads during the testing of these two bulkheads, care was taken to look for any evidence of pre-existing cracking during the fractographic examination of the failed specimens. No evidence of pre-existing damage was found, which was expected since the area from which the specimens were cut is known to be lightly loaded and the loading direction during the Y488 testing was perpendicular to the loading direction used to test these specimens.

Experience with fatigue cracking in these types of specimens indicated that critical cracks could occur up to 15mm on either side of the specimen centre. Using, for simplicity a constant width of 25mm over this region an estimate of the approximate surface area likely to generate a critical crack in each specimen was 1500mm^2. This is an important consideration if these data are to be used to aid in the analysis of F/A-18 critical structural locations, since low Kt areas can have significant scatter in fatigue cracking due to size effects, especially when surface discontinuity densities are low; such as for the occurrence of porosity, mechanical damage and corrosion, as crack initiators.

2.2 Specimen Material Properties

2.2.1 Introduction

All the specimens were cut from what is or was thick section 7050-T74511 aluminium alloy plate. This alloy is one of the high strength Al/ZnMgCu alloys that make up a group of alloys essential for many components in the primary load-carrying structures of modern aircraft. A major limitation on the structural performance of these alloys is that in the peak aged (T6) temper they are all susceptible to stress corrosion cracking (SCC) in the short transverse direction, Speidel and Hyatt, 1972.

Service experience with older alloys like 7075 and 7079 has shown that it is unwise to use them in the T6 temper for thick section components or parts machined from thick section plate because of the risk of SCC. In the mid-1960s to the early 1970s two possible methods to improve stress corrosion resistance were investigated. One was to overage the alloys to a T7 condition, Mehr et al, 1971. For 7075 the highly SCC resistant T73 temper was developed. However, a strength loss of about 15% occurred, Mehr et al, 1971. Subsequently the T736 temper was developed for 7075 and 7175, which enabled SCC resistance intermediate between T76 and T73 to be obtained at T6 strength levels, Speidel and Hyatt, 1972. Despite these developments there remained the need for deep hardenable alloys combining good thick section properties with a high resistance to SCC and improved fracture toughness at strength levels equivalent to the T6 condition in the older alloys. These requirements were the basis for development of alloys like 7010, 7049 and 7050, Renolds and Harris, 1974, Staley and Hunsicker, 1970.

For the alloy of interest here, 7050, the result of this alloy and temper development was an alloy which contains zirconium rather than chromium for controlling recrystallization and grain growth, Staley, 1973. The use of zirconium decreases quench sensitivity, which means that uniform properties are more easily achieved in thick sections. A consequence of this is a greater sensitivity to corrosion pitting when compared to 7075-T73, Wanhill, 1995, which necessitates a good surface corrosion protection scheme if corrosion pitting is not to adversely affect fatigue life.

2.2.2 Specimen properties

The KW plate was certified by British Aluminum USA to conform to the requirements of the specification AMS 4050. The plate came from Lot No. 27-412-8340 R, and was produced in 1998. Table 1 shows the chemical composition specification and the results of analysis of the KW, FT488/1, FT488/2 and the KS plates. The FT488/1 plate was used in the first of the Y488 full-scale component fatigue tests carried out at DSTO, Anderson and Revill, 1990. It was produced by Alcoa and came from Lot No. 603501, casting date unknown, although most probably after 1985. The bulkhead made from this plate had been coated all over with IVD and was tested in this condition (unpainted). The 144mm thick FT488/2 plate was produced by Alcoa (heat Lot unknown) and had a casting date of 16 May, 1992. The bulkhead made from this plate had been coated all over with IVD, shot peened and cold coined in critical locations, and painted, Athiniotis et al, 2003.

Table 1 Specification AMS 4050E compared to the chemical composition% measured for each of the plates examined here

Element	Min AMS 4050E	Max AMS 4050E	Analysis of KW plate	Analysis of FT488/1	Analysis of FT488/2	Analysis of KS plate
Zinc	5.7	6.7	6.18	5.89	5.69	6.42
Copper	2	2.6	2.13	2.07	1.95	2.20
Magnesium	1.9	2.6	2.26	2.05	2.02	1.99
Zirconium	0.08	0.15	0.13	0.11	0.13	0.08
Iron	--	0.15	0.06	0.09	0.08	0.06
Silicon	--	0.12	0.04	0.04	0.03	0.03
Manganese	--	0.1	<0.01	0.01	0.01	0.01
Titanium	--	0.06	0.035	0.07	0.14	0.04
Chromium	--	0.04	<0.005	0.005	0.005	0.005
Other Impurities, each	--	0.05	Ni <0.01	Ni <0.01	Ni <0.01	Ni <0.01
Other Impurities, total	--	0.15	<0.1	<0.1	<0.1	<0.1
Aluminium		Remainder	Remainder	Remainder	Remainder	Remainder

An examination of Table 1 reveals that some of the alloying elements were outside the limits for the material taken from the two bulkheads. This is probably the result of alloy segregation during casting of the original ingot, since the analysis samples were taken from the centre of the plates of both Y488 bulkheads. Table 2 shows the mechanical properties and conductivity requirements of 7050-T7451. The supplied mechanical properties and conductivity measurements are shown in Table 3 for the KW-plate. Conductivity and hardness values were measured for each of the materials examined here, and are presented in Table 4.

Table 2 Specification AMS 4050 Mechanical properties and conductivity for 7050 Al.

Nominal Thickness (inches)	Specimen Orientation	Tensile Strength (ksi)	Yield Strength (ksi)	Elongation in 2 inches or 4D (%)
Over 5 to 6	Longitudinal	70	60	8
	Long Trans.	70	60	4
	Short Trans.	67	57	2
Conductivity (IACS)	not less than 38.0 %			

Table 3 Mechanical properties and conductivity as supplied with KW-plate documentation

Plate Thickness (inches)	Specimen Orientation	Tensile Strength (ksi)		Yield Strength (ksi)		Elongation in 2 inches or 4D (%)	
		Min	Max	Min	Max	Min	Max
6.0	Longitudinal	-	73.8	-	65.1	-	12.3
	Long Trans.	73.8	75.3	62.9	64.7	8.2	8.4
	Short Trans.	-	69.3	-	59.6	-	3.0
Conductivity (IACS)	Min 40.7 %	Max 41.5 %					
Fracture Toughness KSI $\sqrt{in}$	L-T 24.3	T-L 26.9		S-L 23.3			

Table 4 Hardness and conductivity measurements taken at DSTO on the KW, KS and the FT488/1 and FT488/2 plates

	Conductivity (IACS)	Hardness Vickers 10KgF
KW-plate	40.0	172
KS- plate	40.1	183
FT488/1-plate	40.0	176
Y488/2-plate	42.0	167

The microstructure of the KW, FT488/1 and FT488/2 materials were consistent with previous 7050-T7451 material used in coupon testing at DSTO, Barter, et al, 1990, Barter, 2003. The structure consisted of large and small grains. The large grains (about 50-100μm in length) were usually associated with large inclusions of $Al_7Cu_2(Fe,Cr)$, Mg_2Si and Al_2CuMg. Near the centre of the plate the $Al_7Cu_2(Fe,Cr)$ still retained some of the shape that it had gained during solidification from the casting process (consistent with solidification at dendrite arm intersections). This is typical of low levels of breakdown from the original ingot. This lead to large grains having a similar shape and tending to surround the finer, equiaxed grains (10-20μm) that made up the bulk of the microstructure. The large grain structure tended to be less obvious, and more broken up nearer the surface of the plate as did the larger precipitates.

This structure was the result of recrystallisation probably during hot rolling. The larger grains reached their increased size due to more rapid grain growth about the larger precipitates since precipitates act as initiation points for recrystallisation. Because the grain structure had not been heavily broken down during rolling, the large and small sub-grains formed have retained some of the properties of their original grains, particularly their crystallographic orientations. Metallographic etching (very mild compared to the pre-IVD etch) of the specimens revealed the size and shape of these original grains. Through most of the plate, the size of these roughly lenticular shaped pre-recrystallisation grains were about 1mm in the rolling direction (Longitudinal, L), 0.5mm Transverse (T) direction and 0.25mm in the through thickness direction (Short, S) at the centre of the plate. Each packet of large and fine grains that recrystallised from the original grain structure would, because of the limited breakdown within the plate during rolling, be expected to have similarly orientated slip systems. This would in turn influence the nature of the fatigue crack growth, in particular the path of crack growth, and in turn the crack surfaces. It could be expected that limited crack deflection would result while the crack was advancing through only a few pre-recrystallisation grains, even though these contained many recrystallised grains, since deflection generally occurs at grain boundaries with misaligned slip systems. (Apart from grain boundary deflection other causes of deflection in the fracture surface can occur. These can include; interactions between and the joining of adjacent cracks, deflection at inclusions, initiation ahead of the crack front at inclusions or voids and subsequent crack interaction, and crack branching due to poorly aligned slip systems or other barriers to crack growth.) The expected low level of crack growth deflection suggests that crack growth rates may be higher in this thick plate material particularly away from the surfaces when compared to more heavily broken down material, such as forgings, thin plate or extrusions, particularly for cracks growing through ideally orientated grains at or near their origin. This will be examined in a following report.

2.3 Surface preparation

This project was developed out of a desire to improve the understanding of fatigue cracking encountered in service and test components from the F/A-18 aircraft. In particular it was found that the IVD aluminium coated 7050-T7451 components of the F/A-18 aircraft cracked preferentially from beneath the intact coating rather than in areas where the coating had been removed and the surface abraded. This was true in several large fatigue test articles, which included the two Y488 standalone bulkhead tests (FT488/1 and FT488/2), several components of the IFOSTP aft empennage full-scale fatigue test (FT46) and centre barrel full-scale fatigue test (FT55). To simulate this surface the KW specimens were etched, as were the KS specimens previously tested, in a 50% nitric acid/1% hydrofluoric acid solution (as per McDonnell Douglas Process Specification P.S. 13143, 1983) for five minutes, while the FT488/1 and FT488/2 specimens were cut from the bulkheads in such a way as to preserve both the IVD finish, and the pre-IVD etched surface beneath for testing.

2.4 Marker loads

To assist with quantitative fractography on the fractures produced during the testing marker-loads were added to the spectrum. These marker loads were the same as used previously in Barter 2003 and Barter 2003a. They consisted of five relatively large compressive loads inserted into the spectrum between the four tensile loads just before one of the spectrum peak loads. A more complete description of the loads and their effect on the fracture surface can be found in both the preceding papers, Barter, 2003, Barter, 2003a.

2.5 Test Matrix

A series of fatigue tests designed to represent typical RAAF service loading was carried out using a computer controlled 100kN servo hydraulic fatigue test machine. Cycling was set at 10Hz. Table 5 shows the test matrix for the three sets of specimens tested here.

Table 5 The test matrix for the KW, FT488/1 and the FT488/2 specimens.

Material source	Stress level (no Kt)	Number of specimens
FT488/1	300MPa	3
	330MPa	3
	360MPa	3
	390MPa	3
	420MPa	2
FT488/2	300MPa	3
	330MPa	4
	360MPa	3
	390MPa	3
	420MPa	3
KW	390MPa	5

Several stress levels were tested for each of the Y488 bulkhead specimen sets while a single stress level was used for the KW plate. A single stress level for the stock plate was used since this was simply a comparison test to compare test results between the KW plate specimens, with their altered configuration, and orientation, to the KS specimens and to see if this orientation and configuration change resulted in a significant life change, that may explain any life change noted between the bulkhead specimens and the KS specimens.

2.6 Testing results

After completion of the testing the results were collated. The results are presented in Table 6 to Table 8. In these tables the estimated number of Simulated Flight Hours (SFH) is included, which is the number of spectra times 324.92 - the number of RAAF F/A18 flight hours that the spectrum was considered to be equivalent to. No account of the effect that the addition of the marker loads on the life has been included. The results are shown graphically on an S-N plot in Figure 3, compared to the etched KS specimen results (Barter, 2003). Each of these results Tables also includes the log mean (μ_{log}) and log standard deviation (σ_{log}) of the results (using base 10), although the low number of specimens tested at each stress level, in the case of the Y488 bulkhead specimens does not allow a definitive estimate of the scatter to be established for these specimens - the numbers supplied should be only taken as indicative. Figure 4 shows the log means of these results also plotted on an S-N presentation.

Table 6. Results for the FT 488/1 Specimens

Stress peak MPa.	Specimen ID.	No. of Spectra to failure	Turning points to failure	SFH to failure[2]	μ_{log} spectra	σ_{log} (low significance due to low number of specimens tested)
300	FT488/1-1	37.52	505704	12191	37.20	0.0510
	FT488/1-2	32.94	444067	10703		
	FT488/1-3	41.65	562459	13533		
330	FT488/1-4	25.26	340469	8208	23.68	0.0430
	FT488/1-5	24.88	335448	8084		
	FT488/1-6	21.13	284784	6866		
360	FT488/1-7	20.51	276527	6664	21.07	0.0562
	FT488/1-8	24.26	326987	7883		
	FT488/1-11	18.81	253532	6112		
390	FT488/1-12	14.39	193969	4676	13.72	0.0445
	FT488/1-13	14.72	198528	4783		
	FT488/1-14	12.2	164391	3964		
420	FT488/1-9	11.7	158993	3801	10.95	0.0406
	FT488/1-10	10.25	138257	3330		

*LSD = Log Standard Deviation

Table 7. Results for the FT 488/2 Specimens

Stress peak MPa.	Specimen ID.	Spectra to failure	Turning points to failure	SFH to failure[2]	μ_{log} spectra	σ_{log} (low significance due to low number of specimens tested)
300	FT488/2-1	37.73	508591	12259	39.14	0.0704
	FT488/2-2	34.00	458292	11047		
	FT488/2-8	46.73	629920	15184		
330	FT488/2-3	20.56	277166	6680.8	26.84	0.0874
	FT488/2-19	33.52	451785	10891		
	FT488/2-6	27.41	369441	8906		
	FT488/2-15	27.49	370566	8932		
360	FT488/2-5	18.79	253324	6105	21.00	0.1113
	FT488/2-11	17.51	236087	5689		
	FT488/2-10	28.15	379443	9147		
390	FT488/2-16	13.39	180488	4351	14.00	0.0388
	FT488/2-9	15.51	209127	5040		
	FT488/2-7	13.2	177872	4289		
420	FT488/2-13	9.2	123948	2989	9.54	0.1193
	FT488/2-12	12.77	172162	4149		
	FT488/2-17	7.4	99602	2404		

[2] This ignores any effect of the marker loads on the SHF.

Table 8. Results for the KW Specimens

Stress peak MPa.	Specimen ID.	Spectra to failure	Turning points to failure	SFH to failure[2]	μ_{log} spectra	σ_{log}
390	KW100	16.20	218299	5705.6	16.45	0.049
	KW101	17.56	236706	6235.2		
	KW102	19.19	258739	5039.5		
	KW103	14.51	195595	4714.6		
	KW104	15.20	204819	4938.8		

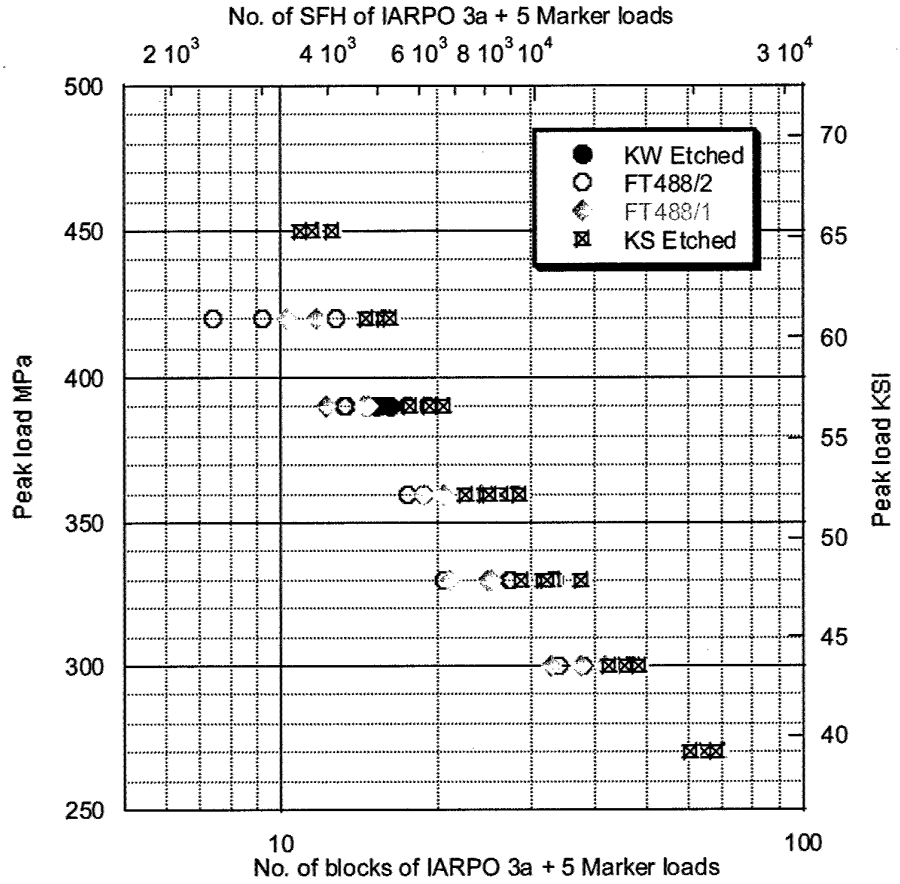

Figure 3 The lives of all the specimens are shown here compared to the KS etched specimens (Barter, 2003) tested previously.

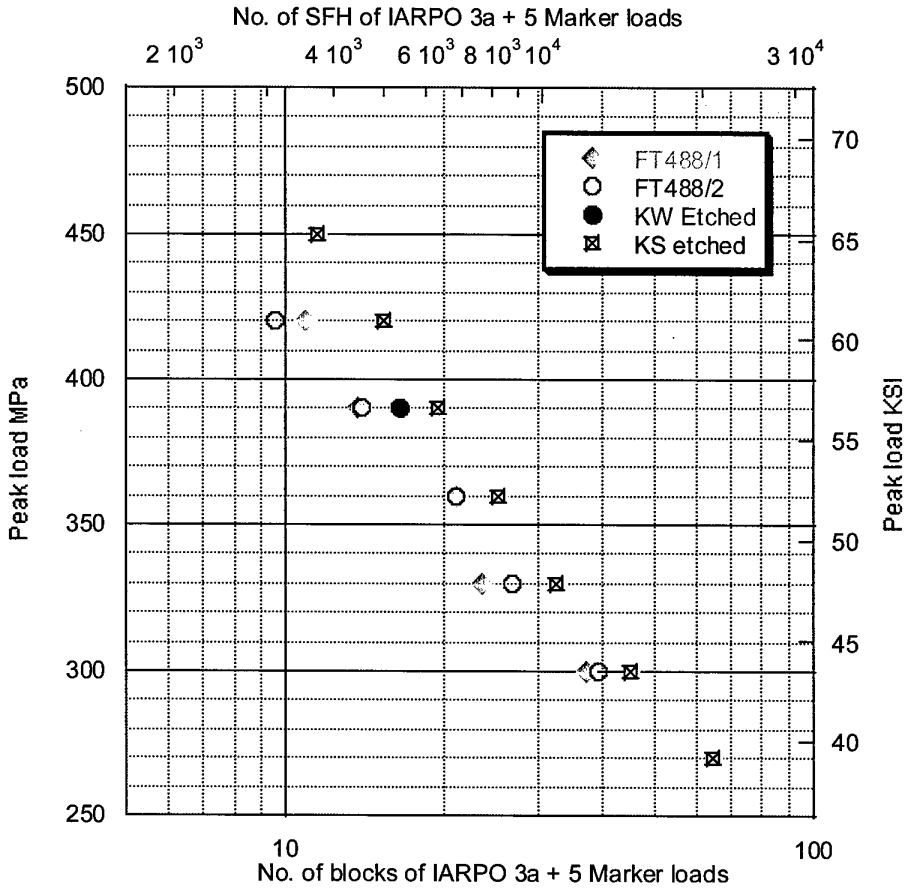

Figure 4 The log mean lives of all the specimens compared to the KS etched specimens tested previously.

2.7 Fracture surface morphology and the secondary cracks

An examination of the fracture surfaces produced during these tests found that many cracks usually intersected the fracture plane. The specimens also had a large number of smaller cracks above and below each fracture plane. There were slight differences; the FT488/1 coupons had a larger number of cracks intersecting the fracture plane, with an apparently reasonably random occurrences compared to the FT488/2 coupons, while the KW specimens had about as many random occurrences as the FT488/1 specimens although the secondary cracks tended to be larger than in the FT488/1 specimens. Figure 5 shows a fracture plane from one of the KW specimens, Figure 6 from one of the FT488/1 specimens and Figure 7 from one of the FT488/2 specimens. The number of fatigue cracks intersecting the fracture surface usually increased with the more highly stressed specimens.

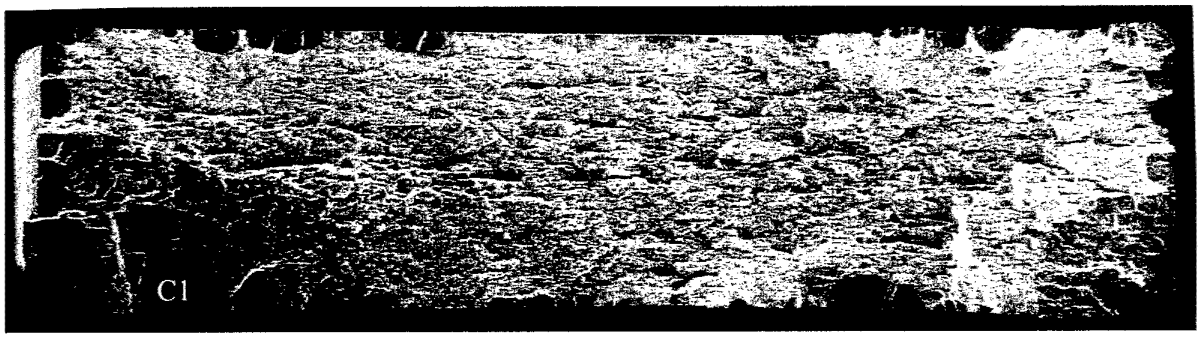

Figure 5. The fracture surface from specimen KW104 which was loaded to a peak stress of 390MPa. Note the large number of fatigue cracks (dark grey areas) that have initiated and grown around the entire circumference of the fracture surface. The largest crack is marked with a C1. The specimen is about 6.4mm thick.

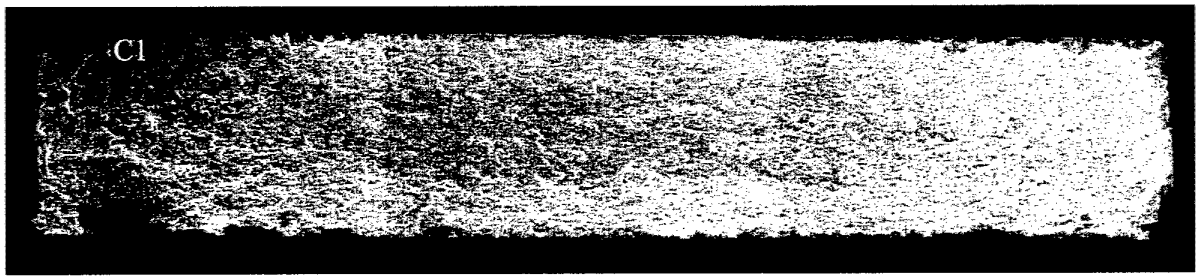

Figure 6. The fracture surface from specimen FT488/1 010 which was loaded to a peak stress of 420MPa. Note the large number of small fatigue cracks (dark grey areas) that have grown either side of the specimen. The largest crack is marked with a C1. The specimen is about 4.5mm thick.

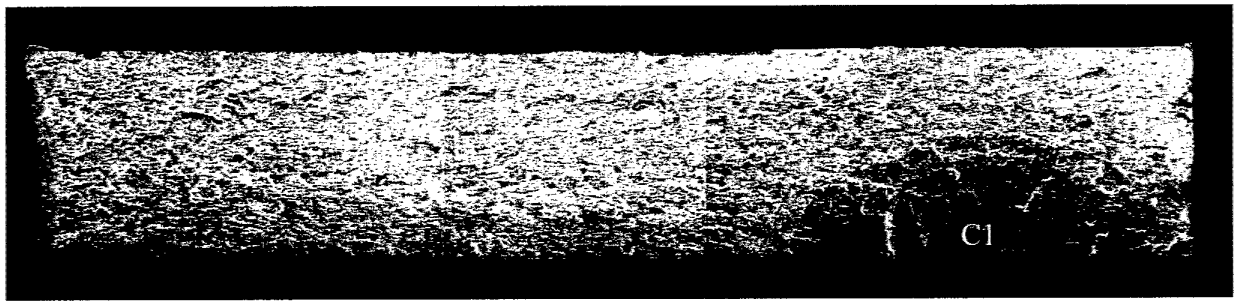

Figure 7. The fracture surface from specimen FT488/2 008 which was loaded to a peak stress of 300MPa. Note the small number of fatigue cracks (dark grey areas) that have grown from either side of the specimen. The largest crack is marked with a C1. The specimen is about 4.5mm thick.

Close examination of the surfaces of the main cracks and many of the secondary cracks revealed that the growth pattern (for example Figure 8) was evident on not only the main crack but also the secondary cracks; except the spacing of the repeating patterns were compressed compared to that of the main cracks. To examine this, several of these cracks had their crack growth measured along with the main cracks (usually the larger secondary cracks). These results and an outline of the measuring method are presented in the next section.

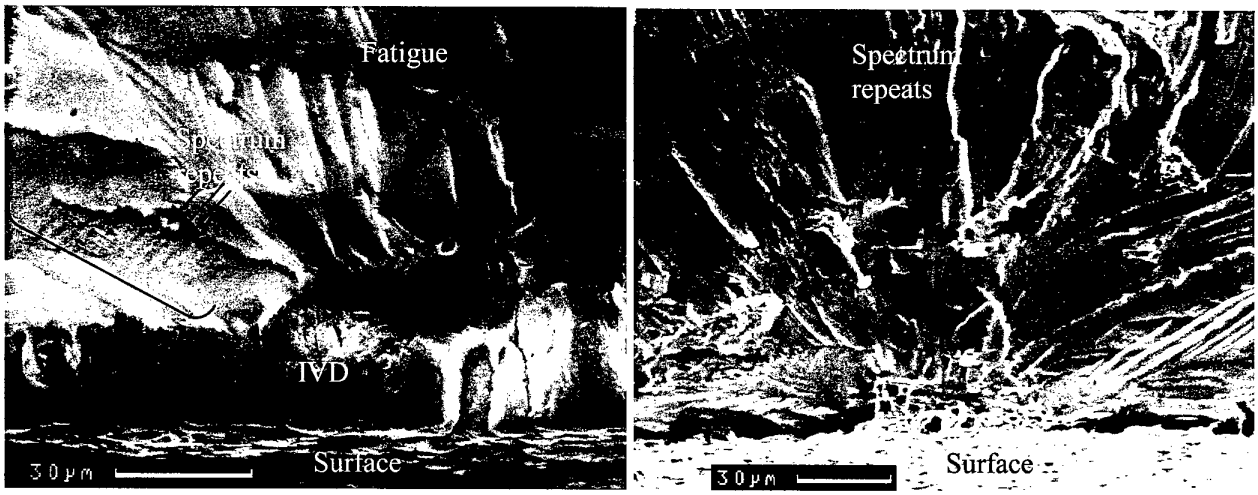

A B

Figure 8. The surface of two secondary cracks showing the repeating pattern caused by the marker loads in the applied loading spectrum. The position of these loads were measured in the quantitative fractography section that follows. A is from FT488/1 02 and B is from KW101. FT488/1 02 had 32 blocks of the spectrum applied while KW101 had 17 blocks applied.

Examining the discontinuities from which the fatigue cracks originated revealed that most of the cracks examined, had initiated from the etch-pits, usually at several locations around each pit. Two of the large cracks from one of the FT488/1 specimens, however, had initiated from porosity. This result supports the view that while the discontinuities caused by the etching are the dominant cause of fatigue crack initiation in these specimens, other populations of different types of discontinuity do exist. While etch pitting is clearly the dominant form of crack initiation in these specimens, their population distribution may be restricted by the physical nature of the etching process, preventing extreme pit sizes, and in effect capping the upper end of the etch pit population distribution, while the population distribution of other flaws may be more continuous. Apart from the etch pitting and the porosity noted here, machining marks, cracked or debonded inclusions (probably a limited upper tail on any population distribution) and corrosion may exist in service components, than would 'fill in' the upper tail of the discontinuity distribution. Further work to adequately resolve the population of discontinuities in components manufactured from this material is to be pursued. The assumption used to present the discontinuity distribution in this report is that the etch pit distribution is continuous and un bounded in the upper tail and therefore gives some information about the probability of extreme values of discontinuities for both the porosity and the etch pits.

In the KW specimens, etch pits were generally either associated with grain boundaries and/or at etched out, or partially etched out inclusions. Examples of the cracking initiating from etch pits are shown in Figure 8 and Figure 9. In the Y488 bulkhead specimens, initiation was still plentiful from grain boundaries and/or at etched out, or partially etched out inclusions although the pitting appeared to be generally less deep, particularly in the FT488/2 specimens. These shallower pits appeared to be associated with machining marks that had been formed in the bulkhead surface during manufacture and then etched as part of the pre-IVD etching

process. As a result shallow pits could be found to run in long groups at the base of these shallow machining marks. This lead to long groups of initiations that closely followed the machining marks. These features can be seen in two FT488/2 specimen fractures as shown in Figure 10.

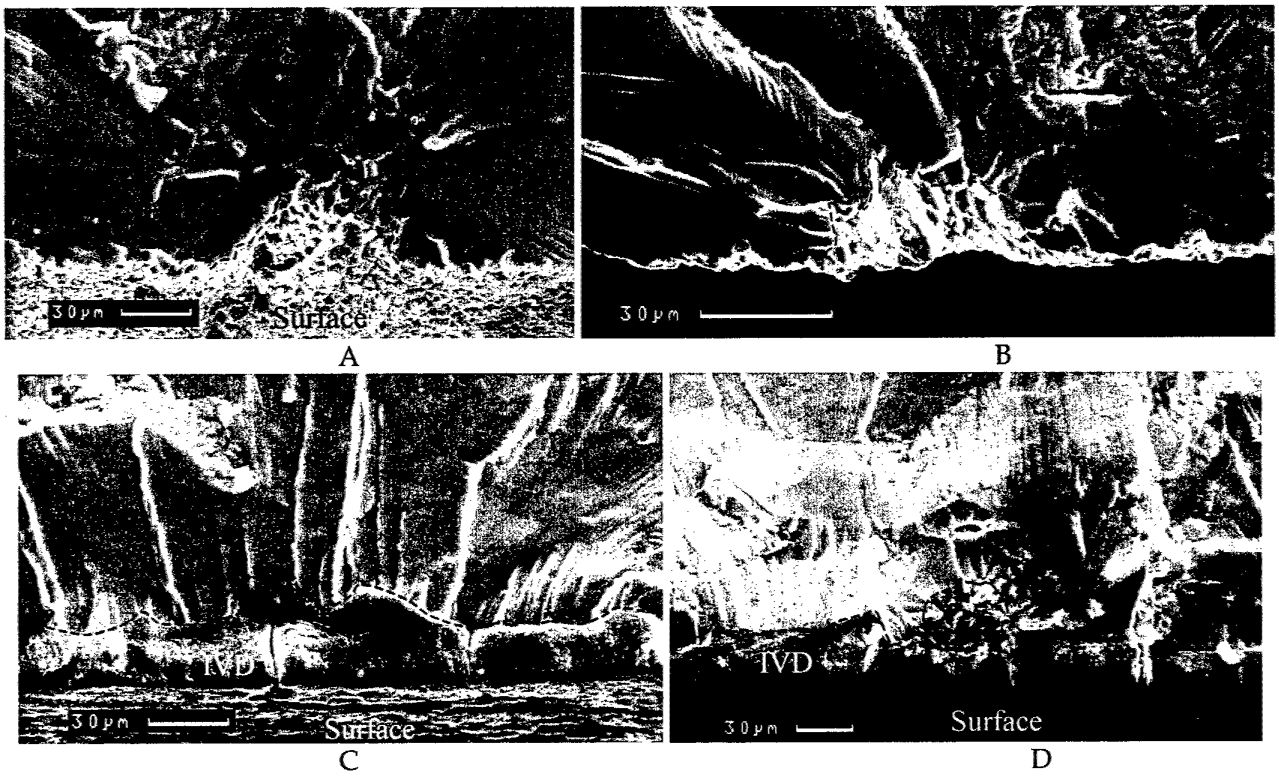

Figure 9 Four examples of initiating flaws created by the etching found in both the KW, (A & B) and 488 bulkhead specimens, (C & D). A dashed line gives the approximate interface between the flaws and the beginning of the fatigue crack growth. The spectrum block repeats can be seen on the fatigue surface in some of these images.

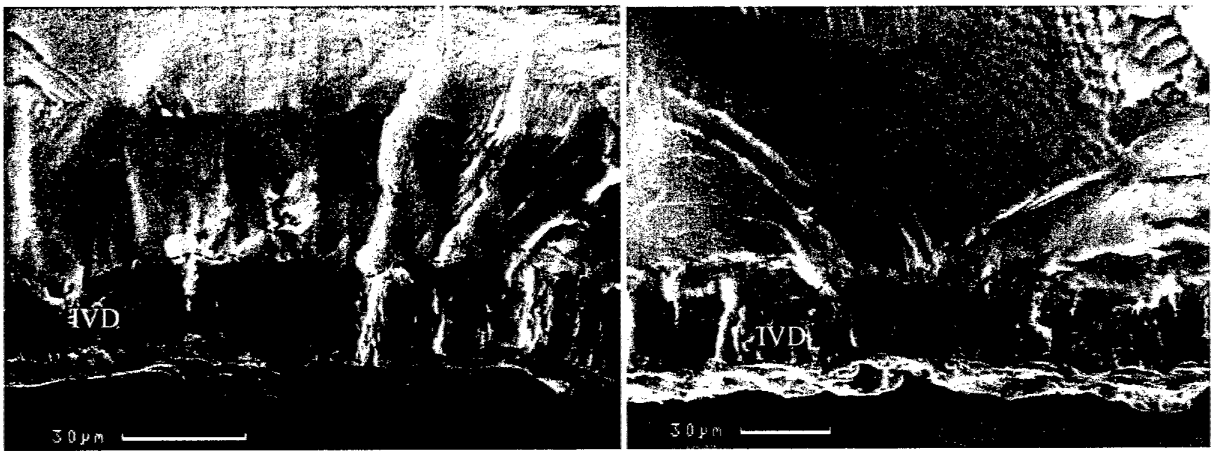

Figure 10 The originating areas of two cracks from the FT488/2 specimens showing the many closely spaced origins and difficult to identify flaw depth, compared to the KW specimens etch pitting. These origins appear to be associated with lines of pits at the base of shallow machining marks.

Two of the larger fatigue cracks from one specimen taken from the FT488/1 bulkhead (specimen 010 (420MPa peak stress)) had initiated from porosity as noted above. These pores were either slightly subsurface or touching the surface at the IVD/7050 interface. The life of this specimen did not appear to be significantly different to the other specimens tested at this stress level, although the porosity, particularly in one case was significantly larger than any etch pit found initiating a fatigue crack or otherwise. These two initiation sites are shown in Figure 11. It should be noted that a large number of crack initiation sites were examined during this part of the investigation; about 400, so the occurrence of porosity as an initiator was about 1 in 200 crack initiations in these specimens. It is unknown if this ratio is applicable to components although most of the specimens tested here had surfaces consistent with service component surfaces. Further assessment of service components is being carried out (Dixon and Molent, 2003) and will be reported on in the future.

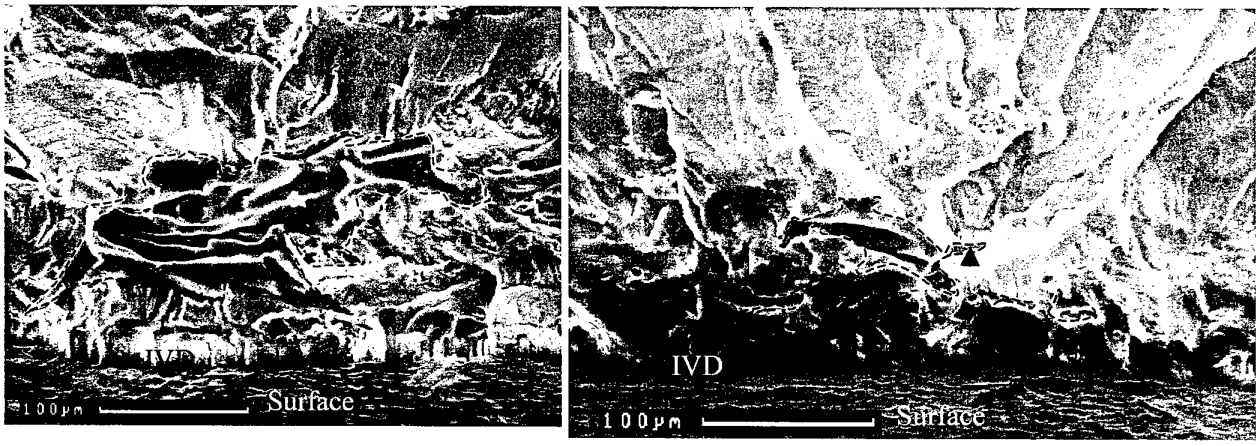

Figure 11 Two crack originating areas from the FT488/1 10 specimen showing the many closely spaced origins around the porosity (outlined with the dashed lines) in the material. In the second example the dominant fatigue crack has started from the region marked with the arrow head.

Examples of cracks that have been opened up, in the regions on the surface of the specimens that were plastically deformed when the specimens failed, are shown in Figure 12. The etching of the surfaces of these specimens is also evident in the KW specimen shown, while the surface produced by the IVD is shown in the FT488/1 specimen. The FT488/2 specimens were not so easily examined since this bulkhead was painted and the paint was very difficult to remove without damaging the IVD coating, making the surface cracking difficult to view. To view the nature of the cracking in the FT488/2 specimens, a spare, thin FT488/2 specimen was fatigue tested to near failure (estimated from the test results) and dye penetrant examined by applying the penetrant while the specimens was under 50% load, and relaxing the load. This revealed multiple cracks and their relationship to shallow machining marks. Measurement of the depth of these marks was difficult, although it was estimated that they did not exceed 0.01mm in depth. A similarly treated etched KW specimen, which does not show any preference for crack position, is included for comparison in Figure 13.

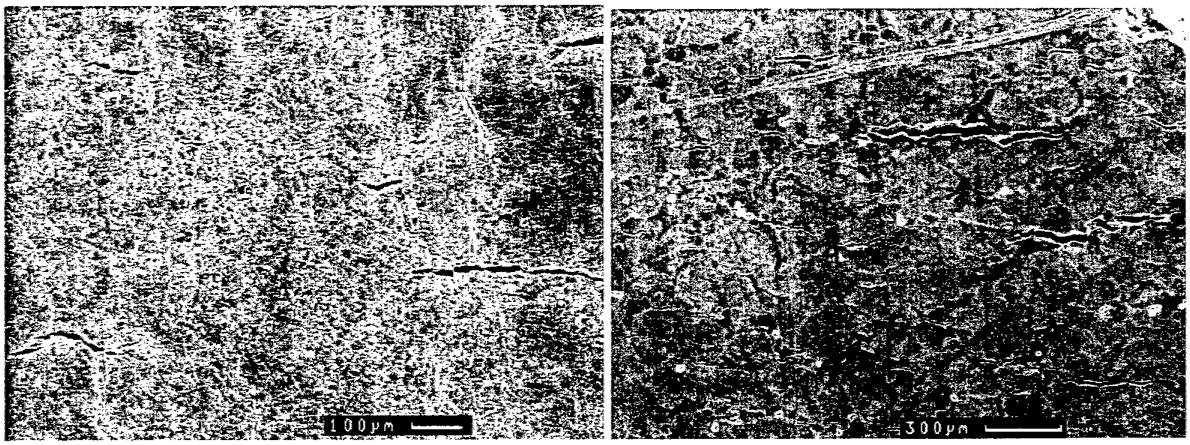

Figure 12. The surface of two specimens (one from the KW set (left) and the other from the FT488/1 set (right)) showing examples of the many secondary cracks found adjacent to the fractures.

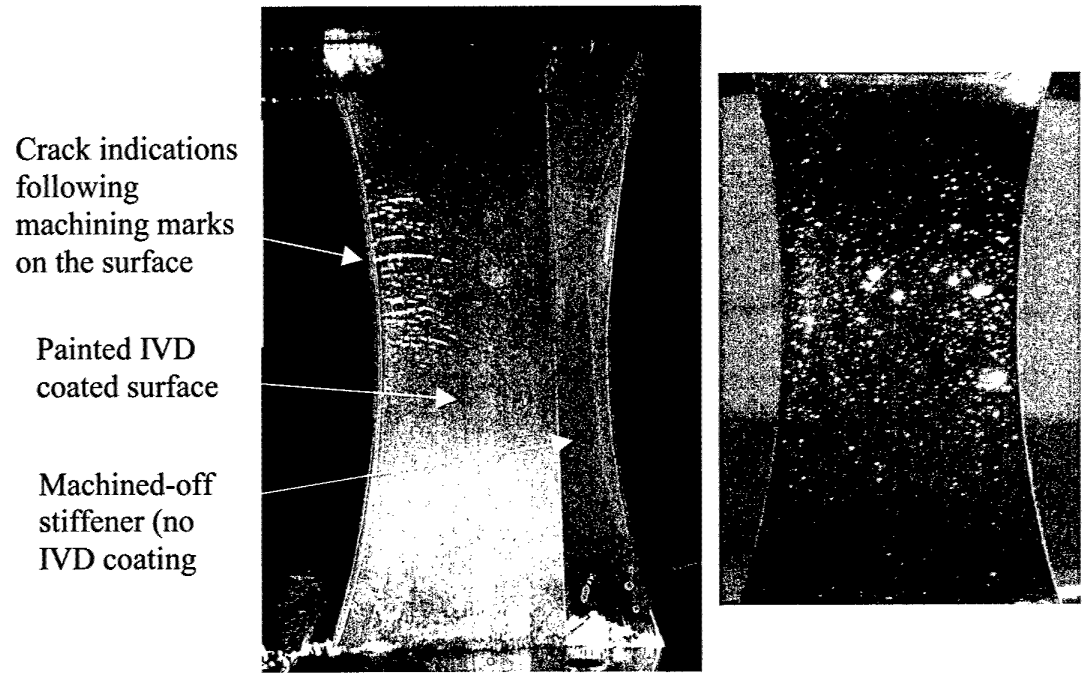

Figure 13 One of the spare thin FT488/2 specimens (left), and a KW specimen, after testing to near failure. Dye penetrant has been used to show the extent of fatigue cracking. The indications for the FT488/2 specimen suggest that the cracking is initiating at the base of shallow machining marks, while the indications for the KW specimen suggest a random distribution of initiations.

2.8 Quantitative fractography

Quantitative fractography was carried out on each of the tested coupons. The largest crack generally was analysed unless it was damaged in which case the second largest crack was analysed. In some specimens the largest and second largest cracks were both analysed. These analyses were made easier by the existence of a fairly distinct repeating pattern aided by the marker loads. Usually the repeating pattern from the repeat of the spectrum was fairly easily found, although its distinctness varied from

area to area on the fracture surface. By tracking the most distinct areas and some of the less distinct areas of the repeating patterns and combining the data from these regions, a relatively complete picture of the crack growth was assembled, assuming that each repeat of the pattern was equivalent to a single load spectrum. This was supported by previous examinations of fatigue fracture surfaces in 7050 aluminium alloy, which have undergone similar fatigue testing, Barter, 1990a, Barter et al, 1991, Barter, 1998, Barter and Price, 2000, Barter, 2003.

As used in the previous reports in this series (Barter, 2003 and Barter, 2003a) the method of calculating the crack depth during measurement of crack growth was to take an 'x' and 'y' reading measured from a zero position set at the interface between the initiating discontinuity and the start of the fatigue crack growth. The 'x' and 'y' positions are fitted to a circular model i.e. the depth of a particular mark is the calculated radius to the position of the mark from the initiation/fatigue interface. To prevent crack growth distortion due to non semi-circular cracking, measurement was confined to a small quadrant centred along the line between the initiation point on the discontinuity-to-fatigue interface and the deepest part of the crack. This is shown schematically in Figure 14. A more complete description of the measuring method and the artefacts that can occur in the crack growth curves due to measuring difficulties is included in the two preceding reports.

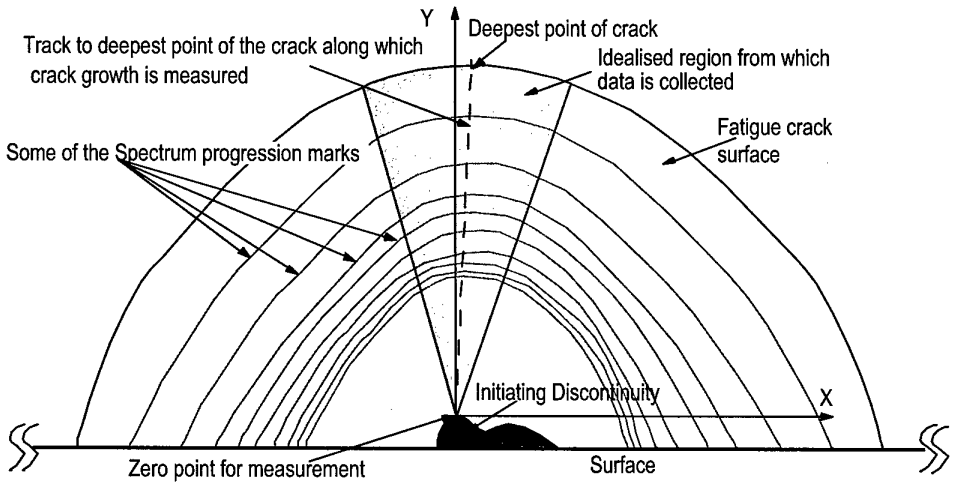

Figure 14 A schematic drawing of the method and track used to measure the fatigue crack growth by quantitative fractography.

Measuring from the discontinuity-to-crack interface was used in these specimens because of the etching. This etching made the surface difficult to define, making the measured discontinuity's depth uncertain. Nevertheless the discontinuity depths were estimated and these will be used for comparison in the estimate of the crack-like effectiveness of each initiating discontinuity.

Despite any limitations with the method of measurement good crack growth curves were produced for each of the specimens tested. Figure 15A&B to Figure 19A&B present the crack growth curves produced for the FT488/1 test specimens, Figure 20A&B to Figure 24A&B show the curves for the FT488/2 test specimens and Figure 25 shows the results for the KW test specimens. These crack growth curves do not include the size of the discontinuity at the crack origin. The crack growth curves are

considered to be a reasonable representation of the rate of cracking in each of these tests. Crack growth curves are also included for some secondary cracks, usually the second or third largest. In these cases the primary crack is marked C1 and the secondary crack/s C2, C3…., or C2, C2.1 for a secondary origin in the second crack. To improve the clarity of the rate of growth while the cracks are small the data has also been plotted on log crack depth versus life axes. The data points for these graphs are contained in Appendixes A, B and C.

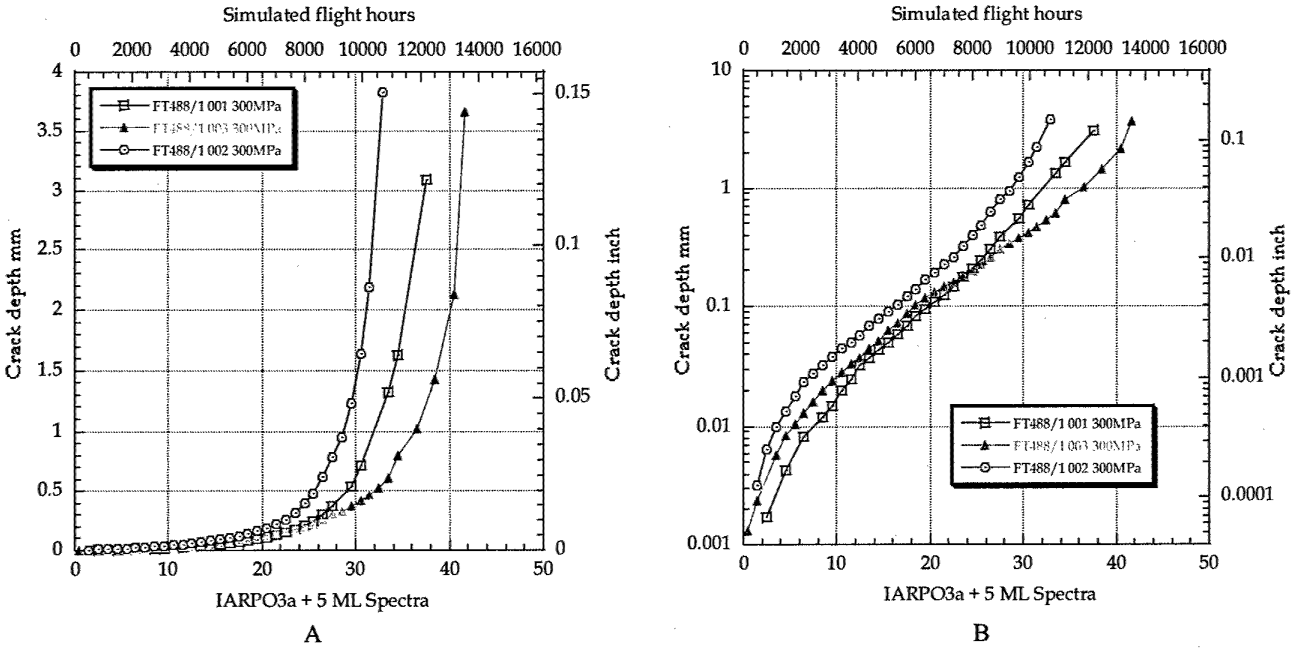

Figure 15 The result of the quantitative fractographic examination of cracks in the FT488/1 specimens loaded to a peak stress of 300MPa. Plot 'A' presents the results plotted on a linear/linear axes. Plot 'B' presents the same data plotted on log/linear axes.

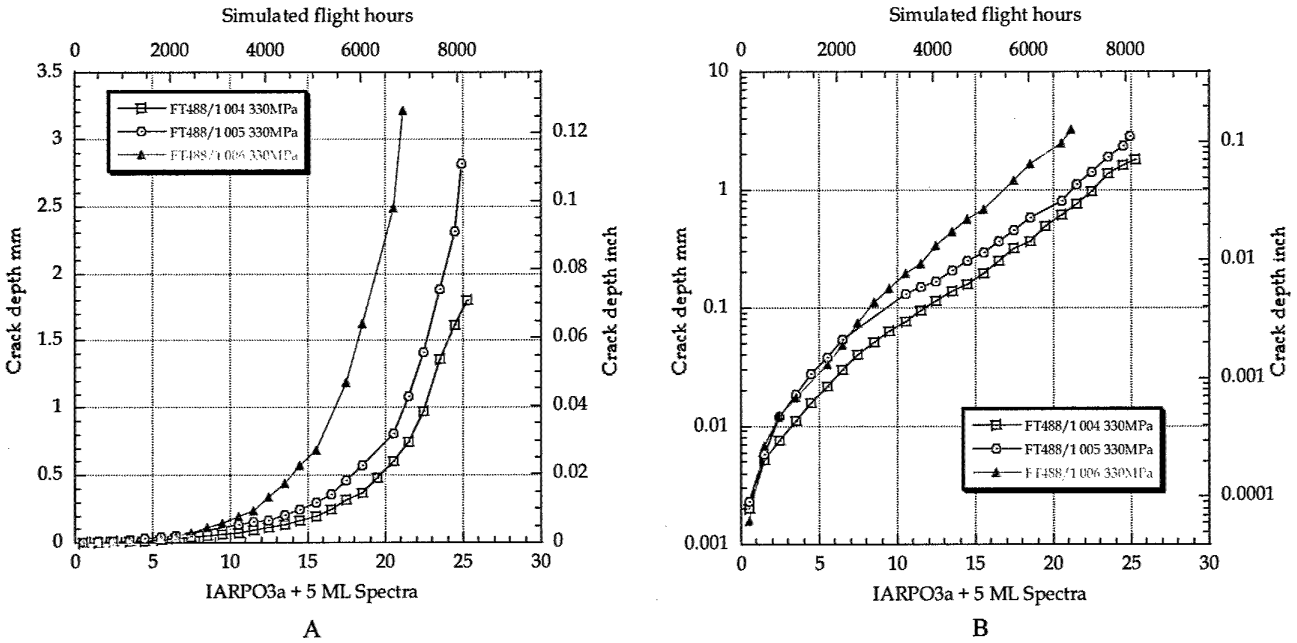

Figure 16 The result of the quantitative fractographic examination of cracks in the FT488/1 specimens loaded to a peak stress of 330MPa.

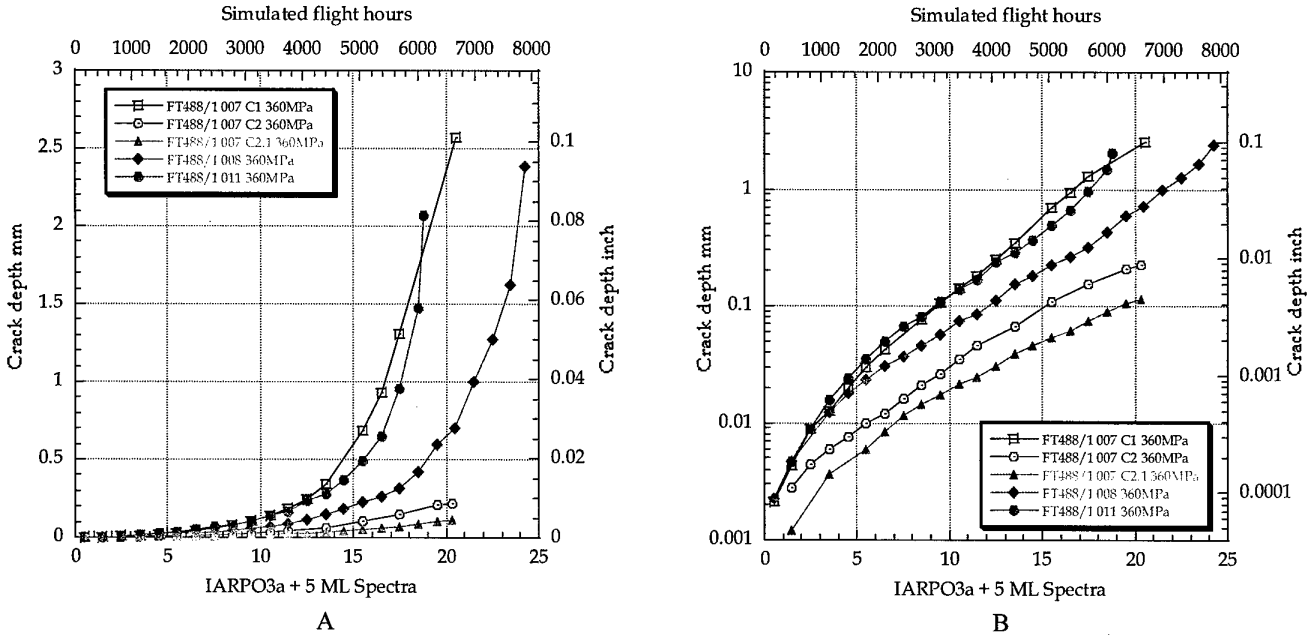

Figure 17 The result of the quantitative fractographic examination of cracks in the FT488/1 specimens loaded to a peak stress of 360MPa.

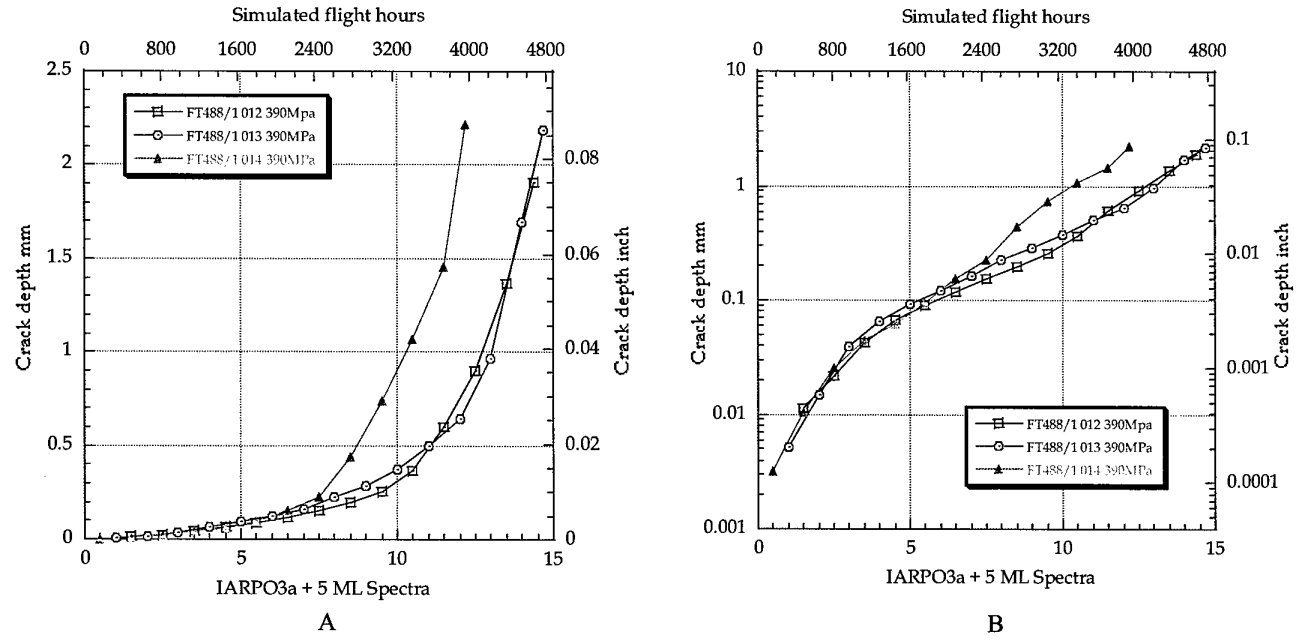

Figure 18 The result of the quantitative fractographic examination of cracks in the FT488/1 specimens loaded to a peak stress of 390MPa.

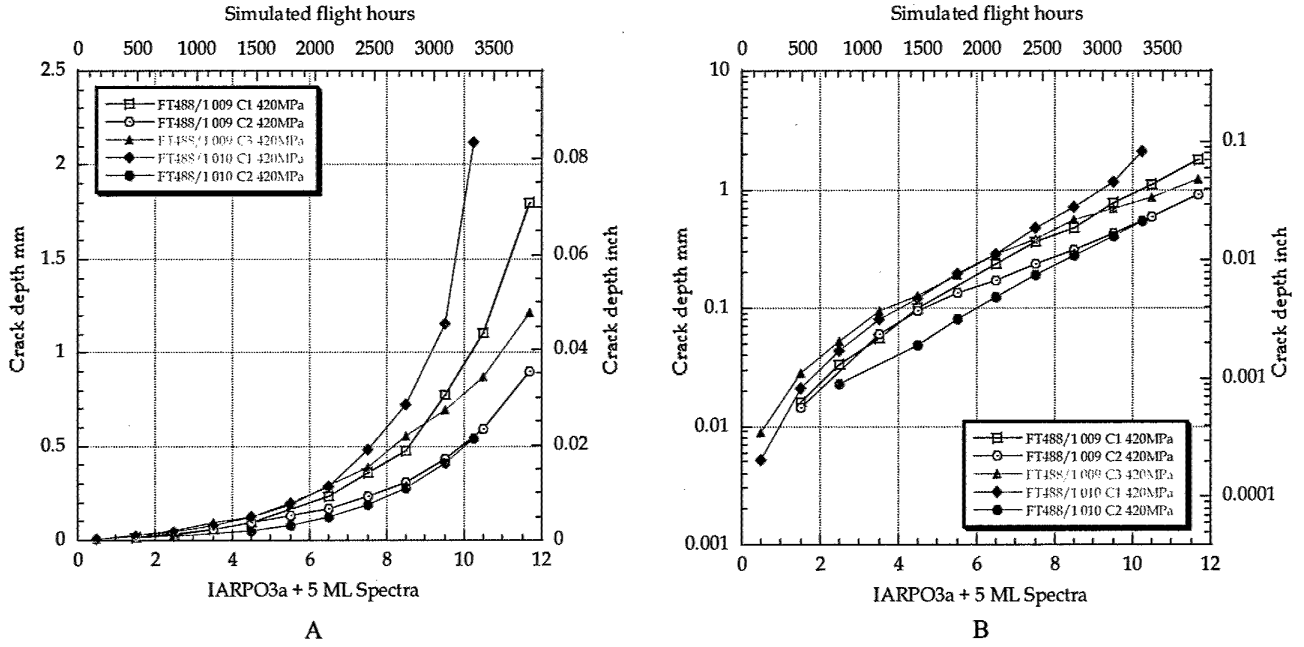

Figure 19 The result of the quantitative fractographic examination of cracks in the FT488/1 specimens loaded to a peak stress of 420MPa.

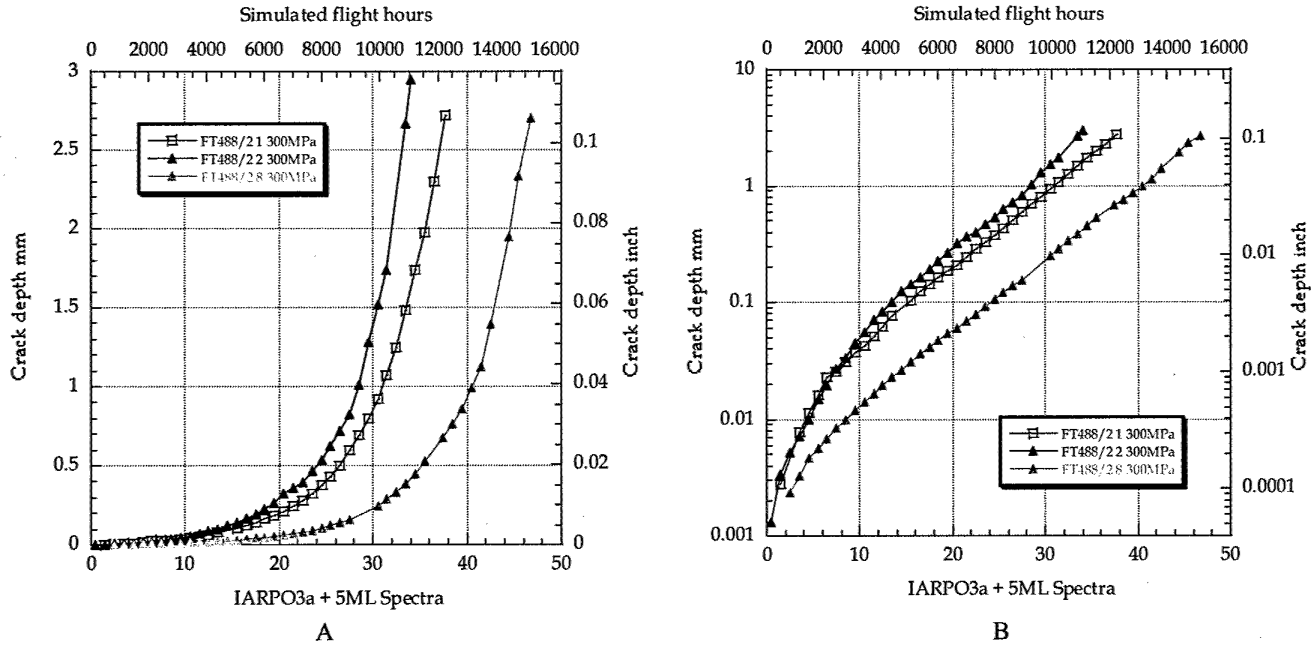

Figure 20 The result of the quantitative fractographic examination of cracks in the FT488/2 specimens loaded to a peak stress of 300MPa.

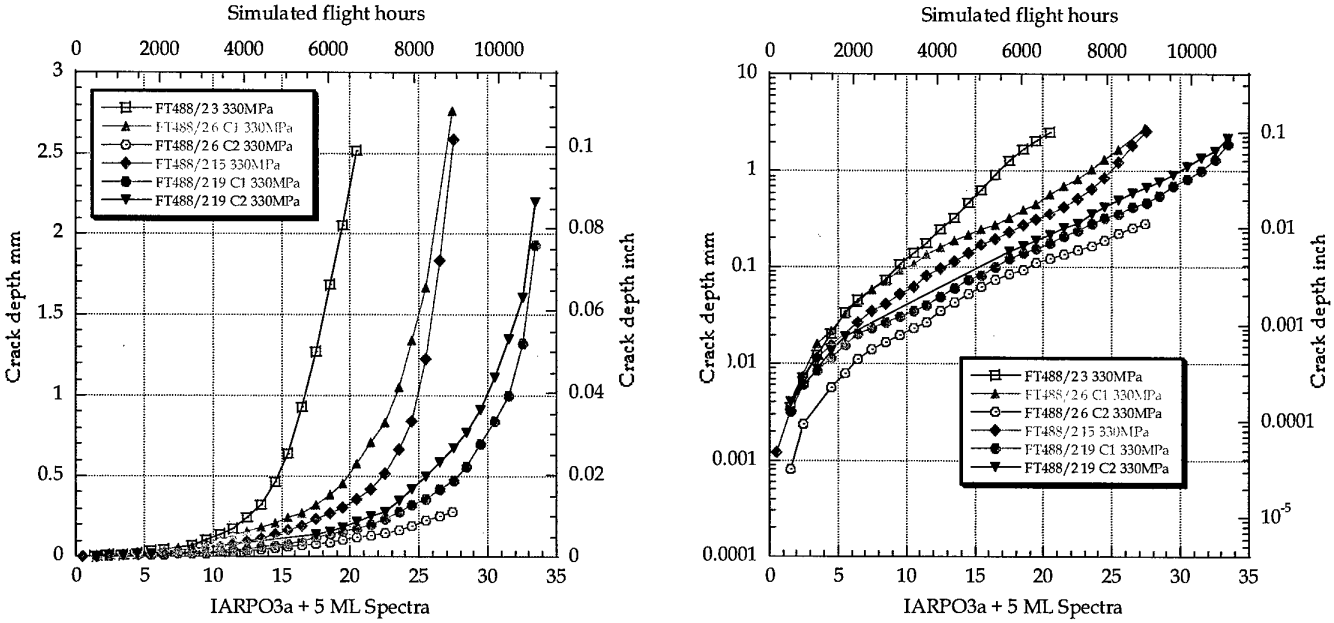

Figure 21 The result of the quantitative fractographic examination of cracks in the FT488/2 specimens loaded to a peak stress of 330MPa.

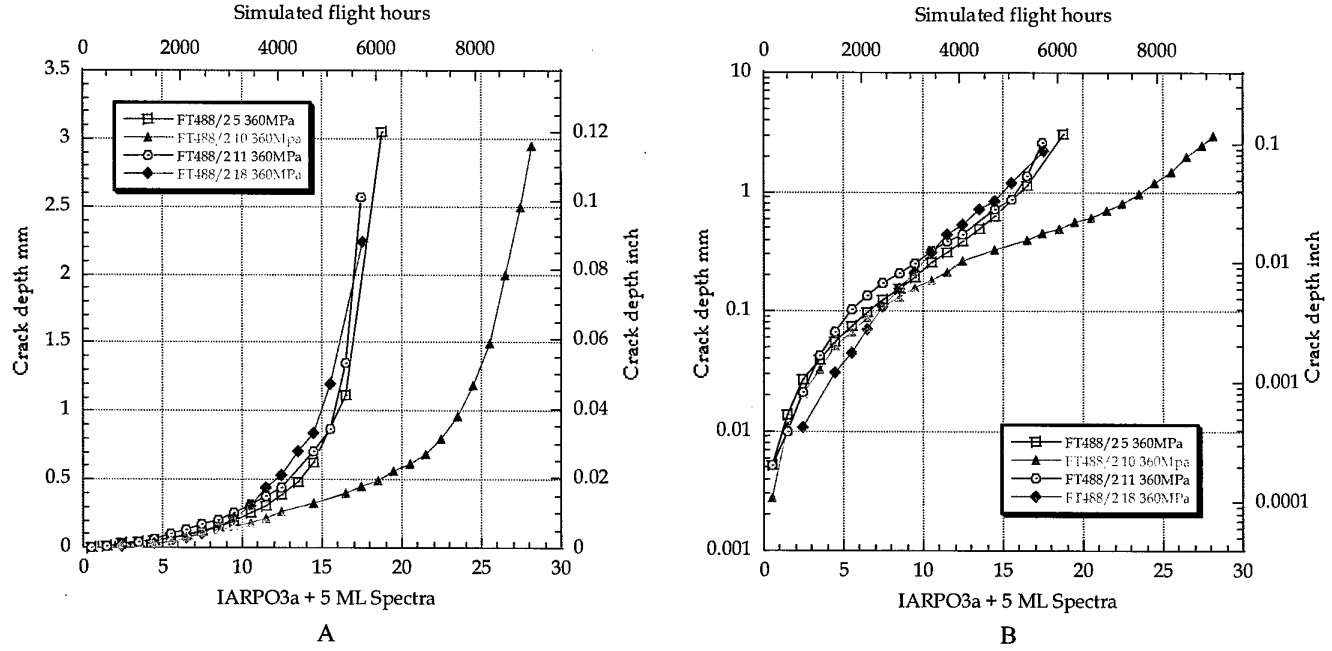

Figure 22 The result of the quantitative fractographic examination of cracks in the FT488/2 specimens loaded to a peak stress of 360MPa.

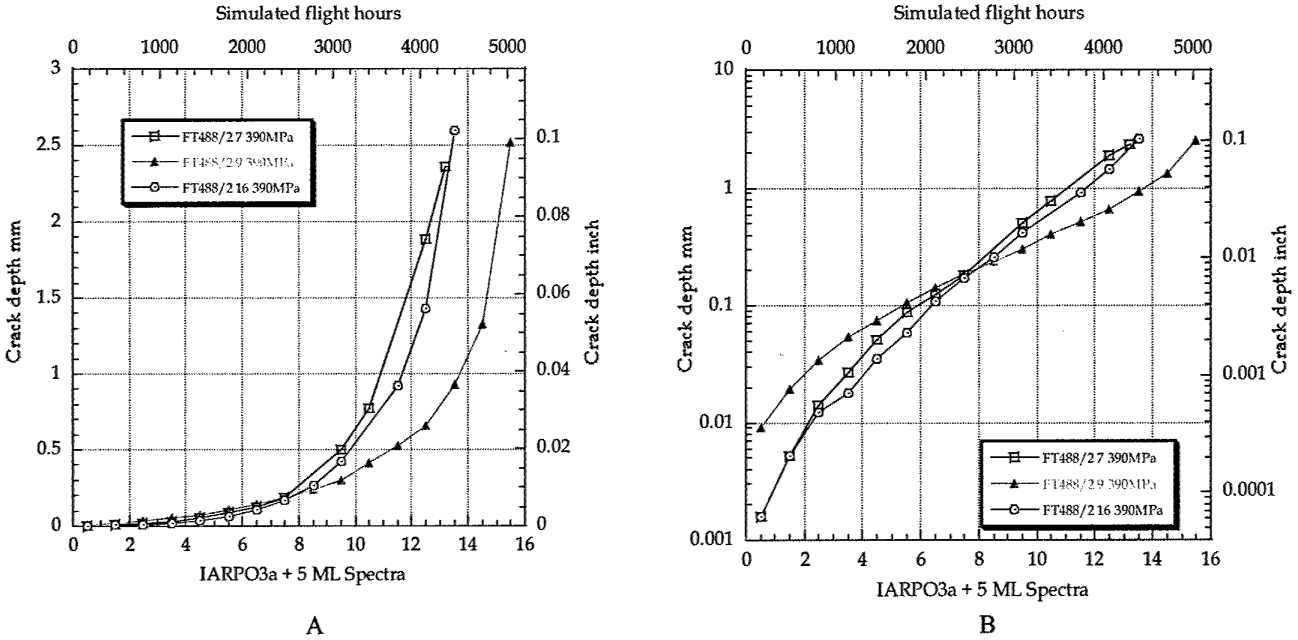

Figure 23 The result of the quantitative fractographic examination of cracks in the FT488/2 specimens loaded to a peak stress of 390MPa.

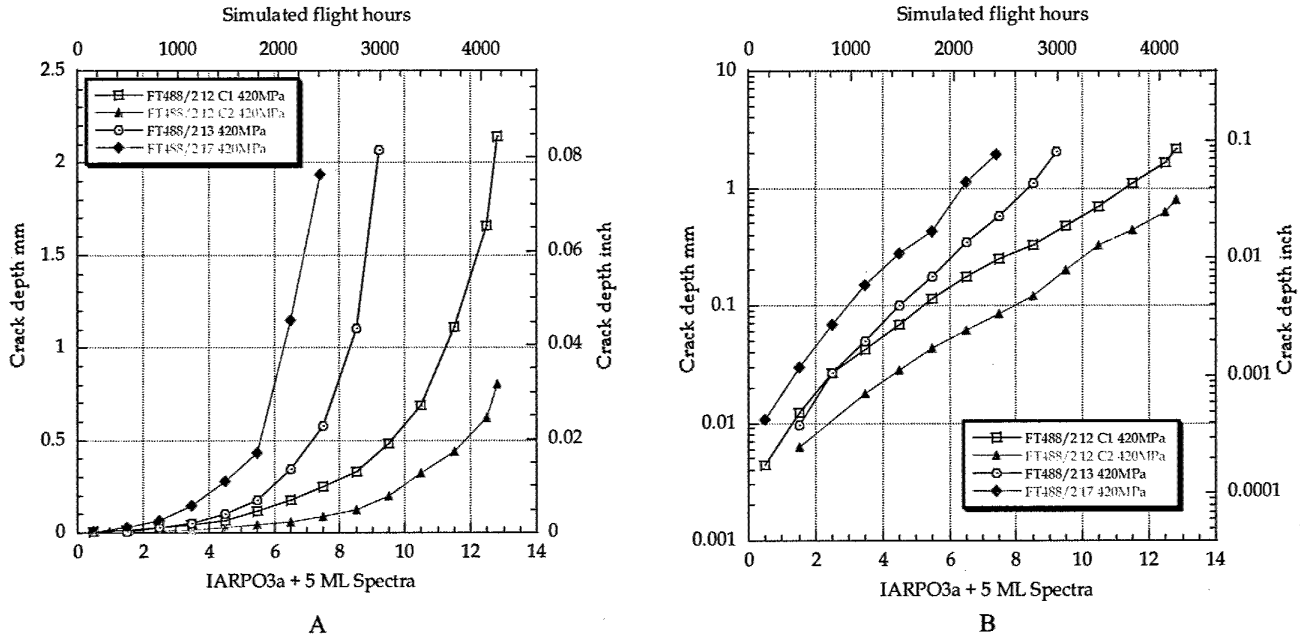

Figure 24 The result of the quantitative fractographic examination of cracks in the FT488/2 specimens loaded to a peak stress of 420MPa.

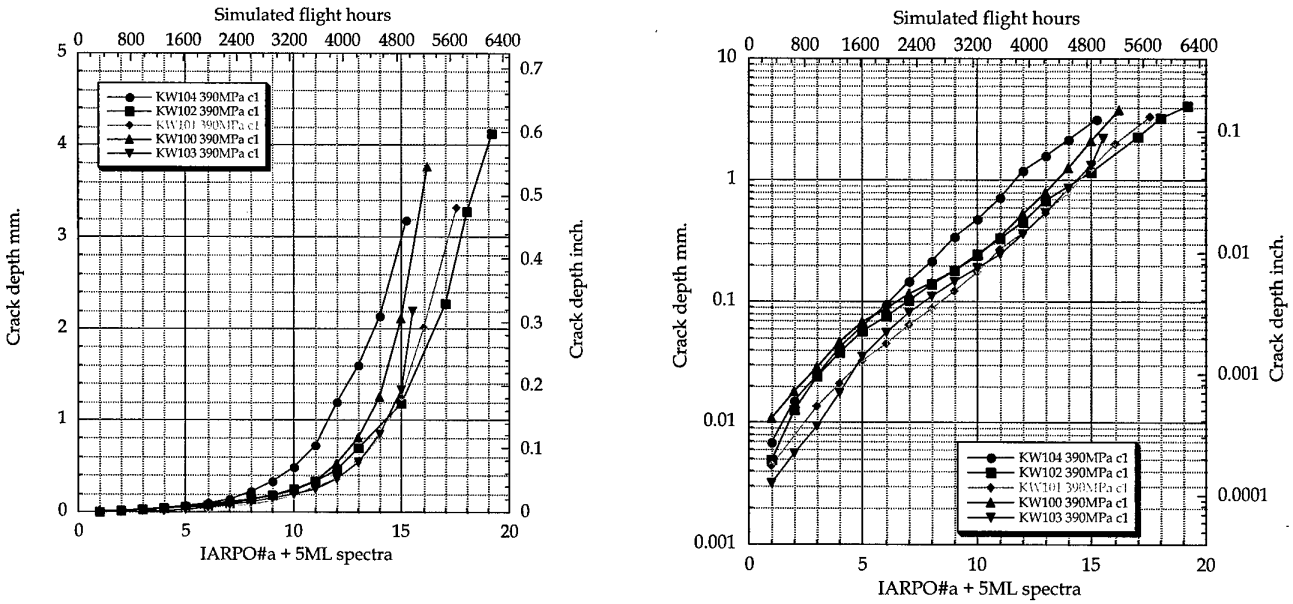

Figure 25 The result of the quantitative fractographic examination of cracks in the KW specimens loaded to a peak stress of 390MPa.

3. Analysis and Discussion

3.1 General observations

The total life of each of the specimens was compared to the life of the previously tested KS specimens. The apparent difference in the life to failure of the KS plate specimens compared to the specimens tested here may be due to one or a combination of; the specimen size and configuration, the position from which the specimens were cut in the plate, the more fatigue resistant orientation of the KS specimens and/or the higher hardness (and therefore strength) of the KS plate. To further investigate this an examination of the crack growth curves produced, and the discontinuities from which the cracks initiated (and how these should be accounted for) was carried out.

3.2 Estimating the effect of the initiating discontinuities

The examination of the fatigue crack origins found that in most cases the cracking initiated from etch pitting in these specimens, as it had in the previous tests reported in Barter, 2003. The other origin types observed were two cases of porosity and the association of some of the etch pitting with shallow machining marks. Most of the pits were associated with grain boundaries, even those in the shallow machining marks. Others were associated with partially or fully etched out inclusions. The crack-like effect of these types of flaws is unclear from their size alone: their shape is not typically that of a thumbnail type crack, and measuring the depth (a difficult proposition to carry out with accuracy due to the rough nature of the etched surface or due to the coating of IVD that existed on most of the specimens) does not give a

robust estimate of the crack-like nature of these flaws, Barter, 2003. To quantify the crack effectiveness of the etch pitting, the combined influence of the etch pitting at the base of machining marks and the porosity where it had initiated cracking, the quantitative fractography data were further assessed in the same manner as the previous two reports; Barter, 2003 and Barter, 2003a.

Using an exponential rate as a model of growth for each crack measured, of the form:

$$a = a_0 e^{\beta(N)} \qquad (1)$$

where 'a' is the crack depth, 'a_0' is the apparent crack depth at the commencement of loading, 'N' is the life and 'β' is the slope of the curve, or a measure of the rate of crack growth, and assuming this growth is true at the beginning of the crack growth curve, then an estimate of the crack-like effectiveness of the flaw at the start of growth can be extracted by fitting this curve to the data. Adding the calculated a_0 to the log depth versus life curves shown in Figure 15 to Figure 25 removes the apparent distortion from the start of the crack growth curves. The amount added is designated, here as the EPS for Estimated Pre-Crack size, (although other names have previously been suggested, such as EIFS (Equivalent Initial Flaw Size, Yang & Manning, 1980 & 1988, Yang, 1995,) and IDS (Initial Discontinuity Size) neither of which make it clear that it is the crack like nature of the flaw or discontinuity or combination of discontinuities that is important, not their mere presence. Also, the measured flaw depths (taking into consideration the difficulties of making this measurement as noted above) were collected for comparison.

The selected amount that best corrects the distortion is an estimate of the effective 'crack-like' size of the flaw prior to any loading and any anomalous growth associated with early crack growth. This also assumes that there is no delay (or very little) in the commencement of cracking after the beginning of the application of loading. In the specimens examined here this has been found to be valid for the data collected from all the cracks considered.

Since the specimens are of a simple configuration with low Kt details and no alternative load paths, the exponential rule would be expected to apply, and appears to give a good representation of the crack growth, as shown in Figure 15 to Figure 25 where most of the crack growth appears as a straight line on these log crack depth versus linear life plots.

The use of QF to assess regions of crack growth very close to the discontinuity/fatigue interface ensures that real crack growth data are being used, rather than crack growth rate estimates derived from models using long crack data. Using real crack growth rates eliminates a large part of the sensitivity of the life-based estimation method to the model and its data selection. This has been used effectively on a number of occasions to avoid the problems associated with the modelling approach when crack configuration is complex, or when the stress history is very complex or incomplete, eg. Athiniotis et al, 1999.

Although the EPS achieved by the method considered above appears to be simple, there are several possible variations that may affect the value. The easiest approach for the fractographer who is interactively examining a particular crack and the measurements taken from that crack, is to add amounts of EPS until a reasonably straight line is achieved on a log depth versus linear life plot of the measurements. This 'anticipation by eye' approach allows a 'first cut' at the data, which is used to

highlight obvious errors in the measurements so that re-assessment of the measurements can be carried out on the specimen in real-time. This helps prevent 'uninformed' data correction while re-measuring poorly defined areas on the fracture surface. For instance a sudden jump in the crack growth rate may be the result of a missed measurement of a repeat in the loading pattern due to surface damage or orientation, preventing this repeat from being seen, or it may be due to the presence of a tear band, a strong probability with some spectrums near the end of a crack's life. Plotting the data during the collection of the measurements and correcting for the anticipated EPS, finding the jump and re-examining the fracture surface to ascertain the most probable cause of that jump, can highlight this. The interactive examination of a crack's surface is a strong advantage of this method, while the dependence of the result on the skill and consistency of the fractographer is a disadvantage as far as reproducibility is concerned.

After the initial data have been collected and the initial best-fit EPS estimated, other mathematical methods were investigated to estimate EPS. One of these is listed below along with the two measures of the flaw effectiveness mentioned previously. Each method has been designated as an EPS Type:

Type I. 'Measured flaw depth'. This is usually the depth of the discontinuity at the point from which crack measurement was started (not the deepest part of the discontinuity), and has a level of uncertainty associated with the difficulty of defining the surface of the specimens on a micro-scale due to the etching, or the presence of the IVD coating.

Type II. The measure that was used during the collection of the QF data, which was estimated to be the EPS. This value is usually weighted towards the data near the beginning if the cracking since a reasonably smooth curve at the start of cracking is the desired outcome. Consequently the fractographer usually gives little weight to the growth of the crack once it has passed about 0.5mm in depth other than to consider if any of the repeats are missing, or have been counted twice. For the data collected here this means that about the first 2/3rds for the data are used to make this EPS estimate.

Type III. Fitting the data to the exponential model (equation 1) using a curve fitting program, and optimising the initial crack depth added to the raw crack size (offset value), checking the 'goodness of fit' (R^2 value), and refining the depth added until the maximum R^2 is reached. This method can be used to produce the curve that best fits the total data. The a_0 of this equation gives a zero life intercept value. It is this zero life intercept value which was thought to be the best measure of the two possible EPSs (the offset applied to the data to give the optimised equation (Type IIIA) or intercept used in the optimised equation (Type III)).

Examples of the curves produced for each of these methods have been previously shown in Barter, 2003, and Figure 26 to Figure 36 for this work.

3.3 The application of EPS to the data

Generally for the data gathered for pre-IVD etched specimens the Type III EPS produces reasonably consistent agreement with the Type II EPS used during the QF, as shown in Barter, 2003. The exception being where cracks have accelerated more

rapidly at the end of growth, which gives a 'kick upward' at the end of the crack. This kick was most notable in some of the cracks examined from the Y488 bulkhead specimens tested here, where crack interaction, from multiple closely spaced etch pitting at the base of shallow machining marks lead to very broad cracking early in the cracks depth and therefore led to more rapid final growth. This kick has the effect of lowering the estimated Type III EPS making the estimate less conservative. This occurs since the Type III EPS uses all the data collected for each crack, a requirement not needed since the growth close to the initiation is probably the most important for EPS estimation. In these cases, some judgment is required about which data points should not be included in the optimisation. The most robust method for including as much data as possible so as to produce the most consistent result is still being investigated.

Since an EPS is a hypothetical crack assumed to exist in a component prior to loading, it characterises the fatigue effect of the actual initiating detail, regardless of its type; pitting, scratches, machining marks, inclusions etc. One of the interesting aspects of this method is that the distributions of EPS values that can be built-up for a particular material and surface condition should be, given that the growth is exponential for the cracking being investigated, applicable to that material and surface condition regardless of changes to the loading spectrum. However, this assertion certainly requires further investigation.

Alternatively, to the methods used to calculate EPS, either Type II or III, the measured value of the flaw size can be used to indicate the relative severity of a flaw. Unfortunately, using the flaw measurement alone will not necessarily indicate the actual effect of the flaw on fatigue life. For example examine the crack growth curves with the measured flaw size added against the crack growth curves with the Type II EPS added in Figure 26A & B to Figure 36A & B. (The data used to produce these curves are included in Appendix A, B and C). Although the flaw depth was found in most cases to be very similar to the Type II EPS, and produced approximately linear curves on log crack depth versus linear plots, there were significant differences. The flaw depth (Type I EPS) and the Type II EPS for all the cracks examined are presented in Table 9 to Table 11. The Type III EPS values are not presented due to the issue of lower than expected values caused by the 'kick' in growth found in several of the Y488 crack growth curves.

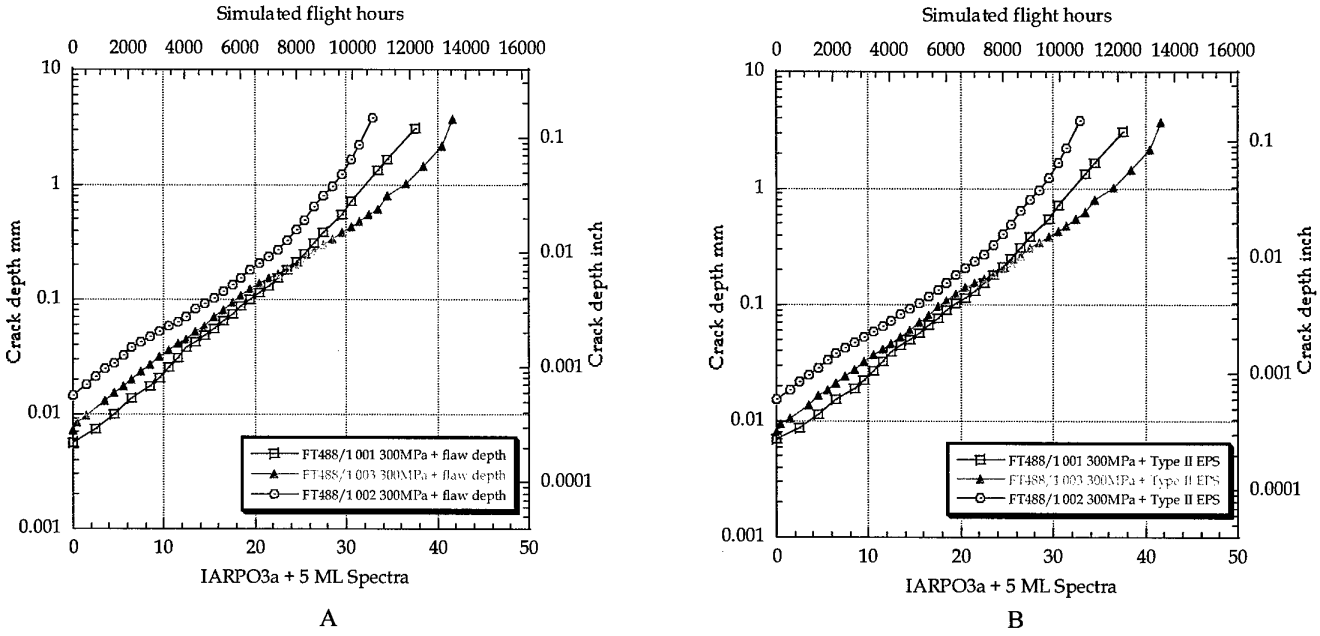

Figure 26 The crack growth plots for the 300MPa peak stress level for the FT488/1 specimens, with log depth versus spectra after correction using the measured flaw depth (A) and the Type II EPS (B).

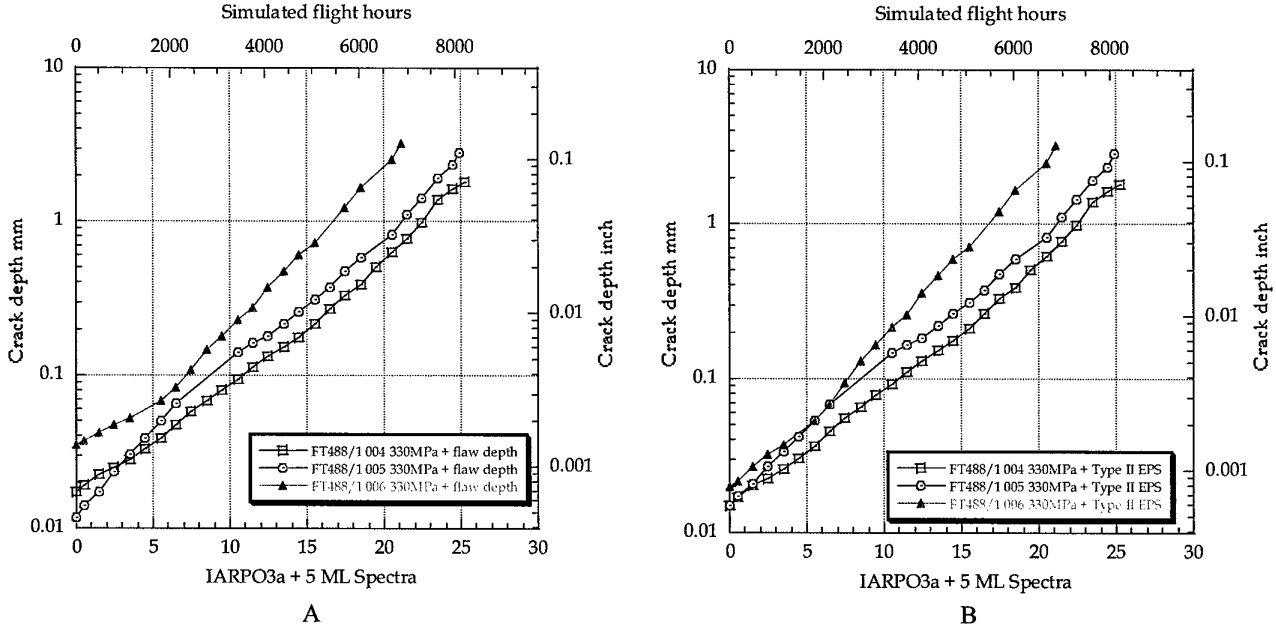

Figure 27 The crack growth plots for the 330MPa peak stress level for the FT488/1 specimens, with log depth versus spectra after correction using the measured flaw depth (A) and the Type II EPS (B).

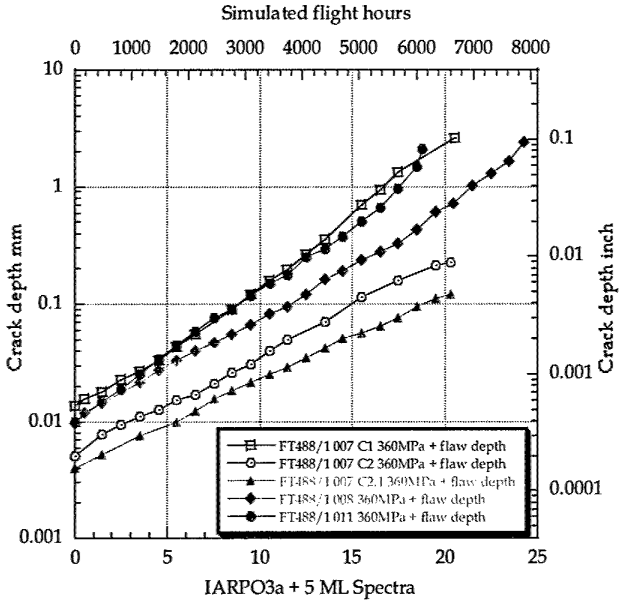

A

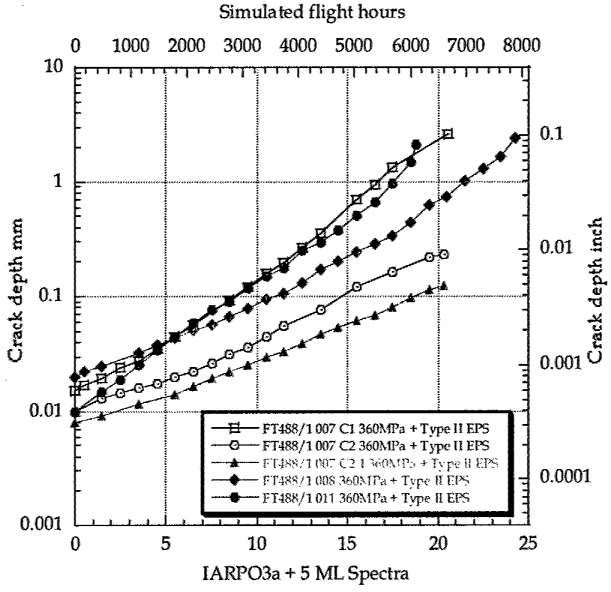

B

Figure 28 The crack growth plots for the 360MPa peak stress level for the FT488/1 specimens, with log depth versus spectra after correction using the measured flaw depth (A) and the Type II EPS (B).

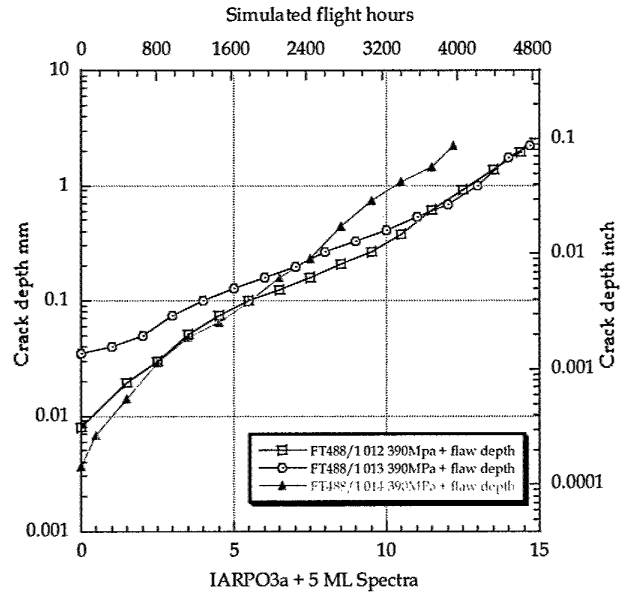

A

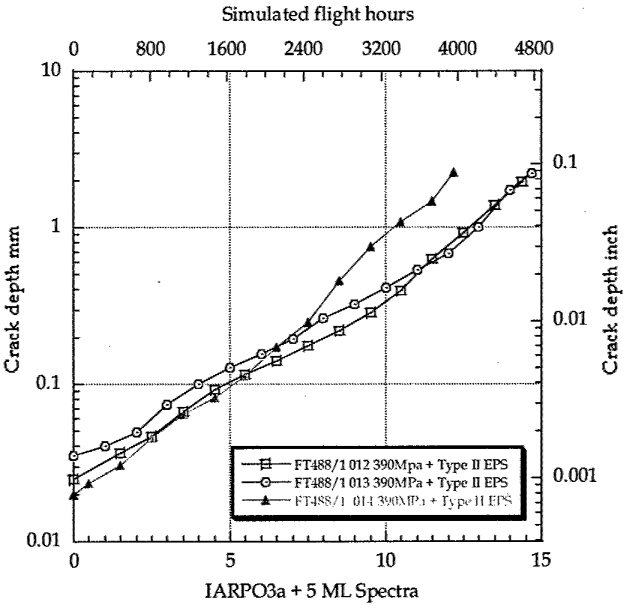

B

Figure 29 The crack growth plots for the 390MPa peak stress level for the FT488/1 specimens, with log depth versus spectra after correction using the measured flaw depth (A) and the Type II EPS (B).

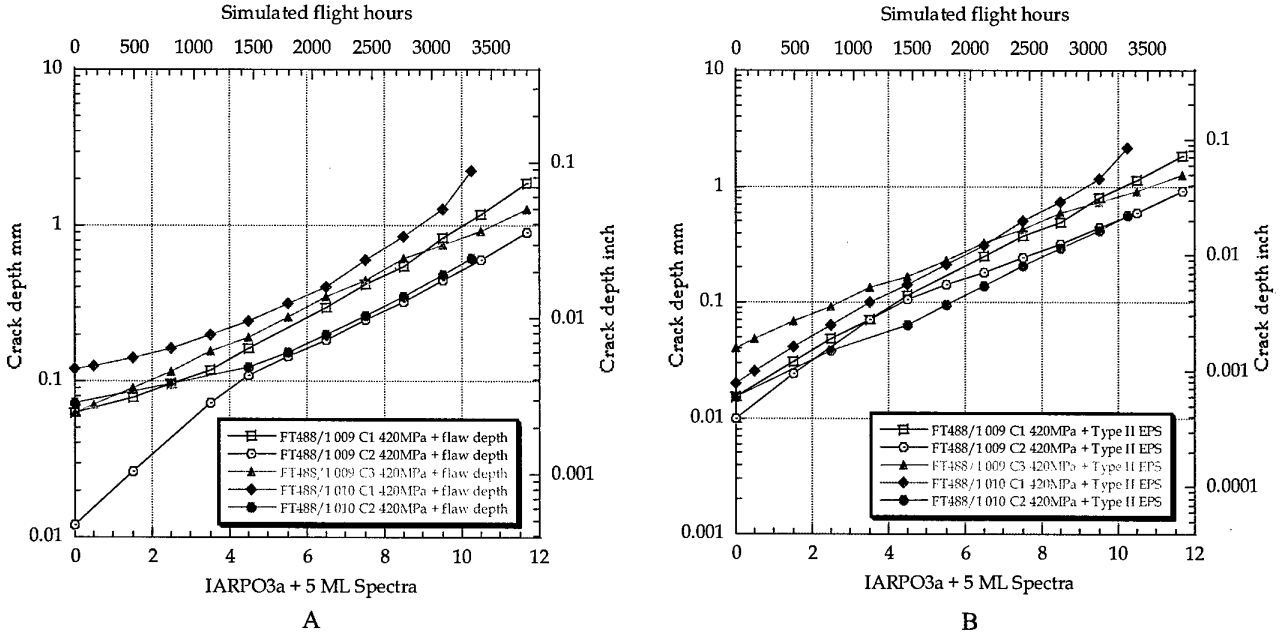

Figure 30 The crack growth plots for the 420MPa peak stress level for the FT488/1 specimens, with log depth versus spectra after correction using the measured flaw depth (A) and the Type II EPS (B).

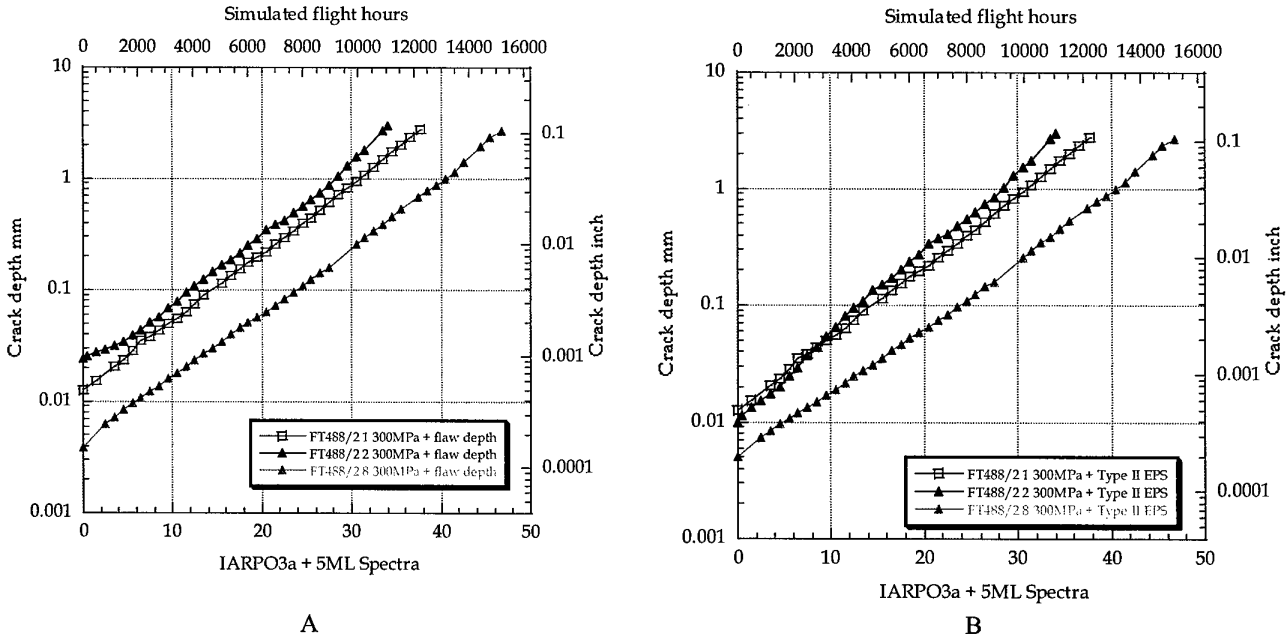

Figure 31 The crack growth plots for the 300MPa peak stress level for the FT488/2 specimens, with log depth versus spectra after correction using the measured flaw depth (A and the Type II EPS (B).

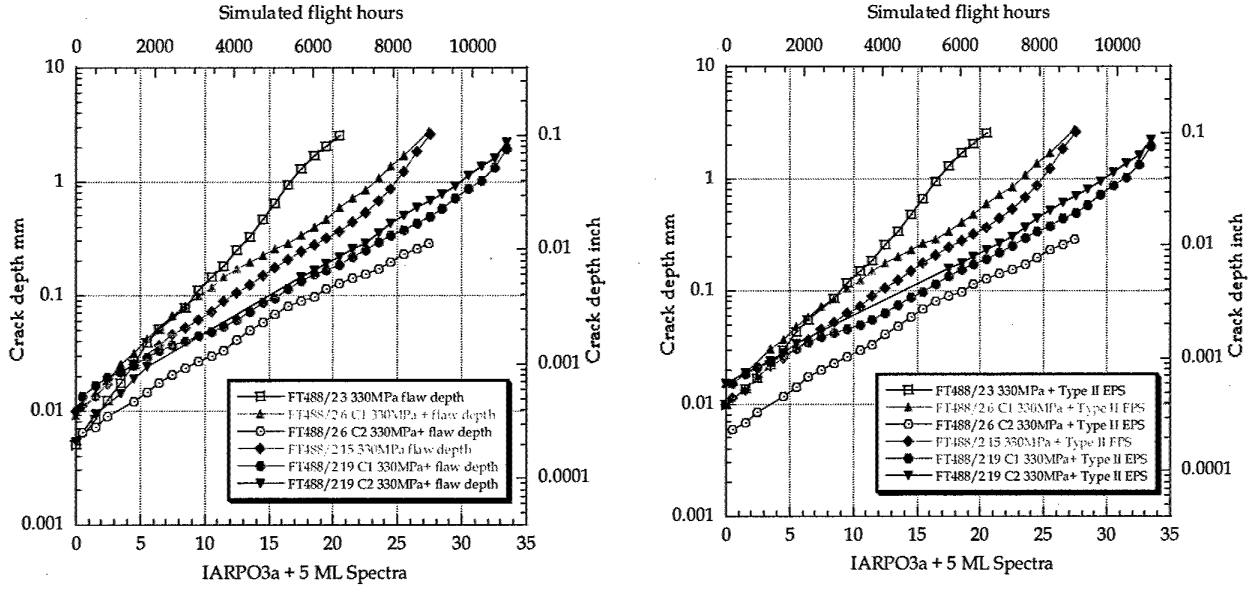

Figure 32 The crack growth plots for the 330MPa peak stress level for the FT488/2 specimens, with log depth versus spectra after correction using the measured flaw depth (A) and the Type II EPS (B).

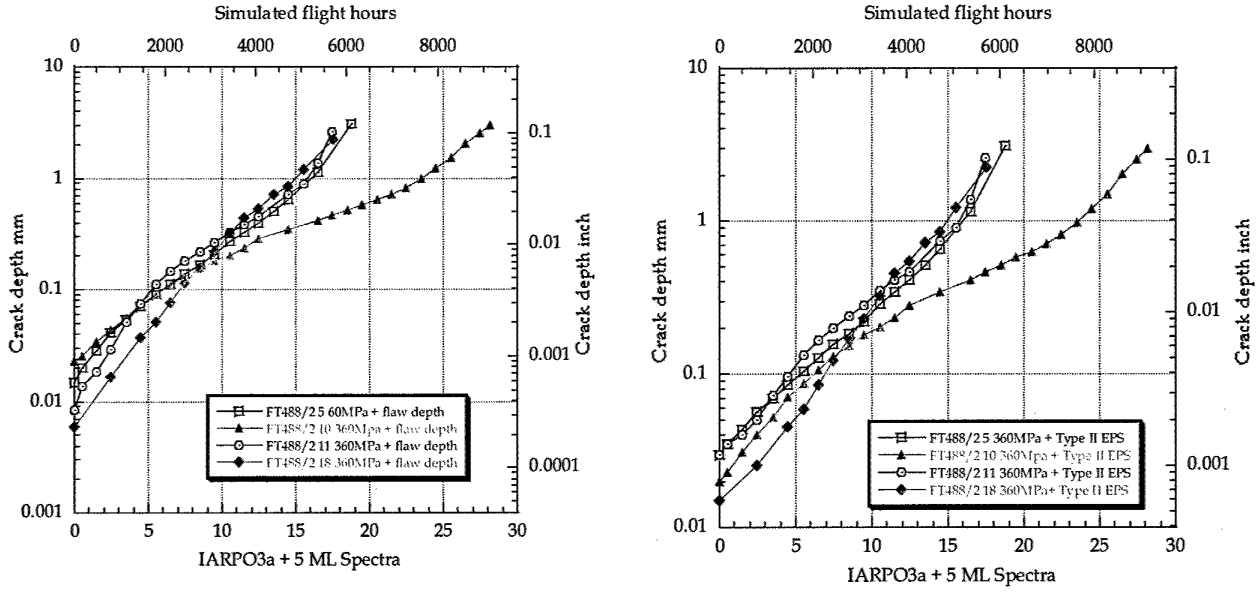

Figure 33 The crack growth plots for the 360MPa peak stress level for the FT488/2 specimens, with log depth versus spectra after correction using the measured flaw depth (A) and the Type II EPS (B).

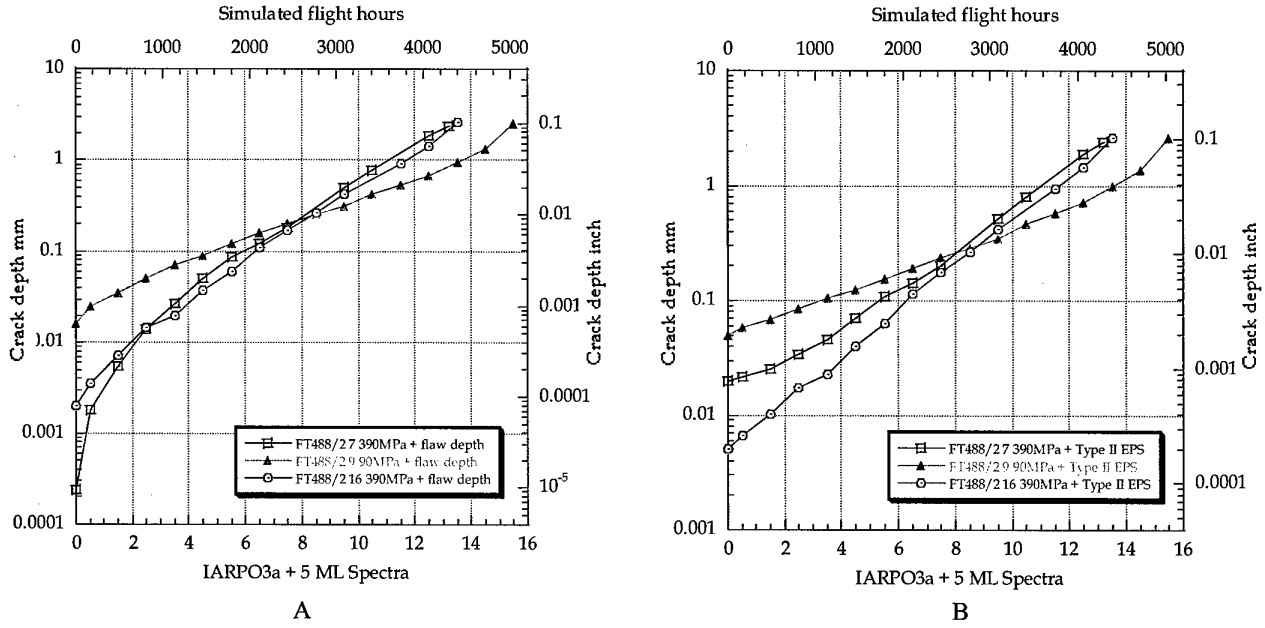

Figure 34 The crack growth plots for the 390MPa peak stress level for the FT488/2 specimens, with log depth versus spectra after correction using the measured flaw depth (A) and the Type II EPS (B).

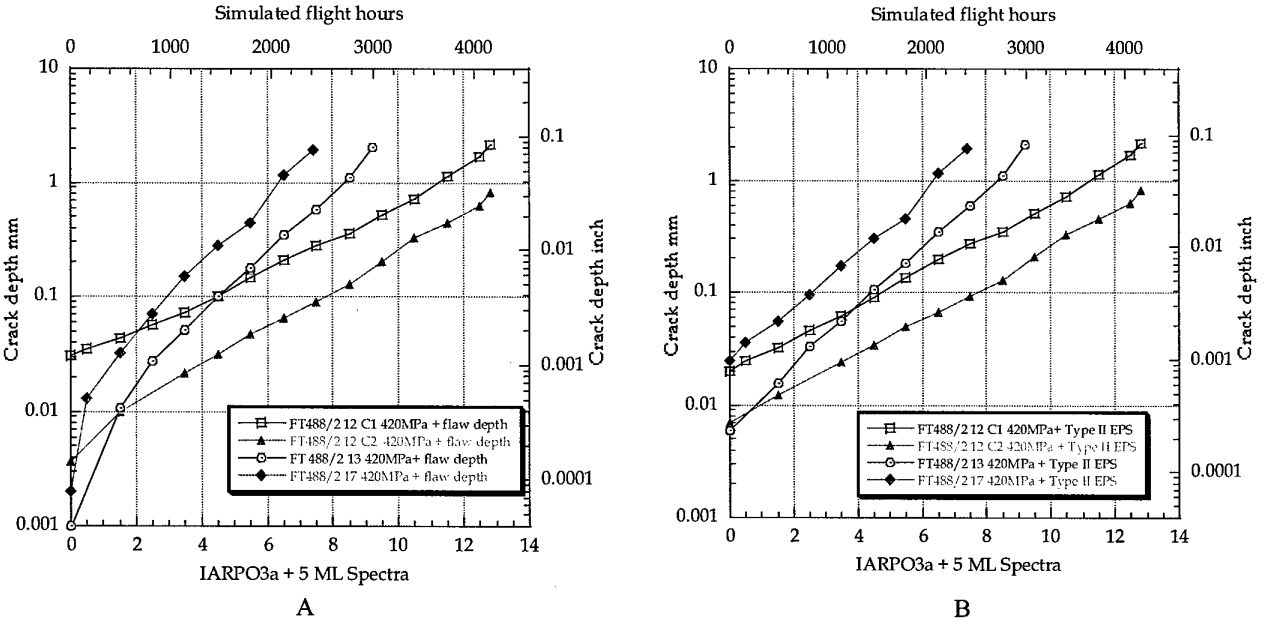

Figure 35 The crack growth plots for the 420MPa peak stress level for the FT488/2 specimens, with log depth versus spectra after correction using the measured flaw depth (A) and the Type II EPS (B).

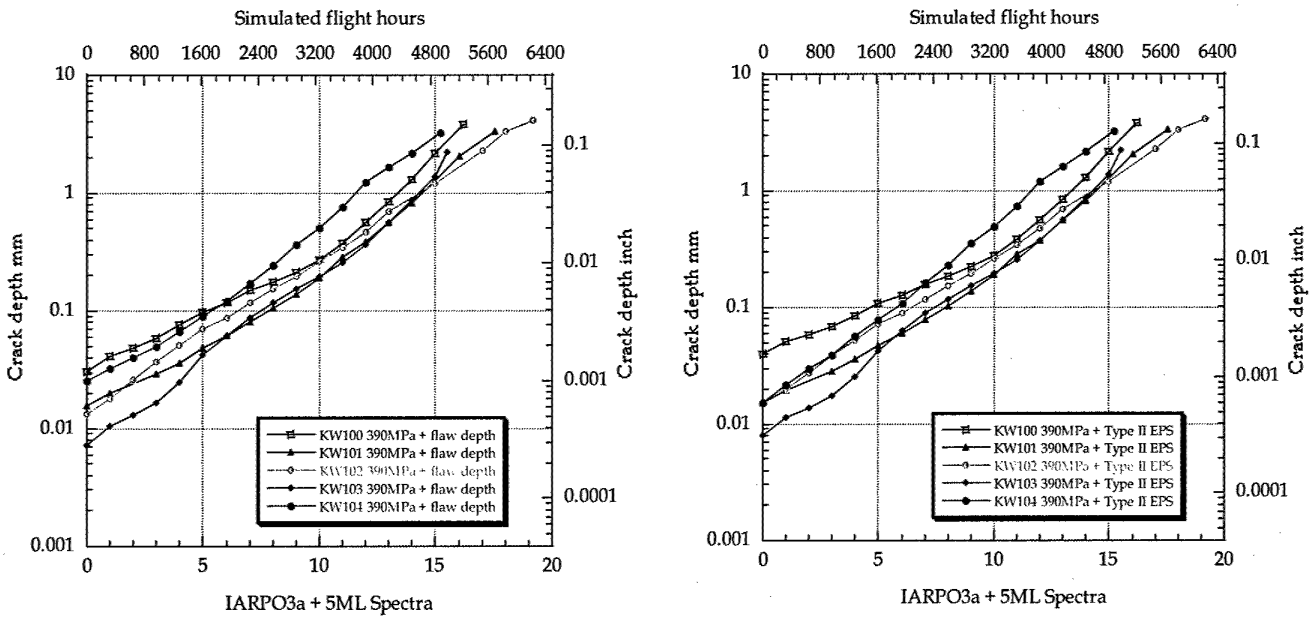

Figure 36 The crack growth plots for the 390MPa peak stress level for the KW specimens, with log depth versus spectra after correction using the measured flaw depth (A) and the Type II EPS (B).

Table 9. EPS and Flaw sizes for the FT488/1 specimens

Peak stress level MPa	Specimen Designation	Type I (Measured flaw depth) mm	Type II EPS mm	Mean Type I /Type II EPS
300	FT488/1-1	0.0056	0.007	0.0091/0.0100
	FT488/1-2	0.0145	0.015	
	FT488/1-3	0.0071	0.008	
330	FT488/1-4	0.0172	0.015	0.0214/0.0167
	FT488/1-5	0.0117	0.015	
	FT488/1-6	0.0353	0.02	
360	FT488/1-7	0.0137	0.015	0.0111/0.0150
	FT488/1-8	0.0096	0.02	
	FT488/1-11	0.01	0.01	
390	FT488/1-12	0.008	0.025	0.0155/0.0267
	FT488/1-13	0.0348	0.035	
	FT488/1-14	0.0036	0.02	
420	FT488/1-10	0.1204	0.02	0.0916/0.0175
	FT488/1-9	0.0628	0.015	
Mean (normal)		0.0171	0.0253	
Standard Deviation		0.0072	0.0318	
Log Mean		0.0158	0.0154	

Table 10. EPS and Flaw sizes for the FT488/2 specimens

Peak stress level MPa	Specimen Designation	Type I (Measured flaw depth) mm	Type II EPS mm	Mean Type I /Type II EPS
300	FT488/2 001	0.0125	0.0125	0.0135/0.0092
	FT488/2 002	0.024	0.01	
	FT488/2 008	0.0039	0.005	
330	FT488/2 003	0.005	0.01	0.0085/0.0130
	FT488/2 015	0.0099	0.01	
	FT488/2 019 C1	0.0132	0.015	
	FT488/2 019 C2	0.0053	0.015	
	FT488/2 006	0.0092	0.015	
360	FT488/2 005	0.0148	0.03	0.013/0.0238
	FT488/2 010	0.0228	0.02	
	FT488/2 011	0.0084	0.03	
	FT488/2 018	0.006	0.015	
390	FT488/2 007	0.00024	0.02	0.0061/0.0250
	FT488/2 009	0.016	0.05	
	FT488/2 016	0.002	0.005	
420	FT488/2 012	0.0308	0.02	0.0113/0.0170
	FT488/2 013	0.001	0.006	
	FT488/2 017	0.002	0.025	
Mean (normal)		0.0104	0.0174	
Standard Deviation		0.0087	0.0111	
Log Mean		0.0064	0.0146	

Table 11. EPS and Flaw sizes for the KW specimens

Peak stress level MPa	Specimen Designation	Type I (Measured flaw depth) mm	Type II EPS mm
390	KW100	0.0308	0.04
	KW101	0.0156	0.015
	KW102	0.0132	0.015
	KW103	0.0072	0.008
	KW104	0.0252	0.015
Mean (normal)		0.0181	0.0168
Standard Deviation		0.222	0.256
Log Mean		0.0164	0.0143

3.4 Comparison with the KS-plate results

The slopes of the crack growth curves, the effectiveness of the discontinuities and the nature of the fracture surfaces of the test specimens reported here were compared to the results of the previously tested KS plate specimens. These comparisons are presented in the following sections.

It should be noted that the cracks investigated here, and in the previous report, Barter, 2003, were almost exclusively the cracks that caused the failure of the specimens (or would have cause failure of the specimens had they survived for only a short interval after the failure; i.e. the second largest cracks), yet each specimen had secondary cracking, sometimes many hundreds of secondary cracks (see Section 2.7). It is for this reason that it might be supposed that the cracks measured constitute the population of the fastest cracks likely in the materials (at these orientations) tested here. This is not a certainty where the population of flaws is low, indeed the etched surfaces with their numerous etch pits most probably allow the fastest or near fastest cracking to achieve failure whereas for a similar specimen with a good as-machined surface and cracked inclusions as crack initiators the fatigue crack initiator density would be such that the probability of achieving complete representation of fastest crack growths would be reduced. This aspect will need further examination, but has

been clearly demonstrated in Pell et al, 2003, and in work to be published in a following report. The work presented in this paper on flaw type, and distribution and the to-be-released Peel QF work on KS specimens loaded with a similar wing root bending moment spectrum and with as-machined finished specimens will be compared in a future paper.

3.4.1 Growth rate

Each of the crack growth curves available for each peak stress level (for the plots containing the Type II EPS value) were plotted on single graphs and compared in Figure 37 to Figure 41. The growth rates were found to be very consistent. Most of the scatter in the final lives appears to be the result of variations in the EPS. It should be noted that although the EPS scatter accounts for a large portion of the crack life variation, crack growth variation is also evident and significant in several of the specimens - particularly those of the FT488/2 group and to a lesser extent the FT488/1 growth curves. The tendency being for a greater acceleration rate towards the end of growth in these specimens. This may be in-part the result of the reduced thickness[3] of these specimens compared to the KW and KS specimens, or due to the broad nature of the cracking because of multiple initiation at the base of the shallow machining marks.

[3] Although the Y488 bulkhead specimens were thinner than the KW and KS coupons the load used for testing was calculated on the cross sectional area of all the coupons (at their thinnest cross section), so the nominal loading at the thinnest part of the specimens is as stated for each of the peak stresses tested. It should also be noted that the Y488 bulkhead specimens had been peened on the radii, whereas the KW specimens were not. This was carried out to prevent failure from non-IVD coated parts of the specimen. None of the Y488 bulkhead specimens grew cracks from these peened areas, so the Kt of these areas was not an issue in any noted crack growth for these specimens, and since the crack growths of the KW specimens were similar, the Kt of the radius (which was not peened) did not appear to have a significant effect on crack growth either.

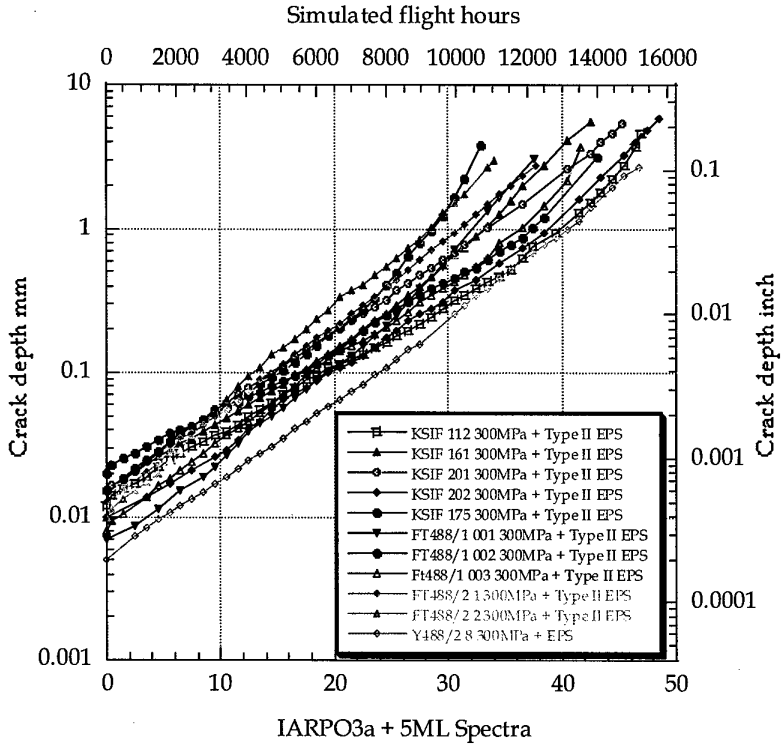

Figure 37. The plots of the two Y488 bulkhead sets of specimens compared to the KS plate data for the 300MPa stress level.

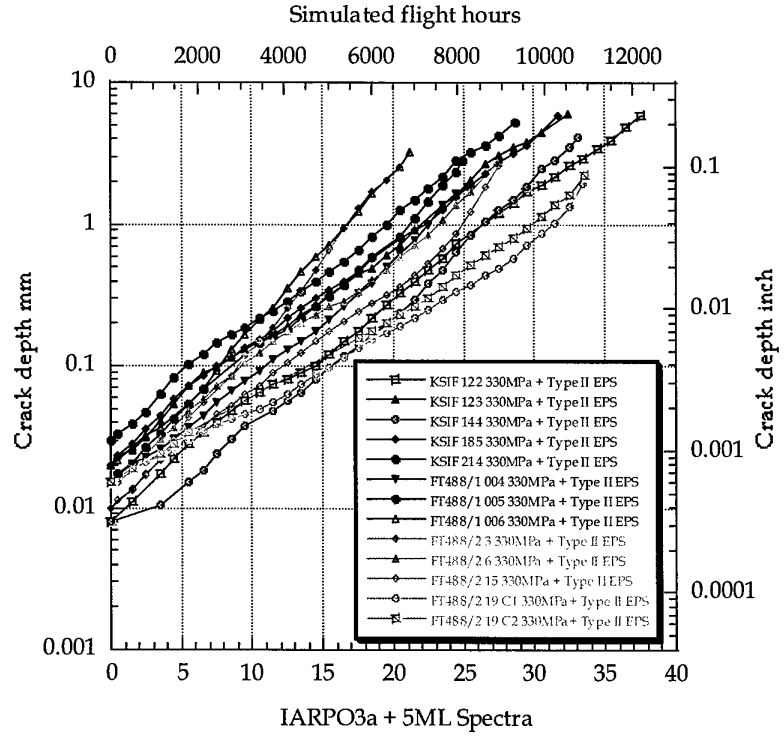

Figure 38. The plots of the two Y488 bulkhead sets of specimens compared to the KS plate data for the 330MPa stress level.

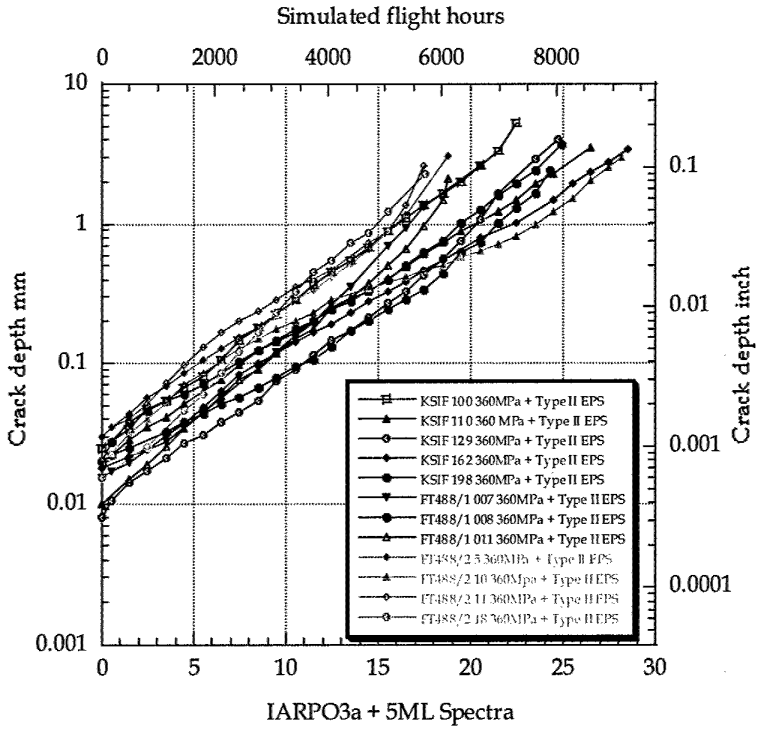

Figure 39. The plots of the two Y488 bulkhead sets of specimens compared to the KS plate data for the 360MPa stress level.

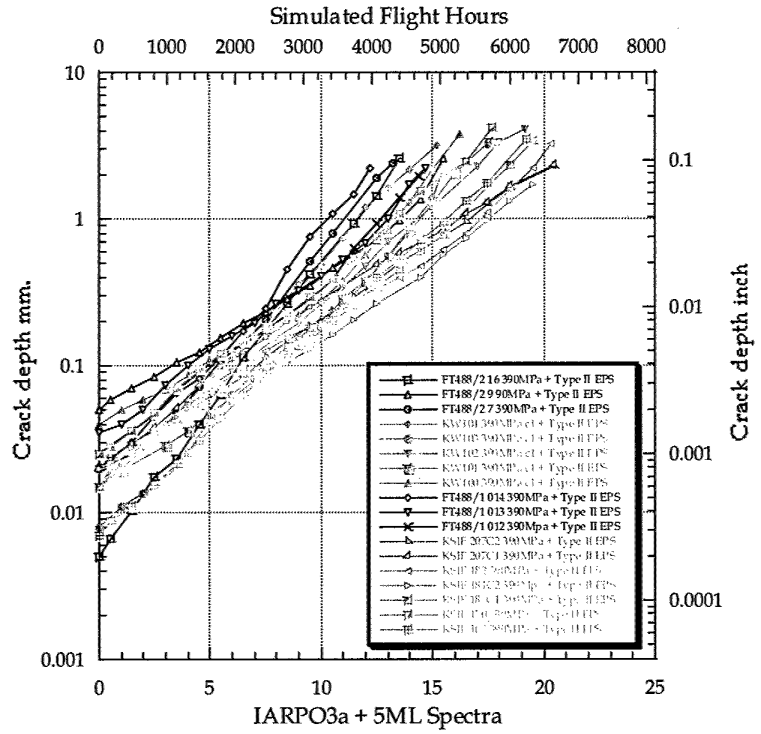

Figure 40. The plots of the two Y488 bulkhead sets of specimens compared to the KS and KW plate data for the 390MPa stress level. Note that the KW data appears to be more like the FT488/1 and 2 data.

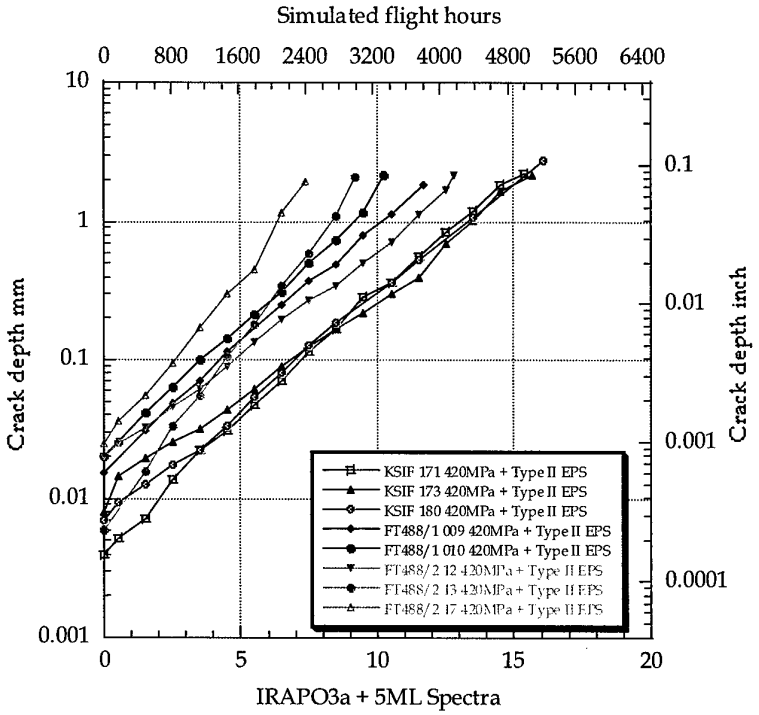

Figure 41. The plots of the two Y488 bulkhead sets of specimens compared to the KS plate data for the 420MPa stress level.

3.4.2 Comparison of the mean slopes

The plots shown in Figure 42 to Figure 46 present crack growth curves using the log means of the slopes (β in equation 1) for each of the crack growth sets compared to the mean slopes of the KS specimens, using 0.01mm as the starting point in all cases. It is notable that the slopes of the crack growth curves for the FT488/1 and 2 specimens were consistently higher than the KS plate specimens. This was expected since the crack growth direction in the FT488/1 and 2 specimens (TS) is known to be preferred over the crack growth direction for the KS plate (LT and LS). Other factors may be the size effect, since the Y488 specimens were thinner than the KS specimens and in addition, the Y488 specimens were cut from the very centre of the plate whereas the KS specimens were taken from random positions within their plate. The centre of the plate is known to be different to the surface material since it is less 'broken down' than the surface material in the plate rolling process.

The starting points for each of the graphs shown in Figure 42 to Figure 46 has been normalised to 0.01mm for comparison purposes while the end points were set to the log mean of the final crack depth for the specimen group in question. The results of the calculation of the a_0 and β for each of the measured crack growth curves were used (including the KS results), and are set out in Table 12 to Table 15. Since the curve fits were carried out on the data including the Type II EPS, the a_0 (the zero life intersect for an approximation of the best offset added to the data) value is approximately the same as the Type III EPS for these data. The Type II EPS and this approximation of the Type III EPS are compared in Table 16. It is notable that the final crack size of the FT488/1 and 2 specimens is always smaller than the KS specimens - due to the smaller thickness of the FT488/1 and 2 specimens.

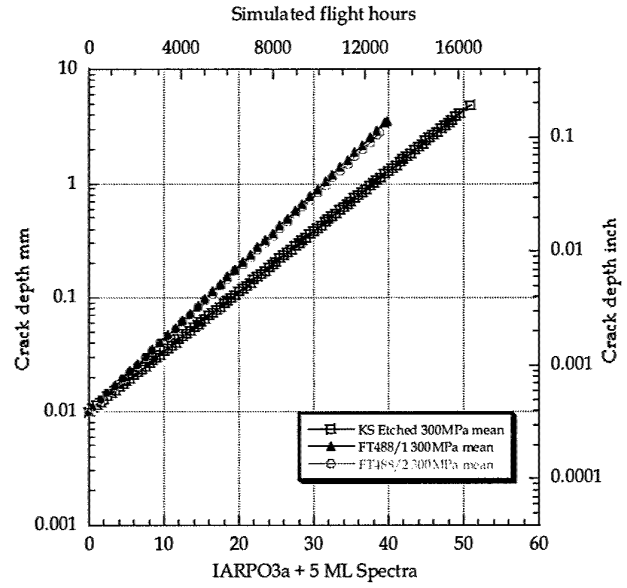

Figure 42. The mean crack growth slopes for the KS plate (Etched) and the two sets of specimens from the FT488/1 and FT488/2 tests, for the 300MPa stress level.

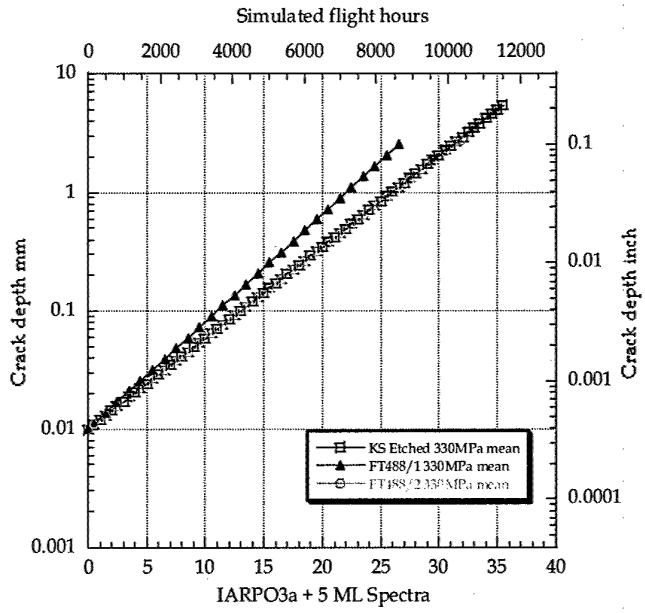

Figure 43. The mean crack growth slopes for each of the data sets at the 330MPa stress level.

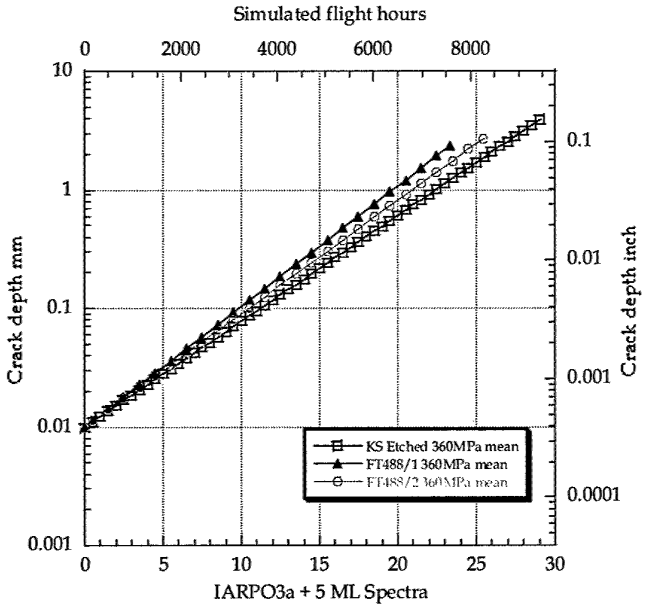

Figure 44. The mean crack growth slopes for each of the data sets at the 360MPa stress level.

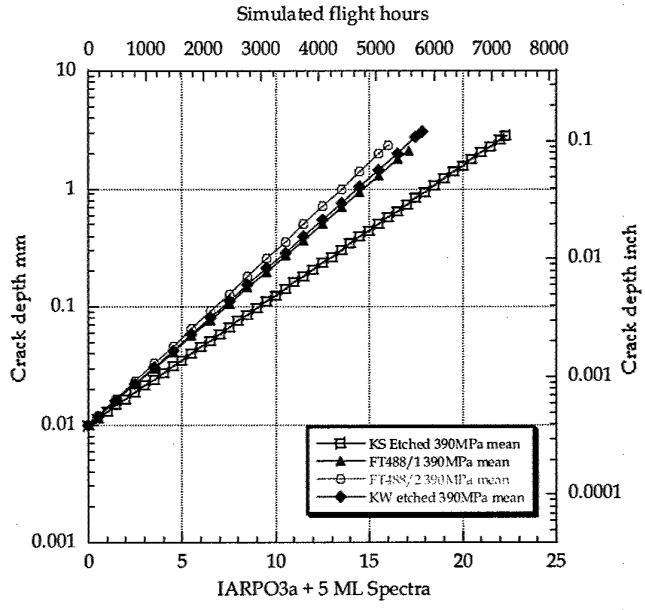

Figure 45. The mean crack growth slopes for each of the data sets at the 390MPa stress level. Note that the KW plate specimens produced a crack growth rate similar to the FT488/1 and 2 specimens.

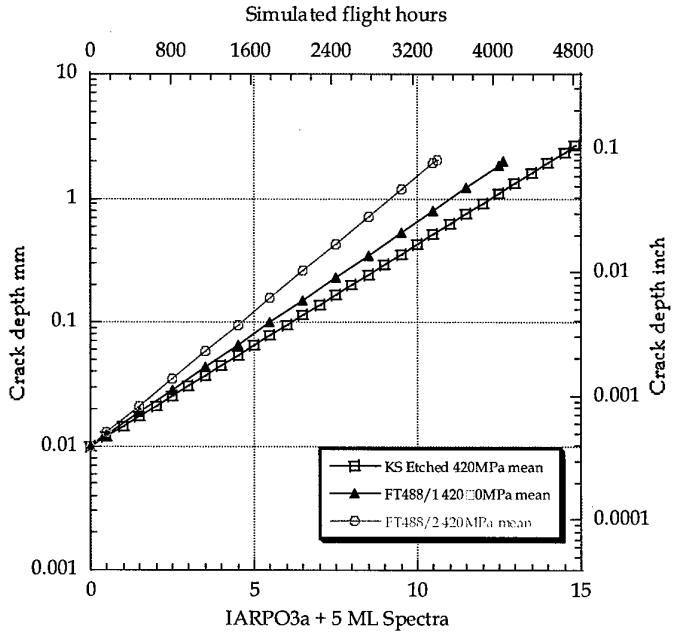

Figure 46. The mean crack growth slopes for each of the data sets at the 420MPa stress level.

Table 12. The FT488/1 specimens mean crack growth curve calculations using the Type II EPS

Peak Stress	Specimen	a_0	β	R (measure of curve fit	μ_{log} of a_0	μ_{log} of β	σ_{log} of a_0	σ_{log} of β	μ_{log} of Max crack depth[4]
300MPa	FT488/1 001	0.0050	0.1602	0.990	0.0081	0.147	0.197	0.0428	3.523
	FT488/1 002	0.0087	0.1322	0.959					
	FT488/1 003	0.0123	0.1509	0.945					
330MPa	FT488/1 004	0.0134	0.1879	0.995	0.0154	0.209	0.0514	0.0593	2.552
	FT488/1 005	0.0161	0.1990	0.992					
	FT488/1 006	0.0168	0.2437	0.998					
360MPa	FT488/1 007	0.0121	0.2565	0.998	0.0122	0.234	0.0936	0.0797	2.348
	FT488/1 008	0.0152	0.1891	0.977					
	FT488/1 011	0.0099	0.2627	0.971					
390MPa	FT488/1 012	0.0224	0.2925	0.991	0.0226	0.314	0.134	0.0813	2.124
	FT488/1 013	0.0309	0.2724	0.982					
	FT488/1 014	0.0167	0.3880	0.996					
420MPa	FT488/1 010	0.0205	0.4330	0.986	0.0186	0.418	0.0578	0.0216	1.973
	FT488/1 009	0.0170	0.4036	0.999					

Table 13. The FT488/2 specimens mean crack growth curve calculations using the Type II EPS

Peak Stress	Specimen	a_0	β	R (measure of curve fit	μ_{log} of a_0	μ_{log} of β	σ_{log} of a_0	σ_{log} of β	μ_{log} of Max crack depth[5]
300MPa	FT488/2 001	0.0127	0.1414	0.999	0.0087	0.145	0.231	0.0463	2.795
	FT488/2 002	0.0108	0.1631	0.997					
	FT488/2 008	0.0047	0.1324	0.997					
330MPa	FT488/2 003	0.0087	0.2783	0.997	0.0124	0.177	0.115	0.124	2.776
	FT488/2 015	0.0105	0.1836	0.964					
	FT488/2 019 C1	0.0132	0.1350	0.970					
	FT488/2 019 C2	0.0141	0.1422	0.988					

[4] Probably influenced by the specimen thickness, hence this value is considerably smaller than in the KW and KS specimens.

[5] Probably influenced by the specimen thickness, hence this value is considerably smaller than in the KW and KS specimens.

	FT488/2 006	0.0171	0.1778	0.990					
360MPa	FT488/2 005	0.0298	0.2219	0.966	0.0250	0.220	0.184	0.114	2.706
	FT488/2 010	0.0312	0.1557	0.985					
	FT488/2 011	0.0316	0.2304	0.955					
	FT488/2 018	0.0133	0.2946	0.999					
390MPa	FT488/2 007	0.0147	0.3757	0.999	0.0152	0.341	0.472	0.154	2.517
	FT488/2 009	0.0457	0.2300	0.957					
	FT488/2 016	0.0052	0.4577	0.997					
420MPa	FT488/2 012	0.0190	0.3550	0.993	0.0142	0.502	0.308	0.131	2.064
	FT488/2 013	0.0063	0.6168	0.994					
	FT488/2 017	0.0238	0.5786	0.995					

Table 14. The KW specimens mean crack growth curve calculations using the Type II EPS

Peak Stress	Specimen	a_0	β	R (measure of curve fit	μ_{log} of a	μ_{log} of β	σ_{log} of a	σ_{log} of β	μ_{log} of Max crack depth
390MPa	KW100	0.0297	0.262	0.962	0.0137	0.312	0.228	0.056	3.22
	KW101	0.0107	0.310	0.994					
	KW102	0.0140	0.360	0.998					
	KW103	0.0071	0.345	0.973					
	KW104	0.0153	0.292	0.998					

Table 15. The KS specimens mean crack growth curve calculations using the Type II EPS

Peak Stress	Specimen	a_0	β	R (measure of curve fit	μ_{log} of a	μ_{log} of β	σ_{log} of a	σ_{log} of β	μ_{log} of Max crack depth
270MPa	KSIF137	0.0199	0.0799	0.988	0.0105	0.0916	0.3	0.0515	5.2
	KSIF128C1	0.00563	0.0948	0.992					
	KSIF189	0.0132	0.0856	0.999					
	KSIF210	0.00457	0.109	0.992					
	KSIF157	0.0192	0.0909	0.996					
300MPa	KSIF112	0.0146	0.126	0.997	0.012	0.122	0.134	0.0445	4.8
	KSIF175	0.0104	0.136	0.984					
	KSIF161	0.00824	0.128	0.988					
	KSIF201	0.0182	0.105	0.944					
	KSIF202	0.011	0.115	0.962					
330MPa	KSIF185	0.0305	0.177	0.998	0.0176	0.172	0.208	0.00716	5.37
	KSIF144	0.0124	0.171	0.997					
	KSIF123	0.00935	0.17	0.997					
	KSIF122	0.0226	0.171	0.995					
	KSIF214	0.021	0.174	0.998					
360MPa	KSIF198	0.0199	0.19	0.996	0.0137	0.214	0.216	0.0792	3.91
	KSIF129	0.0089	0.281	0.998					
	KSIF110	0.00733	0.237	0.985					
	KSIF100	0.0221	0.192	0.983					
	KSIF162	0.0168	0.184	0.997					
390MPa	KSIF181	0.0101	0.287	0.988	0.015	0.259	0.108	0.052	2.83
	KSIF207	0.0192	0.293	0.994					
	KSIF170	0.0169	0.237	0.967					
	KSIF165	0.0167	0.222	0.988					
	KSIF182	0.014	0.261	0.981					
420MPa	KSIF105	0.0059	0.375	0.998	0.00719	0.379	0.172	0.0275	2.68
	KSIF121	0.00747	0.348	0.994					
	KSIF136	0.00853	0.363	0.994					
	KSIF171	0.0124	0.378	0.998					
	KSIF173	0.00782	0.397	0.998					
	KSIF180	0.00379	0.417	0.999					
450MPa	KSIF109	0.00855	0.474	0.978	0.0124	0.439	0.233	0.0607	2.3
	KSIF126	0.0194	0.399	0.992					
	KSIF101	0.00754	0.495	0.983					
	KSIF103	0.0247	0.361	0.99					
	KSIF108	0.00929	0.485	0.996					

Table 16. The Type II EPS values compared to the approximate Type III EPS values.

Peak Stress	Specimen	Type II EPS	Approximate Type III EPS.	% approx Type III of Type II EPS (>100 = smaller approx. Type III EPS)
300MPa	FT488/1 001	0.007	0.0050	71.43
	FT488/1 002	0.015	0.0087	58.00
	FT488/1 003	0.008	0.0123	153.75
330MPa	FT488/1 004	0.015	0.0134	89.33
	FT488/1 005	0.015	0.0161	107.33
	FT488/1 006	0.02	0.0168	84.00
360MPa	FT488/1 007	0.015	0.0121	80.67
	FT488/1 008	0.02	0.0152	76.00
	FT488/1 011	0.01	0.0099	99.00
390MPa	FT488/1 012	0.025	0.0224	89.60
	FT488/1 013	0.035	0.0309	88.29
	FT488/1 014	0.02	0.0167	83.50
420MPa	FT488/1 010	0.02	0.0205	102.50
	FT488/1 009	0.015	0.0170	113.33
300MPa	FT488/2 001	0.0125	0.0127	101.60
	FT488/2 002	0.01	0.0108	108.00
	FT488/2 008	0.005	0.0047	94.00
330MPa	FT488/2 003	0.01	0.0087	87.00
	FT488/2 015	0.01	0.0105	105.00
	FT488/2 019 C1	0.015	0.0132	88.00
	FT488/2 019 C2	0.015	0.0141	94.00
	FT488/2 006	0.015	0.0171	114.00
360MPa	FT488/2 005	0.03	0.0298	99.33
	FT488/2 010	0.02	0.0312	156.00
	FT488/2 011	0.03	0.0316	105.33
	FT488/2 018	0.015	0.0133	88.67
390MPa	FT488/2 007	0.02	0.0147	73.50
	FT488/2 009	0.05	0.0457	91.40
	FT488/2 016	0.005	0.0052	104.00
420MPa	FT488/2 012	0.02	0.0190	95.00
	FT488/2 013	0.006	0.0063	105.00
	FT488/2 017	0.025	0.0238	95.20
390MPa	KW100	0.04	0.0297	74.25
	KW101	0.015	0.0107	71.33
	KW102	0.015	0.0140	93.33
	KW103	0.008	0.0071	88.75
	KW104	0.015	0.0153	102.00
Mean % approx Type III of Type II EPS (>100 = smaller approx. Type III EPS)				95.44

The comparison of the mean crack growth results for the KS plate versus the KW plate growth results revealed that there is a notable increase in the growth rate of the KW specimens. This was consistent with the combined effect of; the altered configuration, and orientation of the KW specimens compared to the KS specimens, and possibly also the increased hardness of the KS material versus the KW material (Table 4).

The mean crack growth rate of the KW specimens was very similar to the mean crack growth rates of the FT488/1 and FT488/2 specimens at the same peak stress level, and the small variation noted was consistent with the variation in the hardness of the three groups. This suggests that hardness has a direct relationship to crack growth rate for the fastest cracks in this material and probably did have an influence on the difference noted between the KS and KW crack growths. At other stress levels this effect is not as well supported although it should be noted that there are only a few crack growth curves in each calculation of the mean crack growth.

If the crack growth for the fastest cracks is directly influenced by the hardness (which has been suggested before for aluminium alloys, Murakami, 1989) then this is an important finding in that the distribution of crack growth might be well modelled by the distribution in hardness values, a much easier value to establish than crack growth rates for a sufficient population of thick section 7050 plate, or even the variation in hardness within a single plate.

The comparison of the Type II EPS values with the approximation of the Type III EPS values as shown in Table 16 suggests, as noted in section 3.3, that the Type III EPS values will be mostly smaller than the Type II values. This makes the Type II value a more conservative (shortening fatigue life) measure of the EPS population. For this reason, only these values are further examined in the following section.

3.4.3 Initial discontinuities

Since the EPS values are likely to represent the larger discontinuities in a specimen rather than the entire population (because they have been determined for the largest cracks) they are unlikely to be well represented by a normal distribution. An extreme value distribution should model the data more accurately and it has been found that two distributions are of particular relevance to discontinuities that grow the largest fatigue cracks in fatigue tests. These are the Weibull and lognormal distributions, with the lognormal distribution being preferred here because it is more conservative (it has a larger upper tail). Knowing the probability of the extreme EPS values are a very important aspect for the prediction of service component fatigue life with an appropriate level of conservatism, White et al, 2002. The following section uses the lognormal distribution, but first the data are tested to determine if they come from the same population, and can be pooled to increase the certainty of the distribution fitted.

To test if the groups of EPS data are independent or belong to the same population, each group of EPS (Type II) values as estimated from the fractography results, were tested against each other group using: the Student t test. Here it was used to determine the t probability for unpaired data with unequal variance. The value determines if there is a statistically significant difference between two means. If this is below a certain level (usually 0.05), the conclusion is that there is a difference between the means of two groups; and the F test, used to determine the F probability. This value determines if the two groups have different variances. A small F probability, (usually <0.05) indicates that the two groups have significantly different variances. Since these two tests assume that the data are normally distributed, the T and F tests were carried out on the logs of the EPS Type II values i.e. the logs of the EPS values appear to be approximately normally distributed. Table 17 gives the t and F statistics for each pair of groups compared.

Table 17 Student t Test for unpaired data with unequal variance for all the Type II EPS data

	G1 vs G2	G1 vs G3	G1 vs G4	G2 vs G3	G2 vs G4	G3 vs G4
Degrees of Freedom	28	7	25	5	26	4
t Value	-0.43	-0.34	0.71	-0.069	1.43	0.81
t Probability	0.67	0.74	0.49	0.95	0.17	0.46
F Value	2.73	1.18	1.54	1.79	1.38	1.30
F Probability	0.18	0.97	0.27	0.38	0.54	0.57

Group 1 (G1): FT488/2 Type II EPS_{log}, Group 2 (G2): FT488/1 Type II EPS_{log}, Group 3 (G3): KW etched Type II EPS_{log}, Group 4 (G4): KS etched Type II EPS_{log}.

These tests on the EPS (Type II) values, indicated that the log means and log standard deviations were reasonably consistent from group-to-group including the KS etched specimens, notwithstanding the slightly different nature of the origins in the FT488/1 and particularly FT488/2 bulkhead specimens.

Since the T and F test results indicate that the variances and means are similar then it is reasonable to pool these pre-IVD etch EPS data (ignoring that two data points are for porosity discontinuities - since they are well within the data bounds) for the purposes of predicting extreme values of the Type II EPS for pre-IVD etched surfaces on thick section 7050 T7451 plate. Figure 47 shows each of the groups of data plotted on a cumulative probability plot using a log EPS axis for the data. It can be seen that each set of data has a reasonable fit (R^2 value) to an exponential line on this plot indicating that a log normal distribution is a reasonable model of the distribution of the Type II EPS values. Figure 48 shows the pooled Type II EPS values also plotted on a cumulative probability plot.

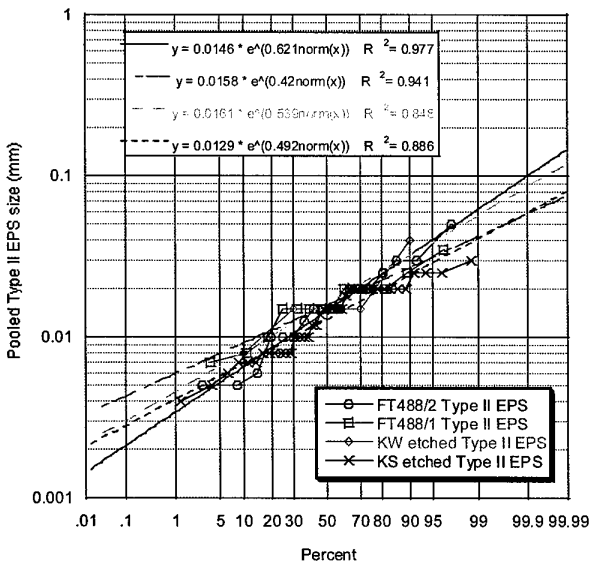

Figure 47 Each of the of the Type II EPS data groups plotted on a cumulative probability plot, with the exponential curve fits.

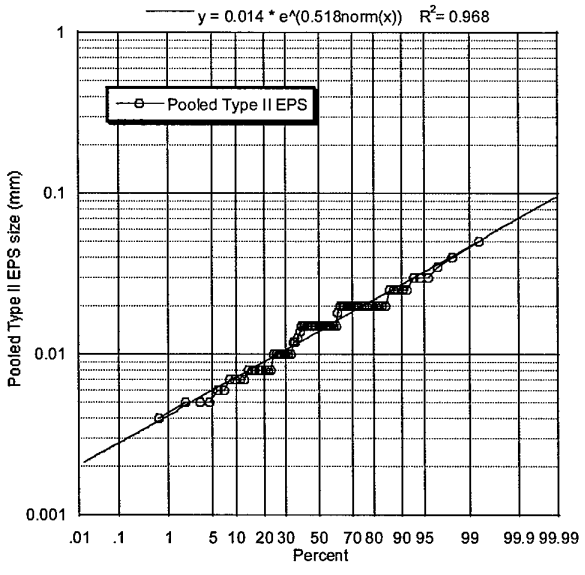

Figure 48 The pooled Type II EPS for all the pre-IVD etched coupons plotted on a cumulative probability plot, with the exponential curve fit.

If the data are log-normally distributed, then the curve fits shown in the above Figures indicate that the results shown in Table 18 can be calculated for extreme values of the Type II EPS, for each set of data. Given the limited data available for each of these data sets, pooling of the data probably gives a better indication of the size of such an extreme Type II EPS for pre-IVD etched 7050-T74511 thick section plate as used in the F/A-18 structure and these values are also noted in the Table. If the Type III EPS data from Barter,2003 is combined with the approx Type III data presented in Table 16 the results shown in the final column of Table 18 are found. These values are larger than the pooled Type II EPS values since the Type III EPS values for the KS specimens were mostly larger than the Type II EPS values for those specimens, the opposite of what was found for the specimens examined in this report.

Table 18 Type II EPS size predicted for pre-IVD etching at two remote probabilities for each data set and the pooled data

Probability level	FT488/2 Type II EPS	FT488/1 Type II EPS	KW etched Type II EPS	KS etched Type II EPS	Pooled etched Type II EPS	Pooled etched specimen data: Type III EPS KS + approx. Type III data generated in this paper
1 in 10^3 specimens	0.098mm	0.057mm	0.084mm	0.058mm	0.070mm	0.084mm
1 in 10^4 specimens	0.147mm	0.075mm	0.120mm	0.081mm	0.095mm	0.123mm

The extreme EPS values presented in Table 18 may be used as the initial crack size for a fracture mechanics assessment of life at the risk levels noted. Of course other unknowns would need to be included to find the true risk of a particular crack size at a particular time, as was attempted using the KS Type III EPS values in White et al, 2002.

As noted in Section 2.7, and assumed here, the bulk of the discontinuities from which the fatigue cracks originated were etch-pits. Other discontinuities either independent or associated with the etch pits were noted; shallow machining marks and on two occasions, porosity. This result supports the view that while the discontinuities caused by the etching are the dominant cause of fatigue crack initiation in these specimens, other populations of different types of discontinuity do exist. While etch pitting is clearly the dominant form of crack initiation in these specimens, their population distribution may be restricted by the physical nature of the etching process, preventing extreme pit sizes, and in effect capping the upper end of the etch pit population distribution, while the population distribution of other flaws may be more continuous. The porosity found here, the machining marks independent of the etching, cracked or debonded inclusions (probably a limited upper tail on any population distribution) and corrosion may exist in service components, than would 'fill in' the upper tail of the discontinuity distribution. Further work to adequately resolve the population of discontinuities in components manufactured from this material is to be pursued. The assumption used to present the discontinuity distribution above is that the etch pit distribution is continuous and un bounded in the upper tail and therefore gives some information about the probability of extreme values of discontinuities for both the porosity machining marks and the etch pits.

3.4.3.1 Topography

The topography of the current set of fracture surfaces were also consistent with the topography of the KS fatigue crack surfaces in that the regions around the origins were usually relatively flat, and intersected very few inclusions. In contrast, when the cracking reached about 0.5mm in depth, depending on the stress level of the applied fatigue loading the surfaces increased in roughness and many inclusions could be seen to intersect the surface from then to the end of the crack. These features suggest that the inclusions in this material do not play a significant role in the growth of the cracks while the cracks are small, even at the higher applied stress levels, although they are known to have a significant effect on crack initiation under some circumstances, Edwards & Newman, 1990. This implies that for cracks to initiate at inclusions, the inclusions need to be cracked, etched/corroded, torn-out or debonded from the matrix prior to the application of fatigue loading, or such damage would need to occur via other than fatigue loading, either before fatigue loading (such as produced by machining) or during the life of the component. This aspect is to be addressed, in part, in the proposed report by Pell on the QF of KS as machined specimens.

For uncracked or debonded inclusions to be involved in fatigue crack initiation, in this material during the life of the component, they would need to either experience very long cycle times, high loads (net section or most likely local; such as in high Kt areas) or damage from corrosion, surface impacts, or wear. In the case of high Kt areas a region at the notch tip can reach yield during fatigue loading and thus produce inclusion cracking.

This suggests that for low Kt regions where the peak stress is insufficient to crack the inclusions for any service load, the removal of surface discontinuities; etching, machining marks, cracked or debonded inclusions, etc., would result in a very significant increase in fatigue life, whereas little advantage will be seen for high Kt detail (except at low applied stresses). There is good evidence to support this proposition in this material and this will be further examined in a following report.

3.4.3.2 Porosity as a crack initiator

Two of the larger fatigue cracks from one specimen taken from the FT488/1 bulkhead (specimen 010 (420MPa peak)) had initiated from porosity as noted in Figure 11. These pores were either slightly subsurface or touching the surface at the IVD-to-7050 interface. The life of these cracks did not appear to be significantly different to the other specimens tested at this stress level, although the porosity, particularly in one case was significantly larger (about 0.14mm deep and 0.3mm long for crack 1 (C1) and, 0.075mm deep and 0.210mm long for crack 2 (C2) compared to a maximum of 0.062 deep for an etch pit) than any etch pit found initiating a fatigue crack. Their physical size was very much larger that their EPS indicating that their physical size is a poor indicator of how crack-like they are. A further examination of the relative effect of porosity as a crack initiator in this material will be presented in a following report.

4. Summary and conclusion

In summary, in this and the previous two papers, the following aspects of fatigue in aluminium alloy 7050 have been investigated using a representative wing root bending moment spectrum to generate the fatigue cracking:

1. A method to produce surfaces on coupons that represent those of F/A-18 aircraft structure.
2. The effect that the surface finish used in the critical aluminium alloy 7050-T7451 structure of the F/A-18 has on the fatigue life, crack initiation and the fatigue crack initiating discontinuity effectiveness.
3. Various methods of using quantitative fractography to measure the metrics of crack initiating discontinuities (mostly etch pitting), and comparing these to the physical size of these discontinuities. (Other types of discontinuities are also being studied and will be the subject of a future report).
4. The apparent probability distributions of the effective fatigue crack size of some of the discontinuities typical for F/A-18 service aircraft structure.
5. The effect that the residual compressive stresses (as developed by a standard life extension technique used on service aircraft) have on life and the type of discontinuity that initiates fatigue cracking after such a surface treatment.
6. A comparison of crack growth rates in several different plates of 7050-T7451 thick section material.

An examination of the results of the testing and analysis carried out here and in a the previous paper, Barter, 2003, suggest that the following conclusions can be made:

1. The comparison of the KS plate test results to the KW plate test results (EPS, life to failure and growth rate), revealed that although the EPS values appear to be similar there is a notable increase in the growth rate of the KW specimens. This was consistent with a combined effect of; the altered configuration, and orientation of the KW specimens compared to the KS specimens, and possibly, the increased hardness of the KS material versus the KW material.
2. The mean crack growth rate of the KW specimens was very similar to the mean crack growth rates of the FT488/1 and FT488/2 specimens at the same peak stress level, and the small variation noted was consistent with the variation in the hardness of the three groups. This suggests that hardness has a direct relationship to crack growth rate for the fastest cracks in this material.
3. The scatter in lives was low compared to typically available figures for low Kt specimens, considering the small number of coupons tested from each material source, with the scatter greatest for the FT488/2 specimens. This was expected considering the reduced number of initiations in these specimens, probably an indicator that the etching was less severe than in the other plates, leading to a reliance in part, on smaller etch pits at the bases of shallow machining marks to initiate the largest cracks.
4. The EPS method appears to account for the crack-like effect of the flaw and the immediately surrounding crack growth more effectively than any measure of the flaw itself. To this end this method gives an excellent measure of the effective size of the flaws in a particular material and the crack-like nature of those flaws.

5. The EPS values were similar for the three plates tested here when compared to each other and to the previously examined etched KS specimens. (This study only considered etched surfaces, a following study will consider as-machined surfaces)
6. Pooling the EPS data appears to be valid for the data presented here, and allows a reasonable estimate of a remotely possible EPS. (Care must be exercised in all extreme value estimation since it is a prediction based on the population near the mean, a population that may not have identified all the possible discontinuities of interest - if the distribution does not adequately represent the less populous but more severe discontinuities then prediction of low levels of their probability will be flawed - further work is being undertaken to address this weakness).
7. Two examples of porosity, of a relatively large size were found to initiate two of the many cracks examined here. Their physical size was very much larger than their EPS indicating that their physical size is a poor indicator of how crack-like they are.

5. Acknowledgements

The author gratefully acknowledges the work of Chris Niessen and Brian Jones of DSTO-PSL for specimen preparation and performing the fatigue tests.

6. Bibliography

Anderson, I. and Revill, G., F/A-18 fuselage station 488 free-standing bulkhead fatigue test, Department of Defence, Defence Science and Technology Organisation report ARL-STRUC-TM-575, 1990.

Athiniotis, N., Barter, S. A and Clark, G., Summary of fatigue cracking in RAAF Macchi MB326H wing spars. Department of Defence, Defence Science and Technology Organisation report ARL-MAT-TR-0747. 1999.

Athiniotis, N., Barter S.A., Bohret D.D., Green A.J., Houston M.I. and Stimson M.G., Final report for the component fatigue test of a F/A-18 Centre Fuselage FS488 Bulkhead - FT488/2, Department of Defence, Defence Science and Technology Organisation report DSTO-TR-0948, 2003.

Barter, S. A and Price, J., Effect of surface preparation treatments on fatigue life of 7050-aluminium alloy. Proceedings of the Structural Integrity and Fracture 2000 Symposium, pp140-153. 2000.

Barter, S. A. Athiniotis, N.and Lambrianidis L., Examination of the microstructure of several samples of 7050 aluminium alloy, Department of Defence, Defence Science and Technology Organisation report ARL-MAT-TM-403. August 1990b.

Barter, S. A., Bishop, B and Clark, G., Defect assessment on F/A-18 488 bulkhead tested at ARL, Department of Defence, Defence Science and Technology Organisation report ARL-MAT-TM-125. 1991.

Barter, S. A., Fatigue Crack growth in 7050T7451 aluminium alloy thick section plate with a surface condition simulating some regions of F/A-18 structure, Department of Defence, Defence Science and Technology Organisation report DSTO-TR-1458. 2003.

Barter, S. A., Fractographic Inspection of the cracking in FT488/2 removed at program 79, Department of Defence, Defence Science and Technology Organisation report DSTO-TN-0170. 1998.

Barter, S. A., The use of the conventional optical microscope for quantitative fractography, Metallography and Mineralogy Conference, Institute of Metals and Materials Australasia Limited, 1991.

Dixon, B. and Molent, L., Ex-service F/A-18 centre barrel fatigue flaw identification test plan, Department of Defence, Defence Science and Technology Organisation report DSTO-TR-1426. 2003.

Edwards, P. R. and Newman, Jr, L. C., Short-crack growth behaviour in various aircraft materials, Advisory Group for Aerospace Research and Development (AGARD) report 767, NATO. 1990.

Mehr, P. L., Spuhler, E. H., Mayer, L. W. and Grant, J. E., Alcoa green letter 7075-T73, Alcoa Green Letter 206, 1971.

Molent L., Ogden R. and Pell R., F/A-18 FS488 Bulkhead fatigue coupon test program, Department of Defence, Defence Science and Technology Organisation report DSTO-TR-0941. 2000.

Murakami, Y., Effects of small defects and nonmetallic inclusions on the fatigue strength of metals, JSME International Journal, Vol 32, No. 2. 1989.

Owen, C. R., Bucci, R. J. and Kegarise, R. J., Aluminium quality breakthrough for aircraft structural reliability, J. Aircraft, 26, 2, pp178-184. 1988.

Pell, R. A., Mazeika, P. J., and Molent, L., The comparison of complex loading sequences tested at several stress levels by fractographic examination, Proc. Of International Committee on Aeronautical Fatigue Conference, Lucerne Switzerland, 2003.

Renolds, M. A. and Harris, J. G., Development of a tough, high-strength aluminium alloy with improved stress-corrosion resistance, Aluminium, Vol. 50, pp502-596, 1974.

Speidel, M. O. and Hyatt, M. V., Stress-corrosion cracking of high-strength aluminium alloys, Advances in corrosion Science and Technology, Plenum Press, Vol. 2, pp115-335, 1972.

Staley, J. T. and Hunsicker, H. Y., Exploratory development of high-strength, stress corrosion resistant aluminium ally for use in thick section applications, Technical Report AMFL-TR-70-256, Air Force Materials Laboratory, Air Force Wright Aeronautical Laboratories, Dayton, 1970.

Wanhill, R. J. H., Damage tolerance engineering property evaluations of aerospace aluminium alloys with emphasis on fatigue crack growth, National Aerospace Laboratory report NLR TP 94177U, NLR Amsterdam, The Netherlands, 1995.

White, P., Barter, S. and Molent, L., Probabilistic fracture prediction based on aircraft specific fatigue test data, In: Proc. 6th Joint FAA/DoD/NASA Aging Aircraft Conference, San Francisco, Sept.16-19, 2002.

Yang, J. N and Manning, S. D. Distribution of equivalent initial flaw size, Proceedings of Annual Reliability and Maintainability Symposium, pp 112-120. 1980.

Yang, J. N and Manning, S. D., Demonstration of probabilistic-based durability analysis method for metallic airframes, Presented as paper 88-2421 at the AIAA/ASME/ASCE/AHS 29th Structures, Structural Dynamics and Materials Conference, 1988.

Yang, J. N, Manning, S. D, Rudd J. L and Bader R. M., Investigation of mechanistic-based equivalent initial flaw size approach, International Committee on Aeronautical Fatigue 18th Symposium Melbourne Australia, 1995.

Appendix A: Crack growth data for the FT488/1 specimens

Table A-1: Results of the quantitative fractography on specimen 001, peak stress 300MPa

No. of spectra IARPO3a + 5 marker loads	Simulated Flight Hours	Measured from flaw to crack mm	Addition of EPS Type I (flaw depth) mm	Addition of EPS Type II mm
0	0		0.0056	0.007
0.5	162.46			
1.5	487.38			
2.5	812.3	0.0017	0.0073	0.0087
3.5	1137.2			
4.5	1462.1	0.0043	0.0099	0.0113
5.5	1787.1			
6.5	2112	0.0081	0.0137	0.0151
7.5	2436.9			
8.5	2761.8	0.0118	0.0174	0.0188
9.5	3086.7	0.0149	0.0205	0.0219
10.5	3411.7	0.02	0.0256	0.027
11.5	3736.6	0.0249	0.0305	0.0319
12.5	4061.5	0.032	0.0376	0.039
13.5	4386.4	0.0371	0.0427	0.0441
14.5	4711.3	0.043	0.0486	0.05
15.5	5036.3	0.0493	0.0549	0.0563
16.5	5361.2	0.0591	0.0647	0.0661
17.5	5686.1	0.0688	0.0744	0.0758
18.5	6011	0.083	0.0886	0.09
19.5	6335.9	0.0949	0.1005	0.1019
20.5	6660.9	0.109	0.1146	0.116
21.5	6985.8	0.1252	0.1308	0.1322
22.5	7310.7	0.1469	0.1525	0.1539
23.5	7635.6	0.175	0.1806	0.182
24.5	7960.5	0.206	0.2116	0.213
25.5	8285.5	0.2453	0.2509	0.2523
26.5	8610.4	0.3057	0.3113	0.3127
27.5	8935.3	0.3798	0.3854	0.3868
28.5	9260.2			
29.5	9585.1	0.5427	0.5483	0.5497
30.5	9910.1	0.7105	0.7161	0.7175
31.5	10235			
32.5	10560			
33.5	10885	1.3243	1.3299	1.3313
34.5	11210	1.6308	1.6364	1.6378
35.5	11535			
36.5	11860			
37.52	12191	3.0935	3.0991	3.1005

Table A-2: Results of the quantitative fractography on specimen 002, peak stress 300MPa

No. of spectra IARPO3a + 5 marker loads	Simulated Flight Hours	Measured from flaw to crack mm	Addition of EPS Type I (flaw depth) mm	Addition of EPS Type II mm
0	0		0.0145	0.015
0.5	162.46			
1.5	487.38	0.0032	0.0177	0.0182
2.5	812.3	0.0064	0.0209	0.0214
3.5	1137.2	0.01	0.0245	0.025
4.5	1462.1	0.0132	0.0277	0.0282

5.5	1787.1	0.018	0.0325	0.033
6.5	2112	0.0233	0.0378	0.0383
7.5	2436.9	0.0277	0.0422	0.0427
8.5	2761.8	0.0321	0.0466	0.0471
9.5	3086.7	0.0377	0.0522	0.0527
10.5	3411.7	0.0441	0.0586	0.0591
11.5	3736.6	0.0493	0.0638	0.0643
12.5	4061.5	0.0569	0.0714	0.0719
13.5	4386.4	0.0689	0.0834	0.0839
14.5	4711.3	0.0784	0.0929	0.0934
15.5	5036.3	0.0889	0.1034	0.1039
16.5	5361.2	0.1039	0.1184	0.1189
17.5	5686.1	0.1203	0.1348	0.1353
18.5	6011	0.1391	0.1536	0.1541
19.5	6335.9	0.165	0.1795	0.18
20.5	6660.9	0.1926	0.2071	0.2076
21.5	6985.8	0.2234	0.2379	0.2384
22.5	7310.7	0.2571	0.2716	0.2721
23.5	7635.6	0.315	0.3295	0.33
24.5	7960.5	0.3943	0.4088	0.4093
25.5	8285.5	0.4769	0.4914	0.4919
26.5	8610.4	0.6248	0.6393	0.6398
27.5	8935.3	0.7869	0.8014	0.8019
28.5	9260.2	0.9431	0.9576	0.9581
29.5	9585.1	1.2236	1.2381	1.2386
30.5	9910.1	1.6362	1.6507	1.6512
31.5	10235	2.1907	2.2052	2.2057
32.5	10560			
32.94	10703	3.8266	3.8411	3.8416

Table A- 3: Results of the quantitative fractography on specimen 003, peak stress 300MPa

No. of spectra IARPO3a + 5 marker loads	Simulated Flight Hours	Measured from flaw to crack mm	Addition of EPS Type I (flaw depth) mm	Addition of EPS Type II mm
0	0		0.0071	0.008
0.5	162.46	0.0013	0.0084	0.0093
1.5	487.38	0.0024	0.0095	0.0104
2.5	812.3			
3.5	1137.2	0.0058	0.0129	0.0138
4.5	1462.1	0.0083	0.0154	0.0163
5.5	1787.1	0.0103	0.0174	0.0183
6.5	2112	0.0128	0.0199	0.0208
7.5	2436.9	0.0162	0.0233	0.0242
8.5	2761.8	0.0198	0.0269	0.0278
9.5	3086.7	0.024	0.0311	0.032
10.5	3411.7	0.0286	0.0357	0.0366
11.5	3736.6	0.0336	0.0407	0.0416
12.5	4061.5	0.0373	0.0444	0.0453
13.5	4386.4	0.0447	0.0518	0.0527
14.5	4711.3	0.0513	0.0584	0.0593
15.5	5036.3	0.0633	0.0704	0.0713
16.5	5361.2	0.073	0.0801	0.081
17.5	5686.1	0.0883	0.0954	0.0963
18.5	6011	0.1016	0.1087	0.1096
19.5	6335.9	0.1176	0.1247	0.1256
20.5	6660.9	0.1327	0.1398	0.1407
21.5	6985.8	0.1459	0.153	0.1539
22.5	7310.7	0.1603	0.1674	0.1683
23.5	7635.6	0.1791	0.1862	0.1871
24.5	7960.5	0.1972	0.2043	0.2052
25.5	8285.5	0.2221	0.2292	0.2301

26.5	8610.4	0.2579	0.265	0.2659
27.5	8935.3	0.2989	0.306	0.3069
28.5	9260.2	0.3333	0.3404	0.3413
29.5	9585.1	0.3749	0.382	0.3829
30.5	9910.1	0.4172	0.4243	0.4252
31.5	10235	0.4654	0.4725	0.4734
32.5	10560	0.532	0.5391	0.54
33.5	10885	0.6089	0.616	0.6169
34.5	11210	0.7977	0.8048	0.8057
35.5	11535			
36.5	11860	1.0195	1.0266	1.0275
37.5	12185			
38.5	12509	1.4229	1.43	1.4309
39.5	12834			
40.5	13159	2.1339	2.141	2.1419
41.5	13484			
41.65	13533	3.6627	3.6698	3.6707

Table A-4: Results of the quantitative fractography on specimen 004, peak stress 330MPa

No. of spectra IARPO3a + 5 marker loads	Simulated Flight Hours	Measured from flaw to crack mm	Addition of EPS Type I (flaw depth) mm	Addition of EPS Type II mm
0	0		0.0172	0.015
0.5	162.46	0.002	0.0192	0.017
1.5	487.38	0.0052	0.0224	0.0202
2.5	812.3	0.0076	0.0248	0.0226
3.5	1137.2	0.0111	0.0283	0.0261
4.5	1462.1	0.0157	0.0329	0.0307
5.5	1787.1	0.0218	0.039	0.0368
6.5	2112	0.0301	0.0473	0.0451
7.5	2436.9	0.0403	0.0575	0.0553
8.5	2761.8	0.051	0.0682	0.066
9.5	3086.7	0.0633	0.0805	0.0783
10.5	3411.7	0.0765	0.0937	0.0915
11.5	3736.6	0.0961	0.1133	0.1111
12.5	4061.5	0.1144	0.1316	0.1294
13.5	4386.4	0.1368	0.154	0.1518
14.5	4711.3	0.1597	0.1769	0.1747
15.5	5036.3	0.1976	0.2148	0.2126
16.5	5361.2	0.2499	0.2671	0.2649
17.5	5686.1	0.3154	0.3326	0.3304
18.5	6011	0.3688	0.386	0.3838
19.5	6335.9	0.486	0.5032	0.501
20.5	6660.9	0.6076	0.6248	0.6226
21.5	6985.8	0.7524	0.7696	0.7674
22.5	7310.7	0.9684	0.9856	0.9834
23.5	7635.6	1.36	1.3772	1.375
24.5	7960.5	1.6148	1.632	1.6298
25.26	8207.5	1.798	1.8152	1.813

Table A-5: Results of the quantitative fractography on specimen 005, peak stress 330MPa

No. of spectra IARPO3a + 5 marker loads	Simulated Flight Hours	Measured from flaw to crack mm	Addition of EPS Type I (flaw depth) mm	Addition of EPS Type II mm
0	0		0.0117	0.015
0.5	162.46	0.0023	0.014	0.0173
1.5	487.38	0.0057	0.0174	0.0207
2.5	812.3	0.0119	0.0236	0.0269
3.5	1137.2	0.0184	0.0301	0.0334

4.5	1462.1	0.0274	0.0391	0.0424
5.5	1787.1	0.0383	0.05	0.0533
6.5	2112	0.0532	0.0649	0.0682
7.5	2436.9			
8.5	2761.8			
9.5	3086.7			
10.5	3411.7	0.1305	0.1422	0.1455
11.5	3736.6	0.1493	0.161	0.1643
12.5	4061.5	0.1674	0.1791	0.1824
13.5	4386.4	0.2053	0.217	0.2203
14.5	4711.3	0.2491	0.2608	0.2641
15.5	5036.3	0.2969	0.3086	0.3119
16.5	5361.2	0.3603	0.372	0.3753
17.5	5686.1	0.4583	0.47	0.4733
18.5	6011	0.5733	0.585	0.5883
19.5	6335.9			
20.5	6660.9	0.8067	0.8184	0.8217
21.5	6985.8	1.0865	1.0982	1.1015
22.5	7310.7	1.4114	1.4231	1.4264
23.5	7635.6	1.8815	1.8932	1.8965
24.5	7960.5	2.318	2.3297	2.333
24.88	8084	2.8191	2.8308	2.8341

Table A-6: Results of the quantitative fractography on specimen 006, peak stress 330MPa

No. of spectra IARPO3a + 5 marker loads	Simulated Flight Hours	Measured from flaw to crack mm	Addition of EPS Type I (flaw depth) mm	Addition of EPS Type II mm
0	0		0.0353	0.02
0.5	162.46	0.0016	0.0369	0.0216
1.5	487.38	0.0068	0.0421	0.0268
2.5	812.3	0.0121	0.0474	0.0321
3.5	1137.2	0.0172	0.0525	0.0372
4.5	1462.1			
5.5	1787.1	0.0332	0.0685	0.0532
6.5	2112	0.0488	0.0841	0.0688
7.5	2436.9	0.0735	0.1088	0.0935
8.5	2761.8	0.1106	0.1459	0.1306
9.5	3086.7	0.1448	0.1801	0.1648
10.5	3411.7	0.1943	0.2296	0.2143
11.5	3736.6	0.2384	0.2737	0.2584
12.5	4061.5	0.3342	0.3695	0.3542
13.5	4386.4	0.4422	0.4775	0.4622
14.5	4711.3	0.5685	0.6038	0.5885
15.5	5036.3	0.6859	0.7212	0.7059
16.5	5361.2			
17.5	5686.1	1.1897	1.225	1.2097
18.5	6011	1.6262	1.6615	1.6462
19.5	6335.9			
20.5	6660.9	2.4845	2.5198	2.5045
21.13	6865.6	3.2147	3.25	3.2347

Table A-7: Results of the quantitative fractography on specimen 007, crack 1, peak stress 360MPa

No. of spectra IARPO3a + 5 marker loads	Simulated Flight Hours	Measured from flaw to crack mm	Addition of EPS Type I (flaw depth) mm	Addition of EPS Type II mm
0	0		0.0137	0.015
0.5	162.46	0.0020999	0.0158	0.0171
1.5	487.38	0.0043	0.018	0.0193

2.5	812.3	0.0088	0.0225	0.0238
3.5	1137.2	0.0127	0.0264	0.0277
4.5	1462.1	0.0198	0.0335	0.0348
5.5	1787.1	0.0299	0.0436	0.0449
6.5	2112	0.0419	0.0556	0.0569
7.5	2436.9			
8.5	2761.8	0.0767	0.0904	0.0917
9.5	3086.7	0.1066	0.1203	0.1216
10.5	3411.7	0.144	0.1577	0.159
11.5	3736.6	0.1827	0.1964	0.1977
12.5	4061.5	0.2479	0.2616	0.2629
13.5	4386.4	0.3445	0.3582	0.3595
14.5	4711.3			
15.5	5036.3	0.6886	0.7023	0.7036
16.5	5361.2	0.9331	0.9468	0.9481
17.5	5686.1	1.3084	1.3221	1.3234
18.5	6011			
19.5	6335.9			
20.51	6664.1	2.5664	2.5801	2.5814

Table A-8: Results of the quantitative fractography on specimen 007, crack 2, peak stress 360MPa

No. of spectra IARPO3a + 5 marker loads	Simulated Flight Hours	Measured from flaw to crack mm	Addition of EPS Type I (flaw depth) mm	Addition of EPS Type II mm
0	0		0.005	0.01
0.5	162.46			
1.5	487.38	0.0028	0.0078	0.0128
2.5	812.3	0.0044	0.0094	0.0144
3.5	1137.2	0.006	0.011	0.016
4.5	1462.1	0.0076	0.0126	0.0176
5.5	1787.1	0.01	0.015	0.02
6.5	2112	0.012	0.017	0.022
7.5	2436.9	0.016	0.021	0.026
8.5	2761.8	0.0212	0.0262	0.0312
9.5	3086.7	0.0257	0.0307	0.0357
10.5	3411.7	0.0347	0.0397	0.0447
11.5	3736.6	0.0453	0.0503	0.0553
12.5	4061.5			
13.5	4386.4	0.0661	0.0711	0.0761
14.5	4711.3			
15.5	5036.3	0.11	0.115	0.12
16.5	5361.2			
17.5	5686.1	0.152	0.157	0.162
18.5	6011			
19.5	6335.9	0.2096	0.2146	0.2196
20.3	6595.9	0.222	0.227	0.232

Table A-9: Results of the quantitative fractography on specimen 007, crack 2.1, peak stress 360MPa

No. of spectra IARPO3a + 5 marker loads	Simulated Flight Hours	Measured from flaw to crack mm	Addition of EPS Type I (flaw depth) mm	Addition of EPS Type II mm
0	0		0.004	0.008
0.5	162.46			
1.5	487.38	0.0012	0.0052	0.0092
2.5	812.3			
3.5	1137.2	0.0036	0.0076	0.0116

4.5	1462.1			
5.5	1787.1	0.006	0.01	0.014
6.5	2112	0.0084	0.0124	0.0164
7.5	2436.9	0.0116	0.0156	0.0196
8.5	2761.8	0.0144	0.0184	0.0224
9.5	3086.7	0.0176	0.0216	0.0256
10.5	3411.7	0.0216	0.0256	0.0296
11.5	3736.6	0.0248	0.0288	0.0328
12.5	4061.5	0.0308	0.0348	0.0388
13.5	4386.4	0.0388	0.0428	0.0468
14.5	4711.3	0.0464	0.0504	0.0544
15.5	5036.3	0.0532	0.0572	0.0612
16.5	5361.2	0.0613	0.0653	0.0693
17.5	5686.1	0.0735	0.0775	0.0815
18.5	6011	0.09	0.094	0.098
19.5	6335.9	0.1062	0.1102	0.1142
20.3	6595.9	0.1157	0.1197	0.1237

Table A-10: Results of the quantitative fractography on specimen 008, peak stress 360MPa

No. of spectra IARPO3a + 5 marker loads	Simulated Flight Hours	Measured from flaw to crack mm	Addition of EPS Type I (flaw depth) mm	Addition of EPS Type II mm
0	0		0.0096	0.02
0.5	162.46	0.0022627	0.011863	0.022263
1.5	487.38	0.0046819	0.014282	0.024682
2.5	812.3			
3.5	1137.2	0.012106	0.021706	0.032106
4.5	1462.1	0.017673	0.027273	0.037673
5.5	1787.1	0.023255	0.032855	0.043255
6.5	2112	0.030442	0.040042	0.050442
7.5	2436.9	0.037234	0.046834	0.057234
8.5	2761.8	0.046028	0.055628	0.066028
9.5	3086.7	0.057622	0.067222	0.077622
10.5	3411.7	0.073617	0.083217	0.093617
11.5	3736.6	0.085821	0.095421	0.10582
12.5	4061.5	0.11102	0.12062	0.13102
13.5	4386.4	0.15382	0.16342	0.17382
14.5	4711.3	0.18289	0.19249	0.20289
15.5	5036.3	0.2245	0.2341	0.2445
16.5	5361.2	0.26703	0.27663	0.28703
17.5	5686.1	0.31764	0.32724	0.33764
18.5	6011	0.42387	0.43347	0.44387
19.5	6335.9	0.5971	0.6067	0.6171
20.5	6660.9	0.70581	0.71541	0.72581
21.5	6985.8	0.9979	1.0075	1.0179
22.5	7310.7	1.2704	1.28	1.2904
23.5	7635.6	1.6273	1.6369	1.6473
24.26	7882.6	2.39	2.3996	2.41

Table A-11: Results of the quantitative fractography on specimen 011, peak stress 360MPa

No. of spectra IARPO3a + 5 marker loads	Simulated Flight Hours	Measured from flaw to crack mm	Addition of EPS Type I (flaw depth) mm	Addition of EPS Type II mm
0	0		0.01	0.01
0.5	162.46			
1.5	487.38	0.0046819	0.014682	0.014682
2.5	812.3	0.0089443	0.018944	0.018944
3.5	1137.2	0.015559	0.025559	0.025559
4.5	1462.1	0.024166	0.034166	0.034166

5.5	1787.1	0.035186	0.045186	0.045186
6.5	2112	0.049076	0.059076	0.059076
7.5	2436.9	0.067002	0.077002	0.077002
8.5	2761.8	0.080568	0.090568	0.090568
9.5	3086.7	0.10852	0.11852	0.11852
10.5	3411.7	0.1381	0.1481	0.1481
11.5	3736.6	0.16822	0.17822	0.17822
12.5	4061.5	0.23721	0.24721	0.24721
13.5	4386.4	0.28441	0.29441	0.29441
14.5	4711.3	0.36641	0.37641	0.37641
15.5	5036.3	0.4904	0.5004	0.5004
16.5	5361.2	0.6536	0.6636	0.6636
17.5	5686.1	0.95225	0.96225	0.96225
18.5	6011	1.4747	1.4847	1.4847
18.81	6111.7	2.0696	2.0796	2.0796

Table A-12: Results of the quantitative fractography on specimen 012, peak stress 390MPa

No. of spectra IARPO3a + 5 marker loads	Simulated Flight Hours	Measured from flaw to crack mm	Addition of EPS Type I (flaw depth) mm	Addition of EPS Type II mm
0	0		0.008	0.025
0.5	162.46			
1.5	487.38	0.0113	0.0193	0.0363
2.5	812.3	0.0217	0.0297	0.0467
3.5	1137.2	0.0424	0.0504	0.0674
4.5	1462.1	0.0664	0.0744	0.0914
5.5	1787.1	0.0908	0.0988	0.1158
6.5	2112	0.1164	0.1244	0.1414
7.5	2436.9	0.1523	0.1603	0.1773
8.5	2761.8	0.1971	0.2051	0.2221
9.5	3086.7	0.2593	0.2673	0.2843
10.5	3411.7	0.3663	0.3743	0.3913
11.5	3736.6	0.6015	0.6095	0.6265
12.5	4061.5	0.9001	0.9081	0.9251
13.5	4386.4	1.3709	1.3789	1.3959
14.4	4678.8	1.9057	1.9137	1.9307

Table A-13: Results of the quantitative fractography on specimen 013, peak stress 390MPa

No. of spectra IARPO3a + 5 marker loads	Simulated Flight Hours	Measured from flaw to crack mm	Addition of EPS Type I (flaw depth) mm	Addition of EPS Type II mm
0	0		0.0348	0.035
1	324.92	0.0052	0.04	0.0402
2	649.84	0.0148	0.0496	0.0498
3	974.76	0.0388	0.0736	0.0738
4	1299.7	0.0652	0.1	0.1002
5	1624.6	0.0934	0.1282	0.1284
6	1949.5	0.1218	0.1566	0.1568
7	2274.4	0.1611	0.1959	0.1961
8	2599.4	0.2271	0.2619	0.2621
9	2924.3	0.289	0.3238	0.324
10	3249.2	0.3731	0.4079	0.4081
11	3574.1	0.4992	0.534	0.5342
12	3899	0.6471	0.6819	0.6821
13	4224	0.9654	1.0002	1.0004
14	4548.9	1.6951	1.7299	1.7301
14.7	4776.3	2.1849	2.2197	2.2199

Table A-14: Results of the quantitative fractography on specimen 014, peak stress 390MPa

No. of spectra IARPO3a + 5 marker loads	Simulated Flight Hours	Measured from flaw to crack mm	Addition of EPS Type I (flaw depth) mm	Addition of EPS Type II mm
0	0		0.0036	0.02
0.5	162.46	0.0032	0.0068	0.0232
1.5	487.38	0.0104	0.014	0.0304
2.5	812.3	0.0252	0.0288	0.0452
3.5	1137.2	0.0445	0.0481	0.0645
4.5	1462.1	0.0617	0.0653	0.0817
5.5	1787.1	0.0937	0.0973	0.1137
6.5	2112	0.1527	0.1563	0.1727
7.5	2436.9	0.2263	0.2299	0.2463
8.5	2761.8	0.4369	0.4405	0.4569
9.5	3086.7	0.7396	0.7432	0.7596
10.5	3411.7	1.0653	1.0689	1.0853
11.5	3736.6	1.4552	1.4588	1.4752
12.2	3964	2.2161	2.2197	2.2361

Table A-15: Results of the quantitative fractography on specimen 009, crack 1, peak stress 420MPa

No. of spectra IARPO3a + 5 marker loads	Simulated Flight Hours	Measured from flaw to crack mm	Addition of EPS Type I (flaw depth) mm	Addition of EPS Type II mm
0	0		0.0628	0.015
0.5	162.46			
1.5	487.38	0.016	0.0788	0.031
2.5	812.3	0.0331	0.0959	0.0481
3.5	1137.2	0.0557	0.1185	0.0707
4.5	1462.1	0.0988	0.1616	0.1138
5.5	1787.1			
6.5	2112	0.234	0.2968	0.249
7.5	2436.9	0.3606	0.4234	0.3756
8.5	2761.8	0.4789	0.5417	0.4939
9.5	3086.7	0.7762	0.839	0.7912
10.5	3411.7	1.107	1.1698	1.122
11.5	3736.6			
11.7	3801.6	1.801	1.8638	1.816

Table A-16: Results of the quantitative fractography on specimen 009, crack 2, peak stress 420MPa

No. of spectra IARPO3a + 5 marker loads	Simulated Flight Hours	Measured from flaw to crack mm	Addition of EPS Type I (flaw depth) mm	Addition of EPS Type II mm
0	0		0.0119	0.01
0.5	162.46			
1.5	487.38	0.0143	0.0262	0.0243
2.5	812.3			
3.5	1137.2	0.0601	0.072	0.0701
4.5	1462.1	0.0959	0.1078	0.1059
5.5	1787.1	0.1332	0.1451	0.1432
6.5	2112	0.1714	0.1833	0.1814
7.5	2436.9	0.2347	0.2466	0.2447
8.5	2761.8	0.3081	0.32	0.3181
9.5	3086.7	0.4324	0.4443	0.4424
10.5	3411.7	0.5893	0.6012	0.5993
11.5	3736.6			
11.7	3801.6	0.9013	0.9132	0.9113

Table A-17: Results of the quantitative fractography on specimen 009, crack 3, peak stress 420MPa

No. of spectra IARPO3a + 5 marker loads	Simulated Flight Hours	Measured from flaw to crack mm	Addition of EPS Type I (flaw depth) mm	Addition of EPS Type II mm
0	0		0.0628	0.04
0.5	162.46	0.0088	0.0716	0.0488
1.5	487.38	0.028	0.0908	0.068
2.5	812.3	0.052	0.1148	0.092
3.5	1137.2	0.0946	0.1574	0.1346
4.5	1462.1	0.1265	0.1893	0.1665
5.5	1787.1	0.1936	0.2564	0.2336
6.5	2112	0.2898	0.3526	0.3298
7.5	2436.9	0.3859	0.4487	0.4259
8.5	2761.8	0.5565	0.6193	0.5965
9.5	3086.7	0.6936	0.7564	0.7336
10.5	3411.7	0.8679	0.9307	0.9079
11.5	3736.6			
11.7	3801.6	1.2136	1.2764	1.2536

Table A-18: Results of the quantitative fractography on specimen 010, crack 1, peak stress 420MPa

No. of spectra IARPO3a + 5 marker loads	Simulated Flight Hours	Measured from flaw to crack mm	Addition of EPS Type I (flaw depth) mm	Addition of EPS Type II mm
0	0		0.1204	0.02
0.5	162.46	0.0052	0.1256	0.0252
1.5	487.38	0.0208	0.1412	0.0408
2.5	812.3	0.0437	0.1641	0.0637
3.5	1137.2	0.0804	0.2008	0.1004
4.5	1462.1	0.1224	0.2428	0.1424
5.5	1787.1	0.1949	0.3153	0.2149
6.5	2112	0.2862	0.4066	0.3062
7.5	2436.9	0.4831	0.6035	0.5031
8.5	2761.8	0.7239	0.8443	0.7439
9.5	3086.7	1.1533	1.2737	1.1733
10.25	3330.4	2.1237	2.2441	2.1437

Table A-19: Results of the quantitative fractography on specimen 010, crack 2, peak stress 420MPa

No. of spectra IARPO3a + 5 marker loads	Simulated Flight Hours	Measured from flaw to crack mm	Addition of EPS Type I (flaw depth) mm	Addition of EPS Type II mm
0	0		0.0727	0.015
0.5	162.46			
1.5	487.38			
2.5	812.3	0.023	0.0957	0.038
3.5	1137.2			
4.5	1462.1	0.0489	0.1216	0.0639
5.5	1787.1	0.0805	0.1532	0.0955
6.5	2112	0.1248	0.1975	0.1398
7.5	2436.9	0.1909	0.2636	0.2059
8.5	2761.8	0.2754	0.3481	0.2904
9.5	3086.7	0.4072	0.4799	0.4222
10.25	3330.4	0.5433	0.616	0.5583

Appendix B: Crack growth data for the FT488/2 specimens

Table B-1: Results of the quantitative fractography on specimen 001, peak stress 300MPa

No. of spectra IARPO3a + 5 marker loads	Simulated Flight Hours	Measured from flaw to crack mm	Addition of EPS Type I (flaw depth) mm	Addition of EPS Type II mm
0	0		0.0125	0.0125
0.5	162.46			
1.5	487.38	0.0028	0.0153	0.0153
2.5	812.3			
3.5	1137.2	0.0078	0.0203	0.0203
4.5	1462.1	0.0112	0.0237	0.0237
5.5	1787.1	0.0159	0.0284	0.0284
6.5	2112	0.0225	0.035	0.035
7.5	2436.9	0.0252	0.0377	0.0377
8.5	2761.8	0.0309	0.0434	0.0434
9.5	3086.7	0.037	0.0495	0.0495
10.5	3411.7	0.0424	0.0549	0.0549
11.5	3736.6	0.0515	0.064	0.064
12.5	4061.5	0.0623	0.0748	0.0748
13.5	4386.4	0.0774	0.0899	0.0899
14.5	4711.3			
15.5	5036.3	0.1025	0.115	0.115
16.5	5361.2	0.1227	0.1352	0.1352
17.5	5686.1	0.1413	0.1538	0.1538
18.5	6011	0.163	0.1755	0.1755
19.5	6335.9	0.1852	0.1977	0.1977
20.5	6660.9	0.2072	0.2197	0.2197
21.5	6985.8	0.246	0.2585	0.2585
22.5	7310.7	0.2838	0.2963	0.2963
23.5	7635.6	0.3265	0.339	0.339
24.5	7960.5	0.3792	0.3917	0.3917
25.5	8285.5	0.4337	0.4462	0.4462
26.5	8610.4	0.5008	0.5133	0.5133
27.5	8935.3	0.5934	0.6059	0.6059
28.5	9260.2	0.6951	0.7076	0.7076
29.5	9585.1	0.7988	0.8113	0.8113
30.5	9910.1	0.9237	0.9362	0.9362
31.5	10235	1.068	1.0805	1.0805
32.5	10560	1.2502	1.2627	1.2627
33.5	10885	1.4802	1.4927	1.4927
34.5	11210	1.7406	1.7531	1.7531
35.5	11535	1.9781	1.9906	1.9906
36.5	11860	2.3	2.3125	2.3125
37.5	12185			
37.73	12259	2.717	2.7295	2.7295

Table B-2: Results of the quantitative fractography on specimen 002, peak stress 300MPa

No. of spectra IARPO3a + 5 marker loads	Simulated Flight Hours	Measured from flaw to crack mm	Addition of EPS Type I (flaw depth) mm	Addition of EPS Type II mm
0	0		0.024	0.01
0.5	162.46	0.0013	0.0253	0.0113
1.5	487.38	0.0034	0.0274	0.0134
2.5	812.3	0.0052	0.0292	0.0152
3.5	1137.2	0.0072	0.0312	0.0172
4.5	1462.1	0.01	0.034	0.02

5.5	1787.1	0.0149	0.0389	0.0249
6.5	2112	0.0193	0.0433	0.0293
7.5	2436.9	0.0265	0.0505	0.0365
8.5	2761.8	0.0332	0.0572	0.0432
9.5	3086.7	0.0444	0.0684	0.0544
10.5	3411.7	0.0548	0.0788	0.0648
11.5	3736.6	0.0697	0.0937	0.0797
12.5	4061.5	0.084	0.108	0.094
13.5	4386.4	0.0996	0.1236	0.1096
14.5	4711.3	0.1237	0.1477	0.1337
15.5	5036.3	0.1414	0.1654	0.1514
16.5	5361.2	0.1628	0.1868	0.1728
17.5	5686.1	0.1895	0.2135	0.1995
18.5	6011	0.2249	0.2489	0.2349
19.5	6335.9	0.2637	0.2877	0.2737
20.5	6660.9	0.3219	0.3459	0.3319
21.5	6985.8	0.3613	0.3853	0.3713
22.5	7310.7	0.3965	0.4205	0.4065
23.5	7635.6	0.4694	0.4934	0.4794
24.5	7960.5	0.5358	0.5598	0.5458
25.5	8285.5	0.6232	0.6472	0.6332
26.5	8610.4	0.7159	0.7399	0.7259
27.5	8935.3	0.8288	0.8528	0.8388
28.5	9260.2	1.0052	1.0292	1.0152
29.5	9585.1	1.2772	1.3012	1.2872
30.5	9910.1	1.5175	1.5415	1.5275
31.5	10235	1.7386	1.7626	1.7486
32.5	10560			
33.5	10885	2.6644	2.6884	2.6744
34	11047	2.9462	2.9702	2.9562

Table B-3: Results of the quantitative fractography on specimen 008, peak stress 300MPa

No. of spectra IARPO3a + 5 marker loads	Simulated Flight Hours	Measured from flaw to crack mm	Addition of EPS Type I (flaw depth) mm	Addition of EPS Type II mm
0	0		0.0039	0.005
0.5	162.46			
1.5	487.38			
2.5	812.3	0.0024	0.0063	0.0074
3.5	1137.2	0.0033	0.0072	0.0083
4.5	1462.1	0.0046	0.0085	0.0096
5.5	1787.1	0.0056	0.0095	0.0106
6.5	2112	0.0068	0.0107	0.0118
7.5	2436.9	0.0083	0.0122	0.0133
8.5	2761.8	0.0098	0.0137	0.0148
9.5	3086.7	0.012	0.0159	0.017
10.5	3411.7	0.0141	0.018	0.0191
11.5	3736.6	0.0166	0.0205	0.0216
12.5	4061.5	0.0194	0.0233	0.0244
13.5	4386.4	0.0225	0.0264	0.0275
14.5	4711.3	0.0259	0.0298	0.0309
15.5	5036.3	0.0304	0.0343	0.0354
16.5	5361.2	0.0364	0.0403	0.0414
17.5	5686.1	0.0414	0.0453	0.0464
18.5	6011	0.0471	0.051	0.0521
19.5	6335.9	0.0533	0.0572	0.0583
20.5	6660.9	0.0602	0.0641	0.0652
21.5	6985.8	0.0689	0.0728	0.0739
22.5	7310.7	0.0782	0.0821	0.0832
23.5	7635.6	0.0921	0.096	0.0971

24.5	7960.5	0.1048	0.1087	0.1098
25.5	8285.5	0.1197	0.1236	0.1247
26.5	8610.4	0.1399	0.1438	0.1449
27.5	8935.3	0.1542	0.1581	0.1592
28.5	9260.2			
29.5	9585.1			
30.5	9910.1	0.2503	0.2542	0.2553
31.5	10235	0.288	0.2919	0.293
32.5	10560	0.3362	0.3401	0.3412
33.5	10885	0.3827	0.3866	0.3877
34.5	11210	0.4501	0.454	0.4551
35.5	11535	0.5286	0.5325	0.5336
36.5	11860			
37.5	12185	0.676	0.6799	0.681
38.5	12509	0.7646	0.7685	0.7696
39.5	12834	0.8635	0.8674	0.8685
40.5	13159	0.9889	0.9928	0.9939
41.5	13484	1.1256	1.1295	1.1306
42.5	13809	1.3936	1.3975	1.3986
43.5	14134			
44.5	14459	1.95	1.9539	1.955
45.5	14784	2.337	2.3409	2.342
46.5	15109			
46.73	15184	2.7014	2.7053	2.7064

Table B-4: Results of the quantitative fractography on specimen 003, peak stress 330MPa

No. of spectra IARPO3a + 5 marker loads	Simulated Flight Hours	Measured from flaw to crack mm	Addition of EPS Type I (flaw depth) mm	Addition of EPS Type II mm
0	0		0.005	0.01
0.5	162.46			
1.5	487.38	0.0035	0.0085	0.0135
2.5	812.3	0.0071	0.0121	0.0171
3.5	1137.2	0.0122	0.0172	0.0222
4.5	1462.1	0.0202	0.0252	0.0302
5.5	1787.1	0.0339	0.0389	0.0439
6.5	2112	0.046	0.051	0.056
7.5	2436.9			
8.5	2761.8	0.0746	0.0796	0.0846
9.5	3086.7	0.1069	0.1119	0.1169
10.5	3411.7	0.1392	0.1442	0.1492
11.5	3736.6	0.1751	0.1801	0.1851
12.5	4061.5	0.2449	0.2499	0.2549
13.5	4386.4	0.325	0.33	0.335
14.5	4711.3	0.4628	0.4678	0.4728
15.5	5036.3	0.6436	0.6486	0.6536
16.5	5361.2	0.9285	0.9335	0.9385
17.5	5686.1	1.2751	1.2801	1.2851
18.5	6011	1.6865	1.6915	1.6965
19.5	6335.9	2.0488	2.0538	2.0588
20.5	6660.9	2.5173	2.5223	2.5273

Table B-5: Results of the quantitative fractography on specimen 006, crack 1, peak stress 330MPa

No. of spectra IARPO3a + 5 marker loads	Simulated Flight Hours	Measured from flaw to crack mm	Addition of EPS Type I (flaw depth) mm	Addition of EPS Type II mm
0	0		0.0092	0.015

0.5	162.46			
1.5	487.38	0.004	0.0132	0.019
2.5	812.3			
3.5	1137.2	0.0159	0.0251	0.0309
4.5	1462.1	0.022	0.0312	0.037
5.5	1787.1	0.0328	0.042	0.0478
6.5	2112	0.0431	0.0523	0.0581
7.5	2436.9	0.0571	0.0663	0.0721
8.5	2761.8	0.0707	0.0799	0.0857
9.5	3086.7	0.092	0.1012	0.107
10.5	3411.7	0.1081	0.1173	0.1231
11.5	3736.6	0.1349	0.1441	0.1499
12.5	4061.5	0.1611	0.1703	0.1761
13.5	4386.4	0.1866	0.1958	0.2016
14.5	4711.3	0.2128	0.222	0.2278
15.5	5036.3	0.2459	0.2551	0.2609
16.5	5361.2	0.2733	0.2825	0.2883
17.5	5686.1	0.3258	0.335	0.3408
18.5	6011	0.3896	0.3988	0.4046
19.5	6335.9	0.458	0.4672	0.473
20.5	6660.9	0.5791	0.5883	0.5941
21.5	6985.8	0.7076	0.7168	0.7226
22.5	7310.7	0.8354	0.8446	0.8504
23.5	7635.6	1.0535	1.0627	1.0685
24.5	7960.5	1.3444	1.3536	1.3594
25.5	8285.5	1.6683	1.6775	1.6833
26.5	8610.4			
27.41	8906.1	2.7608	2.77	2.7758

Table B-6: Results of the quantitative fractography on specimen 006, crack 2, peak stress 330MPa

No. of spectra IARPO3a + 5 marker loads	Simulated Flight Hours	Measured from flaw to crack mm	Addition of EPS Type I (flaw depth) mm	Addition of EPS Type II mm
0.5	162.46		0.0064	0.006
1.5	487.38	0.0008	0.0072	0.0068
2.5	812.3	0.0024	0.0088	0.0084
3.5	1137.2			
4.5	1462.1	0.0056	0.012	0.0116
5.5	1787.1	0.008	0.0144	0.014
6.5	2112	0.0112	0.0176	0.0172
7.5	2436.9	0.014	0.0204	0.02
8.5	2761.8	0.0168	0.0232	0.0228
9.5	3086.7	0.02	0.0264	0.026
10.5	3411.7	0.0236	0.03	0.0296
11.5	3736.6	0.0272	0.0336	0.0332
12.5	4061.5	0.0348	0.0412	0.0408
13.5	4386.4	0.0428	0.0492	0.0488
14.5	4711.3	0.0524	0.0588	0.0584
15.5	5036.3	0.0624	0.0688	0.0684
16.5	5361.2	0.074	0.0804	0.08
17.5	5686.1	0.0832	0.0896	0.0892
18.5	6011	0.0916	0.098	0.0976
19.5	6335.9	0.1088	0.1152	0.1148
20.5	6660.9	0.1212	0.1276	0.1272
21.5	6985.8	0.1344	0.1408	0.1404
22.5	7310.7	0.1485	0.1549	0.1545
23.5	7635.6	0.1655	0.1719	0.1715

24.5	7960.5	0.1899	0.1963	0.1959
25.5	8285.5	0.2258	0.2322	0.2318
26.5	8610.4	0.2519	0.2583	0.2579
27.41	8906.1	0.2808	0.2872	0.2868

Table B-7: Results of the quantitative fractography on specimen 015, peak stress 330MPa

No. of spectra IARPO3a + 5 marker loads	Simulated Flight Hours	Measured from flaw to crack mm	Addition of EPS Type I (flaw depth) mm	Addition of EPS Type II mm
0	0		0.0099	0.01
0.5	162.46	0.0012	0.0111	0.0112
1.5	487.38	0.0033	0.0132	0.0133
2.5	812.3	0.0072	0.0171	0.0172
3.5	1137.2	0.0117	0.0216	0.0217
4.5	1462.1	0.0155	0.0254	0.0255
5.5	1787.1			
6.5	2112	0.0272	0.0371	0.0372
7.5	2436.9	0.0355	0.0454	0.0455
8.5	2761.8	0.042	0.0519	0.052
9.5	3086.7	0.0525	0.0624	0.0625
10.5	3411.7	0.063	0.0729	0.073
11.5	3736.6	0.08	0.0899	0.09
12.5	4061.5	0.0963	0.1062	0.1063
13.5	4386.4	0.1149	0.1248	0.1249
14.5	4711.3	0.1399	0.1498	0.1499
15.5	5036.3	0.1681	0.178	0.1781
16.5	5361.2	0.1975	0.2074	0.2075
17.5	5686.1	0.2336	0.2435	0.2436
18.5	6011	0.27	0.2799	0.28
19.5	6335.9	0.3076	0.3175	0.3176
20.5	6660.9	0.3558	0.3657	0.3658
21.5	6985.8	0.4255	0.4354	0.4355
22.5	7310.7	0.5181	0.528	0.5281
23.5	7635.6	0.6657	0.6756	0.6757
24.5	7960.5	0.8453	0.8552	0.8553
25.5	8285.5	1.2285	1.2384	1.2385
26.5	8610.4	1.8311	1.841	1.8411
27.49	8932.1	2.5888	2.5987	2.5988

Table B-8: Results of the quantitative fractography on specimen 019, crack 1, peak stress 330MPa

No. of spectra IARPO3a + 5 marker loads	Simulated Flight Hours	Measured from flaw to crack mm	Addition of EPS Type I (flaw depth) mm	Addition of EPS Type II mm
0.5	162.46		0.0132	0.015
1.5	487.38	0.0032	0.0164	0.0182
2.5	812.3	0.006	0.0192	0.021
3.5	1137.2	0.0084	0.0216	0.0234
4.5	1462.1	0.0116	0.0248	0.0266
5.5	1787.1	0.0156	0.0288	0.0306
6.5	2112	0.0204	0.0336	0.0354
7.5	2436.9	0.0236	0.0368	0.0386
8.5	2761.8	0.0272	0.0404	0.0422
9.5	3086.7	0.0309	0.0441	0.0459
10.5	3411.7	0.0352	0.0484	0.0502
11.5	3736.6	0.0404	0.0536	0.0554
12.5	4061.5	0.0484	0.0616	0.0634
13.5	4386.4	0.06	0.0732	0.075

14.5	4711.3	0.0736	0.0868	0.0886
15.5	5036.3	0.0824	0.0956	0.0974
16.5	5361.2	0.1008	0.114	0.1158
17.5	5686.1	0.1199	0.1331	0.1349
18.5	6011	0.1403	0.1535	0.1553
19.5	6335.9	0.156	0.1692	0.171
20.5	6660.9	0.175	0.1882	0.19
21.5	6985.8	0.206	0.2192	0.221
22.5	7310.7	0.2376	0.2508	0.2526
23.5	7635.6	0.2811	0.2943	0.2961
24.5	7960.5	0.3227	0.3359	0.3377
25.5	8285.5	0.3604	0.3736	0.3754
26.5	8610.4	0.4195	0.4327	0.4345
27.5	8935.3	0.475	0.4882	0.49
28.5	9260.2	0.5616	0.5748	0.5766
29.5	9585.1	0.6981	0.7113	0.7131
30.5	9910.1	0.8394	0.8526	0.8544
31.5	10235	0.9999	1.0131	1.0149
32.5	10560	1.3218	1.335	1.3368
33.5	10885	1.9331	1.9463	1.9481

Table B-9: Results of the quantitative fractography on specimen 019, crack 2, peak stress 330MPa

No. of spectra IARPO3a + 5 marker loads	Simulated Flight Hours	Measured from flaw to crack mm	Addition of EPS Type I (flaw depth) mm	Addition of EPS Type II mm
0	0		0.0053	0.015
0.5	162.46			
1.5	487.38	0.004	0.0093	0.019
2.5	812.3			
3.5	1137.2	0.0088	0.0141	0.0238
4.5	1462.1	0.0136	0.0189	0.0286
5.5	1787.1	0.0188	0.0241	0.0338
6.5	2112			
7.5	2436.9			
8.5	2761.8			
9.5	3086.7			
10.5	3411.7			
11.5	3736.6			
12.5	4061.5			
13.5	4386.4			
14.5	4711.3			
15.5	5036.3			
16.5	5361.2			
17.5	5686.1	0.1421	0.1474	0.1571
18.5	6011	0.1625	0.1678	0.1775
19.5	6335.9	0.1875	0.1928	0.2025
20.5	6660.9	0.2159	0.2212	0.2309
21.5	6985.8	0.2521	0.2574	0.2671
22.5	7310.7	0.2834	0.2887	0.2984
23.5	7635.6	0.3522	0.3575	0.3672
24.5	7960.5	0.4216	0.4269	0.4366
25.5	8285.5	0.4987	0.504	0.5137
26.5	8610.4	0.588	0.5933	0.603
27.5	8935.3	0.6754	0.6807	0.6904
28.5	9260.2	0.7711	0.7764	0.7861
29.5	9585.1	0.9135	0.9188	0.9285
30.5	9910.1	1.1184	1.1237	1.1334
31.5	10235	1.3548	1.3601	1.3698

32.5	10560	1.6031	1.6084	1.6181
33.52	10891	2.2042	2.2095	2.2192

Table B-10: Results of the quantitative fractography on specimen 005, peak stress 360MPa

No. of spectra IARPO3a + 5 marker loads	Simulated Flight Hours	Measured from flaw to crack mm	Addition of EPS Type I (flaw depth) mm	Addition of EPS Type II mm
0	0		0.0148	0.03
0.5	162.46	0.0052	0.02	0.0352
1.5	487.38	0.0136	0.0284	0.0436
2.5	812.3	0.0268	0.0416	0.0568
3.5	1137.2	0.0392	0.054	0.0692
4.5	1462.1	0.0555	0.0703	0.0855
5.5	1787.1	0.0751	0.0899	0.1051
6.5	2112	0.097	0.1118	0.127
7.5	2436.9	0.1247	0.1395	0.1547
8.5	2761.8	0.1535	0.1683	0.1835
9.5	3086.7	0.1901	0.2049	0.2201
10.5	3411.7	0.2548	0.2696	0.2848
11.5	3736.6	0.3104	0.3252	0.3404
12.5	4061.5	0.3852	0.4	0.4152
13.5	4386.4	0.4846	0.4994	0.5146
14.5	4711.3	0.6209	0.6357	0.6509
15.5	5036.3			
16.5	5361.2	1.1183	1.1331	1.1483
17.5	5686.1			
18.5	6011			
18.79	6105.2	3.0528	3.0676	3.0828

Table B-11: Results of the quantitative fractography on specimen 010, peak stress 360MPa

No. of spectra IARPO3a + 5 marker loads	Simulated Flight Hours	Measured from flaw to crack mm	Addition of EPS Type I (flaw depth) mm	Addition of EPS Type II mm
0	0		0.0228	0.02
0.5	162.46	0.0028	0.0256	0.0228
1.5	487.38	0.0111	0.0339	0.0311
2.5	812.3	0.0206	0.0434	0.0406
3.5	1137.2	0.0326	0.0554	0.0526
4.5	1462.1	0.0514	0.0742	0.0714
5.5	1787.1	0.0662	0.089	0.0862
6.5	2112	0.0867	0.1095	0.1067
7.5	2436.9	0.109	0.1318	0.129
8.5	2761.8	0.1317	0.1545	0.1517
9.5	3086.7	0.1585	0.1813	0.1785
10.5	3411.7	0.1813	0.2041	0.2013
11.5	3736.6	0.2137	0.2365	0.2337
12.5	4061.5	0.2624	0.2852	0.2824
13.5	4386.4			
14.5	4711.3	0.3266	0.3494	0.3466
15.5	5036.3			
16.5	5361.2	0.3957	0.4185	0.4157
17.5	5686.1	0.4481	0.4709	0.4681
18.5	6011	0.4905	0.5133	0.5105
19.5	6335.9	0.5587	0.5815	0.5787
20.5	6660.9	0.6147	0.6375	0.6347
21.5	6985.8	0.69	0.7128	0.71
22.5	7310.7	0.8034	0.8262	0.8234
23.5	7635.6	0.9595	0.9823	0.9795

24.5	7960.5	1.1914	1.2142	1.2114
25.5	8285.5	1.4906	1.5134	1.5106
26.5	8610.4	1.9999	2.0227	2.0199
27.5	8935.3	2.4944	2.5172	2.5144
28.15	9146.5	2.9448	2.9676	2.9648

Table B-12 : Results of the quantitative fractography on specimen 011, peak stress 360MPa

No. of spectra IARPO3a + 5 marker loads	Simulated Flight Hours	Measured from flaw to crack mm	Addition of EPS Type I (flaw depth) mm	Addition of EPS Type II mm
0	0		0.0084	0.03
0.5	162.46	0.0052	0.0136	0.0352
1.5	487.38	0.01	0.0184	0.04
2.5	812.3	0.0208	0.0292	0.0508
3.5	1137.2	0.0428	0.0512	0.0728
4.5	1462.1	0.0667	0.0751	0.0967
5.5	1787.1	0.1022	0.1106	0.1322
6.5	2112	0.1361	0.1445	0.1661
7.5	2436.9	0.1709	0.1793	0.2009
8.5	2761.8	0.208	0.2164	0.238
9.5	3086.7	0.2531	0.2615	0.2831
10.5	3411.7	0.3222	0.3306	0.3522
11.5	3736.6	0.3798	0.3882	0.4098
12.5	4061.5	0.439	0.4474	0.469
13.5	4386.4			
14.5	4711.3	0.7068	0.7152	0.7368
15.5	5036.3	0.8688	0.8772	0.8988
16.5	5361.2	1.3502	1.3586	1.3802
17.5	5686.1	2.5741	2.5825	2.6041

Table B-13 : Results of the quantitative fractography on specimen 018, peak stress 360MPa

No. of spectra IARPO3a + 5 marker loads	Simulated Flight Hours	Measured from flaw to crack mm	Addition of EPS Type I (flaw depth) mm	Addition of EPS Type II mm
0	0		0.006	0.015
0.5	162.46			
1.5	487.38			
2.5	812.3	0.0106	0.0166	0.0256
3.5	1137.2			
4.5	1462.1	0.0306	0.0366	0.0456
5.5	1787.1	0.0448	0.0508	0.0598
6.5	2112	0.0704	0.0764	0.0854
7.5	2436.9	0.1073	0.1133	0.1223
8.5	2761.8	0.1536	0.1596	0.1686
9.5	3086.7	0.2133	0.2193	0.2283
10.5	3411.7	0.3088	0.3148	0.3238
11.5	3736.6	0.4363	0.4423	0.4513
12.5	4061.5	0.5319	0.5379	0.5469
13.5	4386.4	0.7117	0.7177	0.7267
14.5	4711.3	0.8439	0.8499	0.8589
15.5	5036.3	1.1983	1.2043	1.2133
16.5	5361.2			
17.51	5689.3	2.2379	2.2439	2.2529

Table B-14 : Results of the quantitative fractography on specimen 007, peak stress 390MPa

No. of spectra IARPO3a + 5 marker loads	Simulated Flight Hours	Measured from flaw to crack mm	Addition of EPS Type I (flaw depth) mm	Addition of EPS Type II mm
0	0		0.00024	0.02
0.5	162.46	0.0016	0.00184	0.0216
1.5	487.38	0.0052	0.00544	0.0252
2.5	812.3	0.014	0.01424	0.034
3.5	1137.2	0.0264	0.02664	0.0464
4.5	1462.1	0.0512	0.05144	0.0712
5.5	1787.1	0.088	0.08824	0.108
6.5	2112	0.1232	0.12344	0.1432
7.5	2436.9	0.1832	0.18344	0.2032
8.5	2761.8			
9.5	3086.7	0.4992	0.49944	0.5192
10.5	3411.7	0.7729	0.77314	0.7929
11.5	3736.6			
12.5	4061.5	1.8876	1.88784	1.9076
13.2	4288.9	2.3633	2.36354	2.3833

Table B-15: Results of the quantitative fractography on specimen 009, peak stress 390MPa

No. of spectra IARPO3a + 5 marker loads	Simulated Flight Hours	Measured from flaw to crack mm	Addition of EPS Type I (flaw depth) mm	Addition of EPS Type II mm
0	0		0.016	0.05
0.5	162.46	0.0091	0.0251	0.0591
1.5	487.38	0.0193	0.0353	0.0693
2.5	812.3	0.0342	0.0502	0.0842
3.5	1137.2	0.0545	0.0705	0.1045
4.5	1462.1	0.074	0.09	0.124
5.5	1787.1	0.105	0.121	0.155
6.5	2112	0.143	0.159	0.193
7.5	2436.9	0.1854	0.2014	0.2354
8.5	2761.8	0.236	0.252	0.286
9.5	3086.7	0.2997	0.3157	0.3497
10.5	3411.7	0.4092	0.4252	0.4592
11.5	3736.6	0.5233	0.5393	0.5733
12.5	4061.5	0.661	0.677	0.711
13.5	4386.4	0.9308	0.9468	0.9808
14.5	4711.3	1.3264	1.3424	1.3764
15.5	5036.3	2.5218	2.5378	2.5718

Table B-16: Results of the quantitative fractography on specimen 016, peak stress 390MPa

No. of spectra IARPO3a + 5 marker loads	Simulated Flight Hours	Measured from flaw to crack mm	Addition of EPS Type I (flaw depth) mm	Addition of EPS Type II mm
0	0		0.002	0.005
0.5	162.46	0.0016	0.0036	0.0066
1.5	487.38	0.0052	0.0072	0.0102
2.5	812.3	0.0124	0.0144	0.0174
3.5	1137.2	0.018	0.02	0.023
4.5	1462.1	0.0352	0.0372	0.0402
5.5	1787.1	0.0588	0.0608	0.0638
6.5	2112	0.1088	0.1108	0.1138
7.5	2436.9	0.1708	0.1728	0.1758
8.5	2761.8	0.2601	0.2621	0.2651
9.5	3086.7	0.4174	0.4194	0.4224

10.5	3411.7			
11.5	3736.6	0.9228	0.9248	0.9278
12.5	4061.5	1.4333	1.4353	1.4383
13.5	4386.4	2.5987	2.6007	2.6037

Table B-17: Results of the quantitative fractography on specimen 012, crack 1, peak stress 420MPa

No. of spectra IARPO3a + 5 marker loads	Simulated Flight Hours	Measured from flaw to crack mm	Addition of EPS Type I (flaw depth) mm	Addition of EPS Type II mm
0	0		0.0308	0.02
0.5	162.46	0.0044	0.0352	0.0244
1.5	487.38	0.0124	0.0432	0.0324
2.5	812.3	0.0264	0.0572	0.0464
3.5	1137.2	0.0424	0.0732	0.0624
4.5	1462.1	0.0696	0.1004	0.0896
5.5	1787.1	0.1154	0.1462	0.1354
6.5	2112	0.1775	0.2083	0.1975
7.5	2436.9	0.2496	0.2804	0.2696
8.5	2761.8	0.3286	0.3594	0.3486
9.5	3086.7	0.4837	0.5145	0.5037
10.5	3411.7	0.6885	0.7193	0.7085
11.5	3736.6	1.1105	1.1413	1.1305
12.5	4061.5	1.6628	1.6936	1.6828
12.8	4159	2.1405	2.1713	2.1605

Table B-18: Results of the quantitative fractography on specimen 012, creak 2, peak stress 420MPa

No. of spectra IARPO3a + 5 marker loads	Simulated Flight Hours	Measured from flaw to crack mm	Addition of EPS Type I (flaw depth) mm	Addition of EPS Type II mm
0	0		0.0036	0.007
0.5	162.46			
1.5	487.38	0.0062	0.0098	0.0132
2.5	812.3			0.007
3.5	1137.2	0.0181	0.0217	0.0251
4.5	1462.1	0.0281	0.0317	0.0351
5.5	1787.1	0.0438	0.0474	0.0508
6.5	2112	0.0617	0.0653	0.0687
7.5	2436.9	0.0862	0.0898	0.0932
8.5	2761.8	0.1225	0.1261	0.1295
9.5	3086.7	0.2	0.2036	0.207
10.5	3411.7	0.3245	0.3281	0.3315
11.5	3736.6	0.4419	0.4455	0.4489
12.5	4061.5	0.6181	0.6217	0.6251
12.8	4159	0.8056	0.8092	0.8126

Table B-19: Results of the quantitative fractography on specimen 013, peak stress 420MPa

No. of spectra IARPO3a + 5 marker loads	Simulated Flight Hours	Measured from flaw to crack mm	Addition of EPS Type I (flaw depth) mm	Addition of EPS Type II mm
0	0		0.001	0.006
0.5	162.46			
1.5	487.38	0.0096	0.0106	0.0156
2.5	812.3	0.0268	0.0278	0.0328
3.5	1137.2	0.0496	0.0506	0.0556
4.5	1462.1	0.1	0.101	0.106
5.5	1787.1	0.1748	0.1758	0.1808

6.5	2112	0.3428	0.3438	0.3488
7.5	2436.9	0.5804	0.5814	0.5864
8.5	2761.8	1.1008	1.1018	1.1068
9.2	2989.3	2.0688	2.0698	2.0748

Table B-20: Results of the quantitative fractography on specimen 017, peak stress 420MPa

No. of spectra IARPO3a + 5 marker loads	Simulated Flight Hours	Measured from flaw to crack mm	Addition of EPS Type I (flaw depth) mm	Addition of EPS Type II mm
0	0		0.002	0.025
0.5	162.46	0.0108	0.0128	0.0358
1.5	487.38	0.03	0.032	0.055
2.5	812.3	0.0688	0.0708	0.0938
3.5	1137.2	0.1488	0.1508	0.1738
4.5	1462.1	0.2752	0.2772	0.3002
5.5	1787.1	0.4328	0.4348	0.4578
6.5	2112	1.1452	1.1472	1.1702
7.4	2404.4	1.9372	1.9392	1.9622

Appendix C: Growth data for the etched KW plate specimens

Table C-1: Results of the quantitative fractography on KW100, peak stress 390MPa

No. of spectra IARPO3a + 5 marker loads	Simulated Flight Hours	Measured from flaw to crack mm	Addition of EPS Type I (flaw depth) mm	Addition of EPS Type II mm
0	0		0.0308	0.04
1	324.92	0.0108	0.0416	0.0508
2	649.84	0.018	0.0488	0.058
3	974.76	0.0284	0.0592	0.0684
4	1299.7	0.046	0.0768	0.086
5	1624.6	0.0679	0.0987	0.1079
6	1949.5	0.0878	0.1186	0.1278
7	2274.4	0.1172	0.148	0.1572
8	2599.4	0.1442	0.175	0.1842
9	2924.3	0.1823	0.2131	0.2223
10	3249.2	0.2415	0.2723	0.2815
11	3574.1	0.3409	0.3717	0.3809
12	3899	0.5235	0.5543	0.5635
13	4224	0.8031	0.8339	0.8431
14	4548.9	1.2533	1.2841	1.2933
15	4873.8	2.1128	2.1436	2.1528
16	5198.7			
16.2	5263.7	3.7619	3.7927	3.8019

Table C-2: Results of the quantitative fractography on KW101, peak stress 390MPa

No. of spectra IARPO3a + 5 marker loads	Simulated Flight Hours	Measured from flaw to crack mm	Addition of EPS Type I (flaw depth) mm	Addition of EPS Type II mm
0	0		0.0156	0.015
1	324.92	0.0044	0.02	0.0194
2	649.84			
3	974.76	0.0136	0.0292	0.0286
4	1299.7	0.0208	0.0364	0.0358
5	1624.6	0.0323	0.0479	0.0473
6	1949.5	0.0454	0.061	0.0604
7	2274.4	0.0642	0.0798	0.0792
8	2599.4	0.0888	0.1044	0.1038
9	2924.3	0.1237	0.1393	0.1387
10	3249.2	0.1771	0.1927	0.1921
11	3574.1	0.2724	0.288	0.2874
12	3899	0.3647	0.3803	0.3797
13	4224	0.5415	0.5571	0.5565
14	4548.9	0.8038	0.8194	0.8188
15	4873.8	1.255	1.2706	1.27
16	5198.7	2.0192	2.0348	2.0342
17	5523.6			
17.56	5705.6	3.3137	3.3293	3.3287

Table C-3: Results of the quantitative fractography on KW102, peak stress 390MPa

No. of spectra IARPO3a + 5 marker loads	Simulated Flight Hours	Measured from flaw to crack mm	Addition of EPS Type I (flaw depth) mm	Addition of EPS Type II mm
0	0		0.0132	0.015
1	324.92	0.0049	0.0181	0.0199
2	649.84	0.0127	0.0259	0.0277
3	974.76	0.0238	0.037	0.0388
4	1299.7	0.0379	0.0511	0.0529
5	1624.6	0.0573	0.0705	0.0723
6	1949.5	0.0747	0.0879	0.0897
7	2274.4	0.1036	0.1168	0.1186
8	2599.4	0.1388	0.152	0.1538
9	2924.3	0.182	0.1952	0.197
10	3249.2	0.2478	0.261	0.2628
11	3574.1	0.3292	0.3424	0.3442
12	3899	0.4568	0.47	0.4718
13	4224	0.6904	0.7036	0.7054
14	4548.9			
15	4873.8	1.1777	1.1909	1.1927
16	5198.7			
17	5523.6	2.2797	2.2929	2.2947
18	5848.6	3.2756	3.2888	3.2906
19	6173.5			
19.19	6235.2	4.1261	4.1393	4.1411

Table C-4: Results of the quantitative fractography on KW103, creak 1, peak stress 390MPa

No. of spectra IARPO3a + 5 marker loads	Simulated Flight Hours	Measured from flaw to crack mm	Addition of EPS Type I (flaw depth) mm	Addition of EPS Type II mm
0	0		0.0072	0.008
1	324.92	0.0032	0.0104	0.0112
2	649.84	0.0056	0.0128	0.0136
3	974.76	0.0092	0.0164	0.0172
4	1299.7	0.0176	0.0248	0.0256
5	1624.6	0.0348	0.042	0.0428
6	1949.5	0.0552	0.0624	0.0632
7	2274.4	0.0812	0.0884	0.0892
8	2599.4	0.11	0.1172	0.118
9	2924.3	0.1476	0.1548	0.1556
10	3249.2	0.1904	0.1976	0.1984
11	3574.1	0.2482	0.2554	0.2562
12	3899	0.3623	0.3695	0.3703
13	4224	0.548	0.5552	0.556
14	4548.9	0.851	0.8582	0.859
15	4873.8	1.3409	1.3481	1.3489
15.51	5039.5	2.2017	2.2089	2.2097

Table C-5: Results of the quantitative fractography on KW103, creak 1.1, peak stress 390MPa

No. of spectra IARPO3a + 5 marker loads	Simulated Flight Hours	Measured from flaw to crack mm	Addition of EPS Type I (flaw depth) mm	Addition of EPS Type II mm
0	0		0.0168	0.008
1	324.92			
2	649.84	0.004	0.0208	0.012
3	974.76	0.008	0.0248	0.016
4	1299.7	0.0132	0.03	0.0212
5	1624.6	0.0164	0.0332	0.0244
6	1949.5	0.0236	0.0404	0.0316
7	2274.4	0.0344	0.0512	0.0424
8	2599.4	0.0459	0.0627	0.0539
9	2924.3	0.0725	0.0893	0.0805
10	3249.2	0.122	0.1388	0.13
11	3574.1	0.2219	0.2387	0.2299
12	3899	0.4124	0.4292	0.4204
13	4224	0.7883	0.8051	0.7963
14	4548.9			
14.51	4714.6	2.0593	2.0761	2.0673

Table C-6: Results of the quantitative fractography on KW104, peak stress 390MPa

No. of spectra IARPO3a + 5 marker loads	Simulated Flight Hours	Measured from flaw to crack mm	Addition of EPS Type I (flaw depth) mm	Addition of EPS Type II mm
0	0		0.0252	0.015
1	324.92	0.0068	0.032	0.0218
2	649.84	0.0152	0.0404	0.0302
3	974.76	0.0244	0.0496	0.0394
4	1299.7	0.042	0.0672	0.057
5	1624.6	0.0636	0.0888	0.0786
6	1949.5	0.0948	0.12	0.1098
7	2274.4	0.146	0.1712	0.161
8	2599.4	0.2173	0.2425	0.2323
9	2924.3	0.3403	0.3655	0.3553
10	3249.2	0.4798	0.505	0.4948
11	3574.1	0.7201	0.7453	0.7351
12	3899	1.1882	1.2134	1.2032
13	4224	1.6032	1.6284	1.6182
14	4548.9	2.1391	2.1643	2.1541
15	4873.8			
15.2	4938.8	3.18	3.2052	3.195

DISTRIBUTION LIST

Fatigue Crack Growth in Several 7050T7451 Aluminium Alloy Thick Section Plates with Aircraft Manufacturer's and Laboratory Surface Finishes Representing Some Regions of the F/A-18 Structure

S. A. Barter

AUSTRALIA

DEFENCE ORGANISATION

		No. of copies
Task Sponsor	DGTA-ASI1 (SQNLDR J. Medved)	1
S&T Program		
Chief Defence Scientist		
FAS Science Policy	shared copy	1
AS Science Corporate Management		
Director General Science Policy Development		1
Counsellor Defence Science, London		Doc Data Sheet
Counsellor Defence Science, Washington		Doc Data Sheet
Scientific Adviser to MRDC Thailand		Doc Data Sheet
Scientific Adviser Policy and Command		1
Scientific Adviser Joint		1
Navy Scientific Adviser		Doc Data Sheet & Dist List
Scientific Adviser - Army		Doc Data Sheet & Dist List
Scientific Adviser to the DMO M&A		Doc Data Sheet & Dist List
Scientific Adviser to the DMO ELL		Doc Data Sheet & Dist List
Air Force Scientific Adviser		1
Director Trials		1
Platforms Sciences Laboratory		
Director		1
Chief of Air Vehicles Division		1
Research Leader AVD-ASI		1
Task Manager L. Molent		1
Author(s):		
R. Pell		1
S. A. Barter		1
P. White		1
K. Walker		1
Q. Liu		1
IFOSTP filing system		1
DSTO Library and Archives		
Library Fishermans Bend		1
Australian Archives		1
Library, MOD, Pyrmont		Doc Data Sheet
Capability Systems Division		
Director General Maritime Development		Doc Data Sheet

Director General Aerospace Development — Doc Data Sheet
Director General Information Capability Development — Doc Data Sheet

Office of the Chief Information Officer
Deputy CIO — Doc Data Sheet
Director General Information Policy and Plans — Doc Data Sheet
AS Information Structures and Futures — Doc Data Sheet
AS Information Architecture and Management — Doc Data Sheet
Director General Australian Defence Simulation Office — Doc Data Sheet

Strategy Group
Director General Military Strategy — Doc Data Sheet
Director General Preparedness — Doc Data Sheet

HQAST
SO (Science) (ASJIC) — Doc Data Sheet

Navy
Director General Navy Capability, Performance and Plans, Navy Headquarters — Doc Data Sheet
Director General Navy Strategic Policy and Futures, Navy Headquarters — Doc Data Sheet

Air Force
TFSPO Williamtown (Chief Engineer) — 1
RAAF TLO IFOSTP (SQNLDR P. Klose) — 1

Army
ABCA National Standardisation Officer, Land Warfare Development Sector, Puckapunyal — e-mailed Doc Data Sheet
SO (Science), Deployable Joint Force Headquarters (DJFHQ) (L), Enoggera QLD — Doc Data Sheet
SO (Science) - Land Headquarters (LHQ), Victoria Barracks NSW — Doc Data & Exec Summ

Intelligence Program
DGSTA Defence Intelligence Organisation — 1
Manager, Information Centre, Defence Intelligence Organisation — 1 (PDF only)
Manager, Information Centre, Defence Intelligence Organisation — 1
Assistant Secretary Corporate, Defence Imagery and Geospatial Organisation — Doc Data Sheet

Defence Materiel Organisation
Head Airborne Surveillance and Control — Doc Data Sheet
Head Aerospace Systems Division — Doc Data Sheet
Head Electronic Systems Division — Doc Data Sheet
Head Maritime Systems Division — Doc Data Sheet
Head Land Systems Division — Doc Data Sheet
Head Industry Division — Doc Data Sheet
Chief Joint Logistics Command — Doc Data Sheet
Management Information Systems Division — Doc Data Sheet

Head Materiel Finance	Doc Data Sheet

Defence Libraries

Library Manager, DLS-Canberra	Doc Data Sheet
Library Manager, DLS - Sydney West	Doc Data Sheet

OTHER ORGANISATIONS

National Library of Australia	1
NASA (Canberra)	1

UNIVERSITIES AND COLLEGES

Australian Defence Force Academy	
Library	1
Head of Aerospace and Mechanical Engineering	1
Serials Section (M list), Deakin University Library, Geelong, VIC	1
Hargrave Library, Monash University	Doc Data Sheet
Librarian, Flinders University	1

OUTSIDE AUSTRALIA

INTERNATIONAL DEFENCE INFORMATION CENTRES

US Defense Technical Information Center	2
UK Defence Research Information Centre	2
Canada Defence Scientific Information Service	e-mail link to pdf
NZ Defence Information Centre	1

Canada

DTA	1
NRC - D. Simpson	1
Bombardier - Y. Richard	1

ABSTRACTING AND INFORMATION ORGANISATIONS

Library, Chemical Abstracts Reference Service	1
Engineering Societies Library, US	1
Materials Information, Cambridge Scientific Abstracts, US	1
Documents Librarian, The Center for Research Libraries, US	1

INFORMATION EXCHANGE AGREEMENT PARTNERS

National Aerospace Laboratory, Japan	1
National Aerospace Laboratory, Netherlands	1

SPARES	5
Total number of copies:	**48**

DEFENCE SCIENCE AND TECHNOLOGY ORGANISATION
DOCUMENT CONTROL DATA

1. PRIVACY MARKING/CAVEAT (OF DOCUMENT)

2. TITLE

Fatigue Crack Growth in Several 7050T7451 Aluminium Alloy Thick Section Plates with aircraft manufacture's and Laboratory Surface Finishes Representing Some Regions of the F/A-18 Structure

3. SECURITY CLASSIFICATION (FOR UNCLASSIFIED REPORTS THAT ARE LIMITED RELEASE USE (L) NEXT TO DOCUMENT CLASSIFICATION)

Document	(U)
Title	(U)
Abstract	(U)

4. AUTHOR(S)

S. A. Barter

5. CORPORATE AUTHOR

Platforms Sciences Laboratory
506 Lorimer St
Fishermans Bend Victoria 3207 Australia

6a. DSTO NUMBER	6b. AR NUMBER	6c. TYPE OF REPORT	7. DOCUMENT DATE
DSTO-TR-1539	AR-013-004	Technical Report	December 2003

8. FILE NUMBER	9. TASK NUMBER	10. TASK SPONSOR	11. NO. OF PAGES	12. NO. OF REFERENCES
2003/36886/1	AIR00/143	DGTA	72	22

13. URL on the World Wide Web

http://www.dsto.defence.gov.au/corporate/reports/DSTO-TR-1539.pdf

14. RELEASE AUTHORITY

Chief, Air Vehicles Division

15. SECONDARY RELEASE STATEMENT OF THIS DOCUMENT

Approved for public release

OVERSEAS ENQUIRIES OUTSIDE STATED LIMITATIONS SHOULD BE REFERRED THROUGH DOCUMENT EXCHANGE, PO BOX 1500, EDINBURGH, SA 5111

16. DELIBERATE ANNOUNCEMENT

No Limitations

17. CITATION IN OTHER DOCUMENTS Yes

18. DEFTEST DESCRIPTORS

F/A-18 aircraft Aluminium alloys Fatigue (Mechanics) Fatigue tests Fracture mechanics Crack propagation Fractography

19. ABSTRACT

This is the third in a series of papers that examine material factors likely to influence the fatigue life of F/A-18 structure. Work leading up to these papers has highlighted a number of concerns about the fatigue variability of the 7050 aluminium alloy thick section plate and the effect that the surface condition of finished components has on service fatigue crack initiation and life. This report examines a series of fatigue test specimens that were cut from three different 7050 plates, including two aircraft manufacturer's plates. Following the tests, quantitative fractography was used to produce crack growth curves for each fatigue specimen allowing a detailed interpretation of the crack growth to be made, including a measure of the severity of the flaws from which the main fatigue cracks initiated. Comparisons between previously tested 7050 plate, and the three plates tested here were made, with the finding that the crack growth rates and the flaws from which the cracking initiated were very similar to those previously examined.